Mathematical Models in Cancer Risk Assessment


The research presented in this thesis was carried out at the Department of Theoretical Biology, Vrije Universiteit Amsterdam, The Netherlands, and was financially supported by the Netherlands Technology Foundation (STW) and DSM.

VRIJE UNIVERSITEIT

Mathematical Models in Cancer Risk Assessment

ACADEMISCH PROEFSCHRIFT

ter verkrijging van de graad van doctor aan
de Vrije Universiteit Amsterdam,
op gezag van de rector magnificus
prof.dr. T. Sminia,
in het openbaar te verdedigen
ten overstaan van de promotiecommissie
van de faculteit der Aard- en Levenswetenschappen
op dinsdag 9 december 2003 om 13.45 uur
in de aula van de universiteit,
De Boelelaan 1105

door

Ingeborg Minke Martine van Leeuwen

geboren te Voorburg

promotor: prof.dr. S.A.L.M. Kooijman

Aan mijn moeder

Thesis 2003-02 of the Institute of Ecological Science, Vrije Universiteit, Amsterdam, The Netherlands

Contents

Preface

In this **Preface** I give a brief overview of what I have done during the last four years. The primary aim of the work presented in this thesis was to get a quantitative grasp of the process of chemical carcinogenesis with aid of an innovative biologically-based modeling approach. This approach mainly concerned extensions of the Dynamic Energy Budget (DEB) theory to account for several aspects of tumor biology. From the terms DEB-theory and tumor biology, the code-name DEBtum was coined. But, how did I get involved in all this? Well, ...

The first time I knew about the DEBtum project was in October 1998. I was at the Department of Biochemistry and Molecular Biology in Granada, surfing the internet looking for information on protein docking. I ended up at a Russian web-site, where the only readable text was "*Department of Theoretical Biology, Vrije Universiteit, Amsterdam.*" Before I even noticed, I had already clicked on the link and saw a job vacancy "for a mathematician with interest in biology." Five months later I moved back to The Netherlands, which put an abrupt stop to a 21-year period in Spain.

My background is in Pure Mathematics (e.g., Differential Geometry) and Biochemistry (e.g., Protein Engineering). As I had experience with neither mathematical modeling nor cancer biology, I spent most of the first semester in Amsterdam reading about these compelling topics. Soon I became aware of some of the main problems in cancer risk assessment, such as low-dose extrapolation and interspecies extrapolation of risk estimates. Among others, these problems are succinctly discussed in **Chapter I**.

As one of the research objectives was to apply Bas Kooijman's DEB-theory in cancer biology, in the second semester I started to develop some simple DEB-based models to describe the relation between exposure to a chemical and tumor incidence. To facilitate the modeling process, I decided to split up the process of chemical carcinogenesis into 4 steps, namely kinetics, tumor induction, tumor growth and effects. Using this same scheme, I also compared the existing models for chemical carcinogenesis. This gave

rise to a first DEBtum-publication (**Chapter II**). The aim of this article was to provide, for the non-mathematician, a critical overview of models dealing with processes involved in chemical carcinogenesis. Most of the approaches discussed share the following two inconveniences: (*i*) the modeling effort is focused on a single step of the process of chemical carcinogenesis; and (*ii*) a tumor is viewed as an independent group of cells rather than as a part of a host organism.

While I was writing the review article, I programmed a computer tool to efficiently analyze the results of carcinogenicity tests. I extensively used this package to fit the classic models discussed in Chapter II to experimental data from RIVM, TNO and NTP[1] long-term studies. **Chapter III** deals with some of the results achieved during this data-analysis period and includes, in addition, the results of confronting some existing methodology with computer-simulated bioassays.

Once the review article was submitted for publication, I started to work on a new research topic: mathematical modeling of aging. The aging process influences the results of carcinogenicity studies in three ways: (*a*) the chance to develop a tumor depends on age; (*b*) in most carcinogenicity tests the presence of a tumor can only be detected after the death of the host organism. The time to death (aging-mediated, tumor-mediated or sacrifice) thus determines the observed time-to-tumor; and (*c*) the incidence of aging-mediated deaths affects the population size and, consequently, also the number of new cases of cancer.

I formulated a model for aging in which aging-related physiological decline is the result of the accumulation of oxidative damage caused by free radicals. However, when I fitted the new model to experimental data, I was not able to predict the relation between energy intake (food consumption) and life expectancy. It took a long time before I discovered that the problems came from the unexpected feeding behavior of laboratory rodents. Data on food consumption from RIVM and TNO revealed that rats and mice consume an almost constant amount of food during the study period. That is, from the age of one month, food consumption seems to be independent of body size. When I adapted the DEB-model to account for this observation, I succeeded in fitting caloric restriction data. The manuscript describing these results was rapidly accepted for publication (**Chapter IV**).

In the last phase of my research, I extended the DEB-based model to account for tumor growth. The aim was to arrive at a tumor growth model in which a tumor is part of its host organism. Because of the lack of adequate

[1] For the interpretation of the abbreviations, see page 169

tumor growth data, I first developed a general model for the differential growth of body parts. The tumor-growth model derived from the general model is suited to explore the implications of possible interactions between tumor and host. For instance, I investigated the influence of host age and caloric intake on tumor behavior. With regard to the effects of the tumor on the host, I focused on tumor-mediated loss of body weight. The results of these investigations, which have been submitted for publication, appear in this thesis as **Chapter V**.

Acknowledgements

I want to take this opportunity to thank the steering committee of the DEBtum project (Wil ten Berge, Louis Bloemen, Henk van Kranen, Coen van Kreyl, Jaap Krüse, Karel de Raat, Chris Mombers, Wout Slob, and Job van Zorge) for their warm support and helpful suggestions and discussions. I also wish to thank the reading committee (Wil ten Berge, Jaap Krüse, Jan Lankelma, Paul Lohman and Wout Slob) for subjecting this thesis to a critical examination. My thanks are also due to RIVM, TNO and VUMC for sharing their experimental data. I am grateful to the Netherlands Technology Foundation (STW) and DSM for financially supporting the DEBtum project.

I deeply appreciate that Bas Kooijman, my supervisor, afforded me the opportunity to carry out the research on which this thesis is based. It has been a great pleasure to work with Cor Zonneveld, who introduced me to writing scientific publications. I also wish to thank some special friends from Spain: Michele, Hilario, Bori, Eva, Khalid, y Miguel Angel, ¡no sé que hubiera hecho sin vuestro apoyo! I owe a special debt of gratitude to Bernd (p-d-p) who, ever-cheerful, helped me solve many technical problems. I am especially indebted to Wil ten Berge for initiating the DEBtum project. Without his tireless efforts and stimulating enthusiasm, this work could not have been done. Finally, I am also very grateful to many people who have taken the time to read and criticize parts of the manuscript with an expert eye. I thank them separately at the end of the corresponding chapters. Any remaining faults are all my own.

Ingeborg van Leeuwen

Amsterdam,
13th June 2003

I

CANCER RISK ASSESSMENT

> "*When it comes to assessing the impact of chemicals on human health, one has to peel the layers away carefully. We are at the intersection of science, medicine, politics, and law, with a strong flourish of human emotion thrown in to tangle the knot. The answers do not come easily,*" **R.A. Freeze**

Quantitative cancer risk assessment: historical perspectives, basic concepts, and current approaches and uncertainties

I.M.M. van Leeuwen (2003)

I.1 Introduction

In the year 2000, malignant tumors were responsible for 12% of the nearly 56 million deaths worldwide from all causes [214]. The World Cancer Report (2003) also reveals that the number of new cases of cancer is expected to grow by 50% over the next 20 years. Cancer is now globally emerging as a major health problem, but it is far from being a new disease.

Malignant tumors were described in pictures and writings from many ancient civilizations, including those of Asia, South America, and Egypt [221]. Moreover, paleopathological studies [64, 266] have recently led to the identification of several bone tumors in Egyptian mummies dating 1500-500 B.C. and of an adenocarcinoma in the mummy of Ferrante I of Aragón, King of Naples (1431-1494). Furthermore, as early as 400 B.C., Hippocrates compared the long, distended veins radiating from some breast tumors to the limbs of a crab, whence *karkinos* (*καρκινος*) in Greek and *cancer* in Latin [237].

Early cultures attributed the cause of cancer to various gods, and this belief was held generally until the Middle Ages [221]. Hippocrates described cancer as an imbalance between the black humor (from the spleen) and the three bodily humors: blood, phlegm, and bile [221]. Although incorrect this hypothesis was a big step forward, because it attributed the origin of cancer to natural causes. Since then, cancer has been associated with the natural process of aging [134, 201, 244] and with the action of several agents, including radiation [139, 257], viruses [25, 59], natural compounds [32, 261] and man-made chemicals [53, 174]. Table I.1 summarizes the major cancer risk factors.

The hypothesis that some chemicals can cause cancer is at least as old as Percival Pott's (1775) epidemiological study. This English physician observed that young men who had been chimney sweeps as boys had a high chance to develop scrotum cancer [191]. He suggested that chimney soot might be the causative agent. Since Pott identified this first putative car-

cinogenic agent, many chemicals have revealed to possess the ability to induce tumors (see Appendix). The effects such compounds may cause are shown in Table I.2. Nowadays, it has become mandatory to evaluate the carcinogenic potency of chemical compounds before they are manufactured. Such evaluations are intended to ensure that carcinogenic chemicals are either not marketed or withdrawn from use.

Table I.1: The major cancer risk factors [214].

Tobacco smoking	Radiations
Alcohol drinking	Chronic infections
Occupational exposures	Diet & nutrition
Environmental pollution	Immunosuppression
Food contaminants	Genetic susceptibility
Medicinal drugs	Reproductive factors & hormones

Table I.2: Effects carcinogenic agents may cause.

Appearance of unusual tumors
Increase in the occurrence of normal tumors
Appearance of tumors earlier in life
Increased tumor multiplicity

I.2 Regulation and control of cancer risks

The evaluation of the toxicity and carcinogenicity of chemical compounds is carried out world-wide according to guidelines proposed by regulatory institutions (e.g., OECD, IARC, EU, USEPA). For a new chemical, risk assessment involves the following steps:

- *Occupational hazard identification*: evaluation of the hazardous effect of chemical substances on workers exposed due to their work conditions.
- *Ecotoxicological risk assessment:* concerns the fate of chemical substances in the environment and their biological effects on organisms.
- *Human risk assessment:* evaluation of the hazardous effect of chemical substances on the health of the human population. In the EU, new chemicals are investigated according to a tonnage-triggered strategy (see Table I.3). The specific tests (e.g., genotoxicity tests chosen)

vary for pesticides, cosmetics, packing materials, food/feed additives, drugs and veterinary drugs. As can be seen from Table I.3, long-term carcinogenicity tests are mandatory for chemicals with an annual production that exceeds 1,000 ton.

Table I.3: Human-tox tests, according to the EU regulations (J. van Benthem, personal communication). kpa = kilograms per year; tpa = ton per year; CA = chromosomal aberrations; LD_{50} = 50% lethal dose.

Toxicological test	$10–10^2$ kpa	$10^2–10^3$ kpa	1–10 tpa	$10–10^2$ tpa	$10^2–10^3$ tpa	$> 10^3$ tpa
LD_{50} (1 route)	X	X	X	X	X	X
Skin irritation		X	X	X	X	X
Eye irritation		X	X	X	X	X
Skin sensibilization		X	X	X	X	X
Mutagenicity (Ames test)			X	X	X	X
LD_{50} (2 routes)			X	X	X	X
Sub-acute tox (oral)			X	X	X	X
Mutagenicity (CA)			X	X	X	X
Additional mutagenicity			(X)	X	X	X
Fertility				(X)	X	X
Teratogenicity				(X)	X	X
Semi-chronic tox				(X)	X	X
Toxico-kinetics					X	X
Chronic tox					(X)	X
Long-term carcinogenicity						X
Fertility (2nd species)						(X)
Teratogenicity (2nd species)						(X)

Carcinogen risk assessment has been defined as "a scientific attempt to identify and estimate the true cancer risk associated with exposure to chemical agents [238]." The process of carcinogen risk assessment is usually divided into four steps [9, 54, 238].

1. *Hazard identification:* Qualitative identification of the carcinogenic effect a substance has an inherent capacity to cause. It relies on animal data, human data, and supporting data (e.g., pharmacokinetic information and structure-activity relationships). Using these data, chemicals are classified according to the available evidence of carcinogenicity. There is no unanimity about how to classify. Three proposed classification schemes are summarized in Table I.4.

2. *Dose-response assessment:* Estimation of the relationship between dose of, or level of exposure to, a substance and the incidence and severity of the carcinogenic effect (see Table I.2). Incidence concerns the number of new cases occurring. It can, for instance, be expressed as the number of new cases per time unit divided by the population size.

3. *Exposure assessment:* Determination of the emissions, pathways and rates of movement of a substance and its transformation or degradation, in order to estimate concentrations/doses to which human populations or environmental spheres (water, soil and air) are or may be exposed.

4. *Risk characterization:* Estimation of the incidence and severity of the carcinogenic effects likely to occur in a human population due to actual or predicted exposure to a substance.

More than 100,000 chemicals are in commercial use and an estimated 2,000 new ones are introduced annually[1]. As quantitative risk assessment (QRA) of exposure to each of these compounds would be an almost impossible task [84], risk assessment is concerned with setting priorities. This is exemplified by the EU tonnage-triggered strategy shown in Table I.3. Another example is the use of structurally related compounds as reference substances for predicting risks. The USEPA has used the classification in categories A, B or C (Table I.4) as a requisite for entering QRA. As a consequence of setting priorities, only a small percentage of the chemicals in commercial use have been fully tested for their effects on human health [65]. From the perspective of human health, it is desirable that among the few fully tested chemicals are those most likely to be carcinogenic.

[1] Information from [84] and the NTP web-site: `http://ntp-server.niehs.nih.gov/` Downloaded 11 June 2003; Site updated 15 November 2002.

Table I.4: Classification schemes for carcinogens.

Classification of carcinogens according to the USEPA (1986)	
Category A	Known human carcinogen. Proven human carcinogenic substance (see Table I.5 for a list of the substances classified in this category).
Category B1	Probable human carcinogen. Suspected human carcinogenic substance of potential relevance to humans.
Category B2	Probable human carcinogen. Proven animal carcinogenic substance of potential relevance to humans.
Category C	Possible human carcinogen. Suspected animal carcinogenic substance of potential relevance to humans.
Category D	Not classifiable as to human carcinogenicity. Substances not-classifiable with regard to carcinogenicity.
Category E	Evidence of non-carcinogenicity for humans. Negative evidence.
Classification of carcinogens according to the IARC (1987)	
Group 1	Carcinogenic to humans. Sufficient evidence of carcinogenicity in humans.
Group 2A	Probably carcinogenic to humans. Limited evidence in humans and less than sufficient evidence in animals.
Group 2B	Possibly carcinogenic to humans. Limited evidence in humans and no sufficient evidence in animals; or inadequate/non-existent evidence in humans and sufficient evidence in animals.
Group 3	Not classifiable. Agents that are not categorized in any other group.
Group 4	Probably not carcinogenic to humans. Evidence suggesting no carcinogenicity in humans or inadequate data; evidence suggesting no carcinogenicity in animals.
Classification of carcinogens according to the EU (2002)	
Category I	Human carcinogen.
Category II	Probable human carcinogen.
Category IIIA	Insufficient evidence to put in category II, but additional data is unlikely to help.
Category IIIB	Insufficient evidence to put in category II, but additional data is needed.

I.3 Long-term carcinogenicity tests

Carcinogen risk assessment is usually carried out on the basis of long-term rodent bioassays. In such bioassays, test animals are organized in dose-groups that are exposed to different levels of the chemical of interest. Besides the exposed animals, a control group of untreated animals is always included. To mimic lifetime exposure of humans, the animals are exposed chronically for a period of 2 years. To ensure statistically significant tumor incidences, a reasonable number of animals and adequate dose levels are used.

This thesis pays special attention to the long-term carcinogenicity tests carried out by the US National Toxicology Program (NTP). The NTP was established in 1978 by the Department of Health and Human Services (DHHS, USA) to coordinate toxicological testing programs within the Department. Since its foundation, the NTP has evaluated the carcinogenic potency of more than 400 chemicals in rat and mice. The experimental results from these NTP carcinogenicity studies are publicly available from the NTP-server via the internet[2]. Throughout this thesis, data from the NTP long-term carcinogenicity study with 1,3-butadiene will be repeatedly used as an example (Section III.2.1). Our interest for this particular study primarily relies on the relevance of the carcinogenic chemical and on the relatively large number of exposure levels described (6 dose-groups, including control).

The end-points of carcinogenicity studies are primarily pre-neoplastic lesions and neoplasms, but sometimes also include degree of malignancy, time to tumor appearance, multiplicity of (pre-)neoplasia, and occurrence of metastases [58]. "Negative results, in which animals do not have a greater incidence of neoplasia than control animals, do not necessarily mean that a chemical is not a carcinogen, inasmuch as the experiments are conducted under a limited set of conditions. Positive results demonstrate that a chemical is carcinogenic for laboratory animals under the conditions of the study and indicate that exposure to the chemical has the potential for hazard to humans [174]."

Figure I.1 illustrates the two manners in which the results of long-term carcinogenicity tests are often summarized. The upper panel depicts, for each dose-group, the adjusted cumulative incidence (ACI) of deaths with malignant lymphoma as a function of exposure time. The ACI at time t concerns an estimation of the probability that, in absence of competing

[2] `http://ehp.niehs.nih.gov/ntp/docs/ntp.html`
Downloaded 11 June 2003; Site updated 23 May 2003.

causes of death, an animal dies bearing a lymphoma before time t. The lower panel shows the eventual ACI at the end of the exposure period (2 years) as a function of dose. Notice that in the lower panel the information on the time course of tumor occurrence is lost.

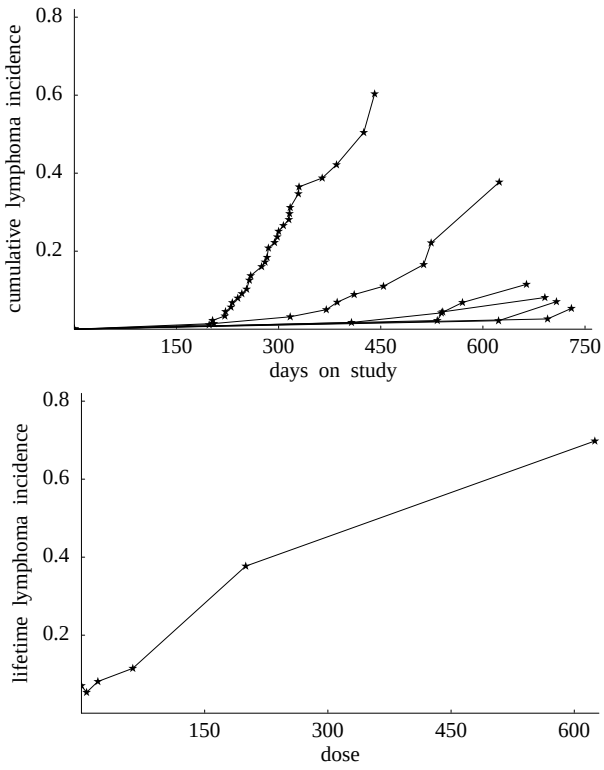

Figure I.1: Cumulative incidence of spontaneous deaths with malignant lymphoma in female mice exposed to 1,3-butadiene. Kaplan-Meier adjusted tumor-bearing fractions. For further information, see Chapter III. Data from the BUT-NTP study (Section III.2.1). *Upper panel:* Cumulative incidence as a function of exposure time. For curves from right to left, the administered 1,3-butadiene dose is 0, 6.25, 20, 62.5, 200 and 625 ppm, respectively. Data points ($\star$) have been joined to distinguish the 6 dose-groups. *Lower panel:* Cumulative incidence after a 2-year (730 days) exposure period as a function of the level of exposure.

I.4 Estimates of the carcinogenic potency

Several types of quantitative information on cancer risk can help decision-makers. Examples are:

- *NOAEL:* No observed adverse-effect level. Exposure level at which there are no statistically significant increases in the frequency or severity of the observed carcinogenic effect between the exposed and control populations [52].
- *ADI & TDI:* Acceptable daily intake & tolerable daily intake. Both concepts concern estimates of a dose without appreciable increase in human risk. ADIs relate to chemicals that have been deliberately added to a product, whereas TDIs concern contaminants whose presence in food or water does not serve, and has never served, any useful purpose. The ADI (or TDI) of a chemical is usually calculated by dividing the animal-derived NOAEL by an uncertainty factor (also called assessment factor or safety factor), which has a default value of 100 [54].
- *MTD:* Maximum tolerated dose. The default MTD is the dose that causes 10% decrement in body growth in the absence of other toxic manifestations.
- TD_{50}: Tumorigenic 50% dose. Dose that, if administered chronically for the standard lifespan of the species, halves the probability of remaining tumorless through that period. Or equivalently, the daily dose that will induce tumors in half of the animals that would have remained tumor-free at zero dose [69].
- *VSD:* Virtually safe dose. Dose with a negligible increase in human risk, such as 10^{-5} or 10^{-6} in a lifetime. It is generally calculated by linear low-dose extrapolation (see Section I.5.4).

The NOAEL is an experimental end-point, as it corresponds to the highest dose that does not cause any observable carcinogenic effect. It is, therefore, very sensitive to the experimental set up and may lead to serious underestimation of the carcinogenic potency of a chemical. The TD_{50} and VSD instead involve non-observed exposure levels and, therefore, entail assumptions on the behavior of the dose-response curve. To extrapolate or interpolate responses from the observed dose-response data, mathematical models can be used. The extrapolation of responses below the lowest experimental dose and the derivation of VSDs are the main topics of Section I.5.4.

I.5 Uncertainties in carcinogen risk assessment

Vinyl chloride [53] and soot [191] have revealed to be carcinogenic first in humans and later in animals. Obviously this is not a preferred sequence of events, although the availability of epidemiological data significantly facilitates the estimation of the carcinogenic potency of a chemical in humans. When animal studies are used for risk assessment, the relationship between dose and response is first established in animals and, thereafter, the risk for human health associated with the human exposure level is calculated. During this process, investigators usually encounter one or more of the difficulties discussed in this Section.

Figure I.2: Skull of a skeleton with burning cigarette, 1886. Vincent van Gogh (1853–1890). Oil on Canvas, 32 x 24.5 cm. Van Gogh Museum, Amsterdam. About one-third of all cancer cases in Europe and North America can be related to the presence of carcinogens in cigarettes and other tobacco products [8, 214].

I.5.1 Exposure to chemical mixtures

Many human cancers can be related to exposures to chemical mixtures. The best known example of a complex carcinogenic mixture is tobacco smoke (Figure I.2). Diet and air pollution are other examples of chemical mixtures that have been associated with an increase in cancer incidence (see

Table I.1). Despite the multifactorial origin of most tumors, environmental exposures are usually studied individually. That is, long-term carcinogenicity tests are carried out with a single chemical compound. To estimate the risk associated with the joint action of several agents, multiplicative or additive effects have been assumed [22, 114].

I.5.2 Intraspecies variability

Significant differences in response to a carcinogenic agent can be observed among different individuals of the same species. Genetic and non-genetic aspects underly this intraspecies variability. The relevance of the former aspects is best exemplified by the existence of heritable genetic disorders that predispose to cancer. Genetic variation can lead to different levels of expression of enzymes involved, for instance, in DNA repair or in activation and detoxication pathways. Gender-related variability in carcinogenic response can be attributed to both endocrine and non-endocrine differences (e.g., Figure I.3). Among the non-genetic aspects involved in intraspecies variability are nutrition, which may influence bioavailability and bioaccumulation, and health status [52].

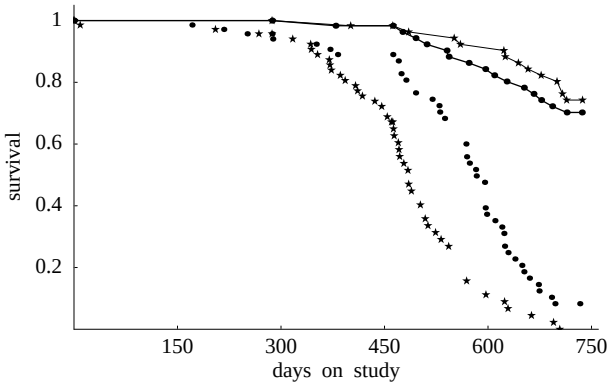

Figure I.3: Survival of mice exposed to 0 and 200 ppm 1,3-butadiene. Kaplan-Meier adjusted survivor-fractions: ($\star$) female and ($\bullet$) male mice. The joined data points correspond to the control-groups. Data from the BUT-NTP study (Section III.2.1). The same external dose of carcinogen causes a sharper decrease in female than in male survival. This gender-related variability may be due, for instance, to differences in effective internal concentration or to differences in the harmful effect caused by this concentration.

Carcinogenesis is usually treated as a stochastic process in which mutations and cell proliferation occur with a certain probability. The observed time-dependent tumor incidence (e.g., Figure I.1) is the result of the intraspecies variability in carcinogenic response, the experimental error, and the stochastic component of the carcinogenic process itself [210]. As can be seen from Chapter II, most mathematical models for chemical carcinogenesis assume implicitly that tumor incidence data can be explained by its stochastic component alone. Indeed, only the so-called tolerance distribution models (Section II.3.2.1) are based on differences in individual susceptibility.

I.5.3 The 'mouse-to-man' problem

The prediction of human responses from animal data is a major issue in quantitative cancer risk assessment. As the species used for carcinogenicity studies is often the mouse, this is known as the mouse-to-man problem. It concerns interspecies scaling of physiological parameters and characteristics, but often also implies extrapolations across routes of exposure, exposure times, and tumor induction mechanisms.

I.5.3.1 Interspecies variability

Variability in the response of different species to a certain chemical compound can, for instance, occur because of differences in uptake, distribution, accumulation, metabolism, excretion or target sensitivity [52]. The most common explanation is that interspecies differences in susceptibility reflect different levels of enzymes that activate or deactivate the putative carcinogen [108]. Examples of compounds that differ significantly in their carcinogenic potency among species are:

- *Aflatoxins* (CAS 1402-68-2, see Table I.5): induces hepatocellular carcinomas in rats, but not in adult mice [151, 175].
- *2-Fluorenylacetamide* (CAS 53-96-3): a very potent carcinogen in one strain of rats; not a carcinogen in another strain [151].
- *Dimethylbenzanthracene* (CAS 57-97-6): produces breast cancers in Sprague-Dawley rats, but not in Wistar rats [108].
- *2-Naphthylamine* (CAS 91-59-8, see Table I.5): much more carcinogenic in humans and dogs than in rats [52].
- *Sulfamethazine* (CAS 57-68-1): induces thyroid follicular cell tumors in rats and mice, but lacks any tumorigenic effect in monkeys [52].

Because of the occurrence of interspecies variability, the extrapolation of tumor incidence information from animal studies to humans must be handled with caution.

I.5.3.2 Interspecies extrapolation

Leaving out of account some chemicals that revealed an extreme divergence in carcinogenic potency among species (see examples above), it has been suggested that "there are good interspecies correlations between the potencies, allowing interspecies extrapolation [40]." Several methods have been proposed to extrapolate physiological characteristics and carcinogenic potencies, the default technique being allometric scaling.

The allometric equation [98] expresses the parameter of interest μ (e.g., TD_{50}) as a power of body weight: $\mu = aW^b$, where W denotes body weight. In a double logarithmic plot, the relation becomes linear: $\log \mu = \log a + b \log W$. It is assumed that the value of b is equal for a wide range of species and chemical compounds, whereas the value of a varies for different chemicals. For a given chemical agent, the value of the parameter μ for humans (μ_h) can then be obtained as follows:

$$\mu_h = \mu_r \left(\frac{W_h}{W_r} \right)^b \tag{I.1}$$

where μ_r is the known value of the same parameter in, for example, a rodent species. The human value μ_h is thus calculated simply by multiplying μ_r by the so-called relative sensitivity factor $(W_h/W_r)^b$, where the symbols W_h and W_r represent the average human and rodent body weights, respectively. Different values for the scaling factor b have been used. Among the most common ones are [42, 49, 231]: (*i*) the body-weight scaling factor, $b = 1$; (*ii*) the body-surface area scaling factor, $b = 2/3$; and (*iii*) Kleiber's scaling factor, $b = 3/4$.

Frequently only the measure of the carcinogenic potency is extrapolated from animals to humans. The use of allometric scaling is then not warranted, however. A carcinogenic potency estimate (e.g., TD_{50}) is a complex quantity that depends on an unknown number of physiological factors as well as on other factors as the exposure time. The choice of one or another scaling factor is thus hard to defend. Alternatively, using a mathematical model for chemical carcinogenesis, such as those discussed in Chapter II, the whole dose-response relationship can be extrapolated. In PBPK models (Section II.3.1), as the parameters have a biological interpretation, the values of the kinetic parameters for rodents may be substituted by values

relevant to humans [10, 154]. For models whose parameters have a less direct empirical link, scaling rules must be defined for the set of model parameters [177, 115]. An important condition for this approach is that scaling relations for different parameters should be compatible with each other. For instance, if two parameters that scale allometrically are proportional, they share the same scaling factor. Moreover, concerning allometric scaling, it is also important to notice that in general a sum of power functions is not a power function. Indeed, if $\mu_1 = a_1 W^{b_1}$ and $\mu_2 = a_2 W^{b_2}$ with $b_1 \neq b_2$, then the parameter $\mu_1 + \mu_2$ does not scale allometrically. Compatible allometric and non-allometric scaling rules are, for example, derived in [115].

I.5.4 Low-dose extrapolation

Besides deducing human carcinogenic responses from animal data, a fundamental problem in risk assessment is the evaluation of the risk associated with the levels to which humans are actually exposed. For practical reasons, such as improving the signal-to-noise ratio and reducing the number of animals required [221, 238], long-term carcinogenicity tests are generally performed using relatively high doses. Consequently, the behavior of the dose-response curve at levels of exposure below the lowest experimental dose is unknown.

The simplest low-dose extrapolation method consists in drawing a straight line from a point of departure to the origin (zero dose, zero additional risk). Possible departure points are, for instance, (LOAEL[3], corresponding additional risk) or (TD_{50}, 0.5). The USEPA uses (LED_{10}, 0.1) as default point of departure, where LED_{10} is the lower 95% confidence limit on a dose that is estimated to cause a 10% increase in tumor incidence [234]. Alternatively, a mathematical model can be used to predict the carcinogenic response in the non-observed low-dose region. It has been shown, however, that different mathematical models can differ significantly in their risk predictions at low doses [54]. Currently, the model most frequently used to carry out low-dose extrapolations is:

$$P(d) = 1 - \mathrm{e}^{-q_0 - q_1 d} \tag{I.2}$$

where $P(d)$ is the probability that an individual exposed to a dose d for its lifetime develops a tumor. As will be explained in Chapter II, this expression can be deduced from the one-hit model (Section II.3.2.3) as well as from the LMS-model (Section II.3.2.4). After fitting the experimental observations, linear low-dose extrapolation is done on the basis of a line with

[3]Lowest observed adverse effect level

slope α, where α is either an estimate of the q_1 parameter or the 95% upper confidence limit of this estimate (for further details, see Figure I.4).

The linear low-dose extrapolation method is used if a linear relationship between dose and response seems reliable for the chemical of interest. This kind of relationship implies that the risk associated with a dose unit is independent of the exposure level. Deviations from this relationship may occur if the mechanism by which an agent induces cancer at high doses is not operative at lower doses [238]. Ames and Gold (1990), for instance, argued that mutagenic carcinogens administered at high doses (e.g., MTD) also stimulate cell proliferation, which enhances tumorigenesis. Moreover, it has been observed that, at low doses of carcinogen, not only the risk per dose unit decreases, but also the time delay until tumor appearance becomes longer [71, 229]. In toxicological tests, with non-carcinogenic end-points, dose-response curves sometimes present an U-shaped behavior (hormesis). This observation led to the hypothesis that, for certain chemical agents, low doses may have a beneficial effect whereas exposure to either a too low or a too high dose may have adverse effects.

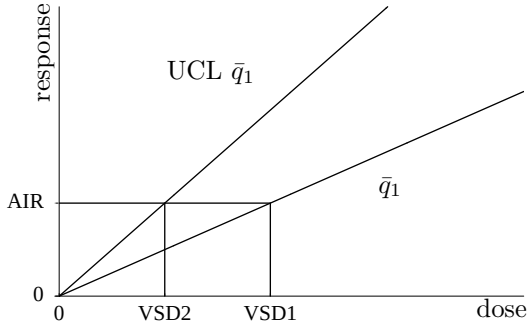

Figure I.4: Low-dose extrapolation is required, for instance, to calculate the virtually safe dose (VSD) associated with a certain acceptable increase in risk (AIR). For genotoxic carcinogens, VSDs are often obtained by linear low-dose extrapolation using equation I.2. VSD1 = virtually safe dose calculated using a straight line with the estimated value $\bar{q}_1$ as slope. VSD2 = virtually safe dose calculated using a line with the 95% upper confidence limit (UCL) of this estimated value as slope. The VSD depends on the slope of the extrapolation line; the larger the slope, the smaller the corresponding VSD.

The shape of the dose-response at low doses is strongly influenced by the presence or absence of dose thresholds. According to the threshold hypoth-

esis "there is a no-effect dose of carcinogen below which induction of cancer cannot occur or occurs with an extremely low probability [151]." The concept of threshold-dose relies on the argument that a single or just a few molecules do not suffice to induce a carcinogenic response. For instance, as long as the amount of carcinogenic compound does not overwhelm defense mechanisms (e.g., detoxication and DNA repair), no response is expected. As thresholds give rise to 'hockey-stick shaped' dose-response curves, the tumor probability may be lower than expected from linear extrapolation. Assuming the existence of a threshold-dose may thus have great impact on the eventual risk estimate.

It has been proposed that carcinogens that act without directly causing DNA damage (non-genotoxic agents) do have a dose threshold, whereas carcinogens that modify the genetic code (genotoxic agents) do not. Therefore, use of the linear low-dose extrapolation method is usually restricted to genotoxic carcinogens, whereas the ADI/TDI approach (Section I.4) is usually used only for non-genotoxic carcinogens. On the basis of the stochastic nature of mutagenesis, it has been argued that a single molecule of a genotoxic agent might cause a DNA mutation leading to malignant transformation. In contrast, a certain concentration of non-genotoxic agent might be required to interfere with processes under homeostatic control. For instance, it seems hard to believe that a single molecule of non-genotoxic agent could suffice to trigger cell proliferation by disturbing cell-cell communication. The mechanistic distinction between two types of carcinogens has been criticized, however. For instance, Waters *et al.* (1999) argued that many chemical carcinogens operate via a combination of both modes of action.

As the behavior of the dose-response curve at low doses is unknown, there is no direct experimental evidence for or against the threshold hypothesis. In the 1970's, Littlefield's group sought to figure out what happens at low levels of 2-acetylaminofluorene (CAS 53-96-3). For this purpose, they exposed more than 24,000 mice to seven different levels of carcinogen [140]. The conclusion from this mega-mouse study was that it is impossible to distinguish between linear and non-linear dose-response curves even when a large number of animals is used.

Acknowledgements

The author thanks Jan van Benthem, Wil ten Berge and Wout Slob for their advice.

Appendix

Table I.5: Agents, substances, mixtures, and medical treatments that have been classified as known human carcinogens [175]. The second column indicates when first included in Category A (See Table I.4)

CAS	Listed	Name or Synonym
1402-68-2	1980	Aflatoxins
	2000	Alcohol beverage consumption
92-67-1	1980	4-Aminodiphenyl
	1985	Analgesic mixtures containing Phenacetin
	1980	Arsenic compounds, inorganic
1332-21-4	1980	Asbestos
446-86-6	1985	Azathioprine
71-43-2	1980	Benzene
92-87-5	1980	Benzidine
	2002	Beryllium and beryllium compounds
542-88-1	1980	Bis(chloromethyl)ether
55-98-1	1985	Busulfan (1,4-butanediol dimethylsulfonate)
106-99-0	2000	1,3-Butadiene
7440-43-9	2000	Cadmium
10108-64-2	2000	Cadmium chloride
1306-19-0	2000	Cadmium oxide
10124-36-4	2000	Cadmium sulfate
1306-23-6	2000	Cadmium sulfide
305-03-3	1981	Chlorambucil
107-30-2	1980	Chloromethyl methyl ether
	1980	Chromium hexavalent compounds
8007-45-2	1980	Coal tar
	1980	Coke oven emissions
8001-58-9	1985	Creosote (coal)
8021-39-4	1985	Creosote (wood)
14464-46-1	2000	Cristobalite
50-18-0	1980	Cyclophosphamide
59865-13-3	1998	Cyclosporin A
56-53-1	1980	Diethylstilbestrol
1937-37-7	2000	Direct black 38
2602-46-2	2000	Direct blue 6
	2000	Dyes that metabolize to Benzidine
	2000	Environmental tobacco smoke
66733-21-9	1980	Erionite
	2002	Estrogens, steroidal
75-21-8	2000	Ethylene oxide
775897-97-6	1980	Lead chromate

continued on next page

continued from previous page

CAS	Listed	Name or Synonym
13909-09-6	1991	MeCCNU
148-82-3	1980	Melphalan
298-81-7	1985	Methoxsalen with ultraviolet A therapy
	1980	Mineral oils
505-60-2	1980	Mustard gas
91-59-8	1980	2-Naphthylamine (2-aminonaphtalene)
	2002	Nickel compounds
7280-37-7	1985	Piperazine estrone sulfate
14808-60-7	2000	Quartz, cristalline (respirable size)
10043-92-2	1994	Radon
	2000	Silica, cristalline (respirable size)
	2000	Smokeless tobacco
16680-47-0	1985	Sodium equilin sulfate
438-67-5	1989	Sodium estrone sulfate
	2000	Solar radiation, sun-lamps, sun-beds
	1980	Soots
	2000	Strong inorganic acid mists containing sulfuric acid
7789-06-2	1980	Strontium chromate
	2000	Tamoxifen
	1980	Tars
1746-01-6	2001	TCDD
52-24-4	1998	Thiotepa (tris(1-aziridinyl)phosphine sulfide)
1314-20-1	1981	Thorium dioxide
	2000	Tobacco smoking
15468-32-2	2000	Tridymite, cristalline (respirable size)
	2002	Ultraviolet radiation, broad spectrum UV radiation
75-01-4	1980	Vinyl chloride
	2002	Wood dust
13530-65-9	1980	Zinc chromate

II

MODELING CHEMICAL CARCINOGENESIS

> "*A statement that is frequently heard from people with a distaste for models is:* 'a model is not more than you put into it.' *Done in the proper way, this is absolutely right and it is the single most important aspect of the use of models,*" **S.A.L.M. Kooijman**

From exposure to effect: a comparison of modeling approaches to chemical carcinogenesis

Adapted from:
I.M.M. van Leeuwen and C. Zonneveld (2001)
Mutation Research, 489(1): 17–45

Abstract
Standardized long-term carcinogenicity tests aim to reveal the relationship between exposure to a chemical and occurrence of a carcinogenic response. The analysis of such tests may be facilitated by the use of mathematical models. To what extent current models actually achieve this purpose is difficult to evaluate. Various aspects of chemically induced carcinogenesis are treated by different modeling approaches, which proceed very much in isolation of each other. With this Chapter we aim to provide for the non-mathematician a comprehensive and critical overview of models dealing with processes involved in chemical carcinogenesis. We cover the entire process of carcinogenesis, from exposure to effect. We succinctly summarize the biology underlying the models and emphasize the relationship between model assumptions and model formulations. The use of mathematics is restricted as far as possible with some additional information relegated to tables.
Keywords
Quantitative cancer risk assessment; Tumor incidence; Chemical carcinogen; Mathematical model; Dose-response relationship.

II.1 Introduction

Despite improvements in prevention, diagnosis and treatment, cancer still strikes one in three people, and one in four will eventually die of the disease [197]. This high incidence is primarily due to two risk factors, namely cigarette smoking [143, 184] and dietary habits [67]. As these concern lifestyle aspects which are in principle subject to personal choice, they can be avoided at the individual level. This does not hold for other risk factors, such as exposure to occupational or environmental agents. These factors

constitute an unintentional risk that can only be avoided through decisions made at the community level.

Since Pott (1775) conducted his historical study on chimney sweeps and identified soot as a carcinogenic agent, extensive testimony has accumulated with regard to the causal relationship between cancer incidence and exposure to chemical compounds. Evidence that chemicals may cause cancer has come, for instance, from experimental tests and epidemiological studies. Nowadays, the carcinogenic effect of a compound is crucial to restrictions on either its production or its emission into the environment. The success of these restrictions might explain the assertion by Ames *et al.* (1997) that food additives and industrial chemicals have had little impact on the overall cancer incidence to date.

Primary prevention of cancer can be accomplished by reducing the number of carcinogens to which humans are exposed, and by reducing the levels of exposure to carcinogens [229]. Clearly, these approaches rely on accurate identification of carcinogens and on reliable quantification of their ability to elicit a carcinogenic response. Both hinge on the adequacy of the tests devised to estimate the carcinogenic potency of chemicals, and on the validity of the conclusions derived from them. These issues are far from settled as the often fierce debates about them illustrate. For two different reasons, society needs a strategy to accurately evaluate the implications of carcinogenicity tests for humans. From the perspective of human health, such a strategy is essential to rule out risk-underestimates. From an economic point of view, the avoidance of risk-overestimates averts costs associated with unnecessary reduction of exposure levels.

The various tests devised to estimate carcinogenic potency differ in many aspects, but they share a common feature: the analysis of their results is facilitated by the establishment of a functional relationship between dose and response [124]. The plethora of mathematical models used for this purpose may at times be disconcerting to experimental scientists. Some modelers have attempted to conciliate experimentalists with the models. Hanes and Wedel (1985), for example, purport to "remove for the nonmathematician some of the mystery as to the derivation of the formulas." Even if they accomplished this aim, they still only consider a small subset of models that are currently in vogue. Other reviews are subject to similar restrictions in scope. For instance, Van Ryzin (1980) only deals with dose-response models for risk assessment, while Kopp-Schneider (1997) focuses on multistep models of tumor induction. None of these works covers the entire area from exposure to effect. The most thorough overview of models involved in the estimation of human cancer risk is by Moolgavkar *et al.* (1999). Due

to its in-depth treatment of the topic, this book is less suited as a gentle introduction to the field. In summary, we think that a general but succinct overview for the non-mathematician is still lacking. The aim of the present work is to provide such an overview.

The remainder of this Chapter is organized as follows. Section II.2 provides a brief description of the biology of chemical carcinogenesis as a four-phase process. We realize that the informed reader will miss many important findings. Their omission derives from the fact that these new findings are not yet used by modelers; we only present a skeletal outline of chemical carcinogenesis relevant for our overview. Section II.3 discusses a representative selection of mathematical models for chemical carcinogenesis, organized according to the phases defined in Section II.2. In our experience, existing explications of the models are either hard to find or hard to follow. Therefore, we aim to make explicit the relationship between model assumptions and model formulations. Finally, in Section II.4, we make some concluding remarks that go beyond the individual models. Although in this Chapter we focus on the conceptual basis of the various models, we cannot always ignore mathematical formulations. Where these become cumbersome, they are confined to tables. The reader not interested in the mathematical niceties may skip these tables without loosing continuity.

In this Chapter we compare some 30 representative modeling approaches. Understandably but regrettably, they do not share a common strategy with respect to their mathematical notation. Different models may therefore use the same symbol for unrelated concepts or variables. To minimize confusion related to the notation, we were forced at times to choose a representation that deviates from the customary. In the few instances where we used the same symbol for different concepts, the context should suffice to disambiguate its interpretation.

II.2 Chemical carcinogenesis

Theoretical studies on tumor biology are far outnumbered by experimental studies. Yet models still abound: for this review, we studied some 100 papers on a variety of models, as well as some monographs. To keep track of all these studies, a natural first step is to contrive some classification. ECETOC's Monograph no. 24 (1996) classifies models for chemical carcinogenesis loosely on the basis of their underlying statistical assumptions [54]. But as the authors remark themselves, "The division between the models is somewhat arbitrary as there is considerable overlap." An alternative criterion classifies

models as either descriptive or mechanistic. This criterion judges the amount of underlying biology involved. From a mathematical point of view, models can be classified as either deterministic (with a single outcome) or stochastic (with more than one possible outcome). Kopp-Schneider (1997) classifies stochastic models for tumor induction on the basis of their intended use, level of biological detail and method used for their analysis. As the method of analysis has only to do with the degree of mathematical complexity, we do not find this criterion very informative.

As an alternative we organize models according to a division of the process of chemical carcinogenesis, from exposure to effect, into four consecutive phases. We briefly define the phases here, while in the subsections below we provide further details. The first phase, referred to as *kinetics*, concerns the relationship between exposure to a (pro)carcinogen and internal dose of carcinogen. The second phase, referred to as *tumor induction*, comprises the toxico-dynamic mechanisms through which the carcinogen induces the transformation of normal cells into tumor cells. The third phase, referred to as *tumor growth*, relates to the clonal expansion of a tumor. During this phase, the tumor's malignancy may increase (tumor progression). The last phase, referred to as *effects*, involves the consequences of tumor development for the organism.

Not all the models discussed in this Chapter have been developed with the aim to contribute to a quantitative understanding of chemical carcinogenesis. For instance, most tumor growth models have been developed with the aim to improve cancer treatment, and have not yet been applied within the context of chemical carcinogenesis. Nevertheless, tumor growth models naturally fit the scheme outlined above because it is only after a tumor reaches a certain size that effects will become apparent. Many other models unambiguously address one of the steps defined above. Hence the classification seems to offer a framework to keep track of the heterogeneous collection of models dealing with aspects of chemical carcinogenesis in its broadest sense.

II.2.1 Exposure and kinetics

As defined above, kinetics concerns the relationship between the exposure of an animal to a (pro)carcinogen and the internal dose of carcinogen at a target tissue. Here we use 'exposure' in a general sense that includes the exposure conditions. Kinetics constitutes an essential phase in chemical carcinogenesis because it is the tissue dose that is responsible for the carcinogenic response. For foreign chemicals, kinetics comprises four biolog-

ical processes, namely uptake, distribution, metabolic transformation, and elimination of the chemical compound.

Uptake consists of two subprocesses: intake and absorption. The result of intake is that the chemical enters either the lung cavity or the gastrointestinal tract. The intake rate depends on the exposure conditions and on the physiology of the animal. For instance, if administration of the chemical is via food, the concentration of the chemical in food and the food ingestion rate determine the intake rate. Intake is bypassed when the chemical is administered directly into the stomach (gavage). Furthermore, intake is absent when the chemical is applied directly on the skin.

Once the chemical is in a body cavity or on the skin, absorption may take place. The result of absorption is that the chemical actually enters the body. Chemicals administered via injections bypass both intake and absorption. There are two major absorption mechanisms, namely passive diffusion and carrier-mediated transport. The latter mechanism is saturable, whereas the former is not. The actual absorption rate, in contrast to the intake rate, depends on physico-chemical properties of the chemical, such as charge and molecular structure [194, 226]. As it also depends on characteristics of the tissue involved (e.g., absorption surface-area), the uptake route is important for the absorption rate. For instance, absorption from the lungs is usually rapid.

Distribution involves partitioning of the chemical among different body parts. It starts from the site where the chemical enters the body. Chemicals absorbed from the gastrointestinal tract first pass through the liver, whereas chemicals absorbed from the lungs directly enter the bloodstream. Consequently, uptake via the lungs usually results in a quick distribution among major organs [226]. Indeed, the site of entry is important for both the distribution rate and the final disposition of the chemical. Distribution of the chemical out of the bloodstream into the target tissues depends on physico-chemical properties of the chemical (e.g., lipophilicity) and on the relative characteristics of the tissues (e.g., relative size and lipid content). As the characteristics of the tissues vary with age, the same holds for partitioning among body parts [240].

Living organisms have a wide range of enzymatic defense mechanisms against toxic compounds. The enzymes involved usually convert lipophilic chemicals into more hydrophilic and, therefore, easier excretable metabolites. Environmental and occupational (pro)carcinogens are also subject to enzymatic transformation [76, 157]. Metabolism of a carcinogen can give rise to transformation into non-carcinogenic metabolites (detoxication). The effect of metabolic transformation on the carcinogenic response of chemicals

is not always favorable, however. Indeed, metabolism of a pro-carcinogen can give rise to an active carcinogen (activation).

Several organs, including skin, kidney, and lung, have the ability to transform chemicals. However, the organ that has the largest capacity for metabolic transformation is the liver [226]. As an effect of detoxication in the liver, the carcinogenicity of a particular chemical is often less by oral ingestion than by other uptake routes. As an effect of activation in the liver, oral ingestion of (pro)carcinogens often results in the development of tumors in this organ. Thus, the uptake route influences metabolic transformation and, therefore, carcinogenic response. This influence may even cause a chemical to be carcinogenic only when uptake occurs via a particular route. A clear example is the situation in which the gastrointestinal microflora transforms a chemical into a potent carcinogen [70].

Detoxication of procarcinogens and carcinogens is clearly an important determinant for the internal concentration and, thus, for the carcinogenic response. Another important determinant is elimination of procarcinogens, carcinogens, and their metabolites from the body. The major elimination routes are urinary and biliary excretion. These routes can saturate, leading to accumulation [226].

II.2.2 Tumor induction

In this subsection we briefly deal with the biological processes underlying the transformation of normal cells into cancer cells. However, we neither attempt to summarize the latest advances in cancer research, nor pretend to deal with all the complexities of the genesis of the disease. Rather, we focus on results used as assumptions in the mathematical models discussed in Section II.3.2.

The current view of tumorigenesis, as expressed by Hanahan and Weinberg (2000), postulates that "tumor development proceeds via a process formally analogous to Darwinian evolution, in which a succession of genetic changes (...) leads to the progressive conversion of normal cells into cancer cells." This model, first proposed by Nowel (1976), is illustrated in Figure II.1 for a tumor that originates from one single normal cell. This is consistent with the observation that most human and animal tumors are monoclonal in composition [173, 57]. The genetic changes shared by all tumor cells accumulate along the single lineage preceding the final single founder cell, whereas heterogeneous changes occur during tumor growth [232] (see Figure II.1).

It is the progressive accumulation of multiple genetic changes that un-

derlies the multi-step nature of tumorigenesis [79, 172]. As many genes are targets of these changes, cancer is essentially a complex genetic disease. Cellular genes implicated in tumor development are usually referred to as cancer genes. It is possible to distinguish between two classes of cancer genes, those directly controlling cell proliferation (Class I) and those maintaining the integrity of the genome (Class II). The former include proto-oncogenes and tumor suppressor genes. In contrast to changes in Class I genes, a change in the normal activity of a Class II gene leads to cancer as a secondary effect. A change in activity of a cancer gene may concern either a change in the level of gene expression (e.g., [89, 248]) or a disruption of the gene product's biological behavior (e.g., [135, 136]). These changes may take place as the ultimate consequence of genetic events such as point mutations, rearrangements or major chromosomal aberrations. Recent studies further indicate that epigenetic events controlling the level of gene expression may play a more important role in tumorigenesis than was previously thought (see [103, 148, 265]).

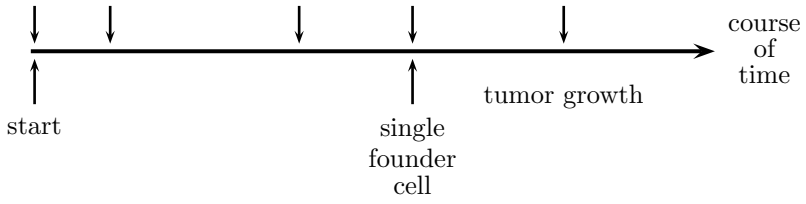

Figure II.1: Tumorigenesis. The start point is the moment at which one normal cell enters the process of tumor evolution. Any down pointing arrow represents the acquisition of one or more new physiological traits, each conferring an additional growth advantage [79]. The single founder cell is the last bottleneck along the evolutionary pathway [232]. The genesis of this cell indicates the beginning of final clonal expansion (tumor growth). In addition to the traits acquired in earlier stages, one or more alterations may occur during tumor growth leading to an increase in malignancy (tumor progression).

The number of changes required to produce a tumor is specific to a particular tumor type. Indeed, the number of cancer genes involved in tumorigenesis varies from one tumor type to another [16, 97]. Moreover, the number of alleles whose activity must change to lead to a phenotypic effect varies from one cancer gene to another. Aberrant genes that act in a recessive manner only have a phenotypic effect when present in the homozygous or hemizygous state, whereas aberrant genes that act in a dominant manner

exert a phenotypic effect even when present in the heterozygous state. With regard to the temporal sequence of the changes, on the one hand it has been proposed that the total accumulation of genetic alterations, rather than their relative order, is most important for tumorigenesis (e.g., [57]). On the other hand there is evidence that the nature and order of genetic changes can have impact on both tumor morphology and the likelihood of tumor progression (e.g., [102]).

Action of chemical carcinogens
Once present in a target tissue, chemical carcinogens can interfere with the process of tumorigenesis at one or more stages. Whichever mechanism is involved, tumor induction implies the interaction of the chemical with one or more cellular components. If the interaction results in DNA damage, the chemical is said to be 'genotoxic.' The potency of a genotoxic compound depends not only on its capacity to cause DNA damage, but also on the rate of cell replication and on the cell's capacity to repair the specific damage inflicted by the chemical compound [19, 147]. Non-genotoxic carcinogens are able to act without causing DNA damage [99, 148]. For instance, they can induce uncontrolled cell proliferation by altering inter-cellular communication [254, 200]. As a final remark, we notice that a carcinogen can have more than one mode of action [238, 243]. For example, a chemical can act as a mutagen at low doses, while on top of this it may be cytotoxic at high doses [7, 69]. See also Chapter I (Section I.5.4).

II.2.3 Tumor growth

Individual tumor cells are not immortal. Death of tumor cells occurs through the processes of apoptosis or necrosis [142, 220]. The latter may take place as a consequence of insufficient supply of nutrients, or as a result of excessive accumulation of metabolic waste products. Survival of chemically induced tumor cells, however, is not only subject to natural death processes: they may also be killed by the immune system of the host organism [176, 196]. The existence of cell loss implies that a tumor clone may regress prior to reaching a detectable size (see Figure II.2).

Even if they are monoclonal in origin, tumor cells are often heterogeneous with respect to properties such as metabolism, cell division rate, and antigenicity. During tumor growth, tumor cells become heterogeneous as a result of the occurrence of additional genetic alterations (tumor progression). The phenotypic heterogeneity of tumor cells is also the result of significant differences among their local environments [215] which define, for instance,

availability of nutrients. A limited supply of nutrients or oxygen commonly occurs in solid tumors, giving rise to a necrotic core [220]. The location of a cell within the tumor may determine its vulnerability to attacks of the immune system. Thus, phenotype and location of individual cells determine the rates of cell gain and cell loss within the tumor.

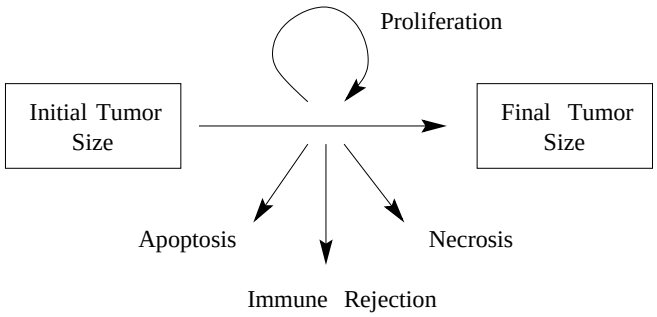

Figure II.2: Tumor growth. Tumor size increases due to cell proliferation. The cell-cycle time and growth fraction determine the rate at which cells are added to the tumor. Tumor size decreases due to cell death and cell killing. The final tumor size may be below the detection limit.

For solid tumors it is possible to distinguish between two growth phases. During the initial phase, or avascular growth phase, the tumor cells obtain nutrients and oxygen by diffusion from the surrounding tissue. When the tumor is no longer able to obtain sufficient nutrients by diffusion alone, tumor cells may start to produce several factors to stimulate angiogenesis [63, 106]. This defines the beginning of the so-called vascular tumor growth phase. During this second phase, tumor cells obtain oxygen and nutrients from the newly formed tumor blood vessels. After vascularization the tumor may become larger.

Once a tumor reaches a detectable size, its growth may be quantified by measuring tumor size as a function of time. However, only few body sites allow more than one measurement of tumor size [212]. The sparsity of data on human tumor growth is even more accentuated because treatment is rarely withheld [213]. As a consequence, available experimental data mainly relate to growth of tumors *in vitro* (tumor spheroids), growth of tumors inoculated in animal models, or growth of natural tumors *in vivo* during a short period of their growth ontogeny.

Experimental results have revealed that growth of solid tumors *in vivo* is often characterized by a late phase of declining growth rate [212]. The

same growth pattern has been observed in studies on tumor spheroids *in vitro* [215]. The growth deceleration has been attributed to several factors such as increase in cell loss, increase in cell-cycle time or decline in the growth fraction [127, 221]. The growth fraction, defined as the ratio of proliferating cells to total cells [156], is a concept frequently used to compare tumors in terms of their growth capacity. Another concept used for this purpose is the tumor doubling time, that is the time a tumor needs to double its size. Tumor doubling time (T_2) is a useful concept if a tumor grows exponentially, because it is then a constant. As soon as exponential growth is no longer realistic, the tumor doubling time becomes less informative.

II.2.4 Effects

In many carcinogenicity tests the time to tumor onset is not observable. The presence of a tumor can only be detected after the death (or sacrifice) of the animal. Thus, though the goal of carcinogenicity studies is to evaluate tumor incidence, one has to confront the topic of tumor lethality. How a tumor causes a decrease in survival is not always clear. The size of the tumor is relevant, but not the cause in itself. Rather, when a tumor reaches a certain size it may either impair the normal function of the host organ [108], or exhaust the organism due to its unrestrained use of resources. Moreover, the probability of invasion and metastasis, which are the most life-threatening aspects of tumor progression [137, 256], increases with the size of the primary tumor [107]. The detrimental effect of a tumor thus depends on its size, but it may also depend on its location in the body. For instance, it is unlikely that a brain tumor causes death through attrition.

II.3 Overview of existing models

To begin with, we want to distinguish between a conceptual model, a mathematical model and a mathematical description. We view a conceptual model as a set of assumptions regarding a certain phenomenon. If the conceptual model is translated into equations, it becomes a mathematical model. The mathematical model thus comprises both the mathematical description and the underlying assumptions (i.e., the conceptual model). Note that this accounts for the possibility that two different mathematical models share the same mathematical description. An good example of a mathematical description that appears in different contexts is the Weibull equation [245]:

$$f(y) = 1 - \mathrm{e}^{-vy^{\tau}} \tag{II.1}$$

where y is some variable. Sometimes $f(y)$ describes the fraction of tumor bearing animals as a function of dose (e.g., equation II.4), sometimes it describes the fraction of tumor bearing animals as a function of time (e.g., equation II.5). That is, the interpretation of the variable y differs. The associated conceptual models are clearly different as they concern different phenomena. More confusing is the situation in which two models for the same phenomenon result in an analogous mathematical description. Despite their outward similarity, we consider such models to be different, because they differ in their underlying assumptions. Naturally, such models are indistinguishable when fitted to experimental data.

II.3.1 Kinetic models

Although an organism is exposed to a certain environmental concentration of a (pro)carcinogen, the relevant concentration for tumor induction is at the target site. This implies that we have to relate the external concentration to the internal. Kinetic models deal with this problem.

Any kinetic model consists of a set of mass balance equations, each equation describing the change in the amount of chemical in a body 'compartment.' A compartment does not necessarily correspond to an organ. For example, the most simple kinetic model treats the entire body as one compartment. The models assume that the chemical is well mixed within each compartment, so it makes sense to define the concentration of the chemical in each compartment. The concentration of the chemical in compartment i is $C_i = Q_i/V_i$, where Q_i and V_i denote the mass of the chemical and the volume of that compartment, respectively. A general mass balance equation for the change in Q_i is:

$$Q_i' = \mathit{flux}_{in} + \mathit{flux}_{ma} - \mathit{flux}_{out} - \mathit{flux}_{md} \tag{II.2}$$

where flux_{ma} stands for production flux (metabolic activation) and flux_{md} for the metabolic-detoxication flux. The actual expressions for the fluxes depend on the specific choice for the kinetic model. In steady state the total positive flux equals the total negative flux, and the mass of the chemical in the compartment is constant.

To give some flavor of kinetic models, we here briefly illustrate the linear one-compartment model that treats the whole body as one compartment. If no metabolic transformation takes place, the amount of chemical in the body is determined by the uptake and elimination processes only. The model assumes that both uptake and elimination follow simple linear kinetics or, equivalently, it assumes that flux_{in} is proportional to external concentration,

while flux_{out} is proportional to internal concentration. Since the physics of transport suggests that flux_{in} and flux_{out} are also proportional to the areas of the surfaces involved in absorption and excretion [117], equation II.2 yields:

$$Q' = \mathit{flux}_{in} - \mathit{flux}_{out} = \delta_\nu A_\nu d - \delta_\eta A_\eta C$$

where d represents the external concentration, C the internal concentration, and A_ν and A_η the effective surface-areas for absorption and excretion, respectively. The interpretation of the proportionality constants δ_ν and δ_η depends on the uptake and elimination routes and on the transport mechanisms.

Body growth can substantially affect the kinetics of a chemical and, thus, its internal concentration. Indeed, if the organism's size (V) is not constant, the effective surface-areas A_ν and A_η are also functions of time. Moreover, due to the increase in size dilution of the chemical occurs. This implies that the change in concentration is not simply proportional to the change in mass of the chemical, which in mathematical terms means $C'(t) \neq Q'(t)/V(t)$. For a discussion on a one-compartment model that accounts for body growth, see references [117, 119]. We here focus on the simple situation where (*i*) the organism does not grow, (*ii*) the external concentration is constant, and (*iii*) the initial internal concentration is zero. Deviation from these conditions complicates the mathematical expressions somewhat. These complications are beyond the aim of our presentation.

If the organism's body size remains constant, $C'(t)$ equals $Q'(t)/V$ and the effective surface-areas A_ν and A_η are constant. The mass balance equation above can then be rewritten as $C'(t) = \nu d - \eta C(t)$, with $\nu = \delta_\nu A_\nu / V$ and $\eta = \delta_\eta A_\eta / V$ the (constant) uptake and elimination coefficients, respectively. The solution of this linear differential equation is $C(t) = \frac{\nu}{\eta}(1 - \mathrm{e}^{-\eta t})d$, which satisfies $C(0) = 0$. The equation gives a saturating curve when internal concentration is plotted against exposure time (see Figure II.3). After some time the term $\mathrm{e}^{-\eta t}$ dies out, and the internal concentration becomes proportional to the external concentration with proportionality coefficient ν/η. In ecotoxicology this ratio is usually called bioconcentration factor [119, 131, 194]. The steady-state proportionality between external and internal concentration is a generic characteristic of linear compartment models. This property breaks down, for example, if metabolic transformation follows the more realistic nonlinear Michaelis-Menten kinetics.

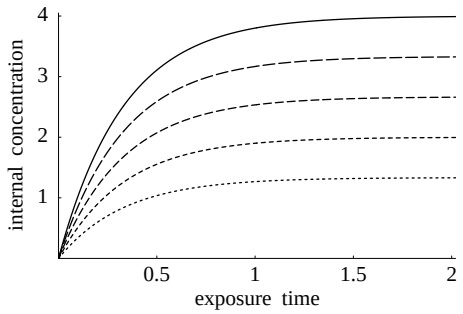

Figure II.3: 1-compartment model. Internal concentration as a function of exposure time. Parameter values: $\nu = 1$ and $\eta = 3$. From top down wards d equals 12, 10, 8, 6, and 4, respectively. For each curve, the asymptotic maximum internal concentration is given by $C_{max} = d/3$.

If any of the assumptions that underly the one-compartment model does not hold, a multi-compartment model can be used. Two main approaches have been pursued in developing multi-compartment kinetic models [9, 35], namely data-based compartmental modeling and physiologically-based compartmental modeling (PBPK, where PK stands for Pharmaco-Kinetics). The former includes empirical models, whose compartments often lack a biological interpretation. The latter includes biologically-based models, whose compartments correspond more closely to anatomical structures. Indeed, a compartment comprises a single organ, or a group of organs that share relevant physiological features.

Most PBPK-models define a central (blood) compartment that is responsible for the distribution of the chemical (e.g., [158]). The amount of chemical entering (or leaving) a compartment via the circulatory system depends on the concentration in the blood and in the compartment, and on the solubility of the chemical in the blood and in the compartment. If distribution among organs is fast in comparison with uptake and elimination, blood flows can be omitted from the model [160]. The alternative is that blood flows function as model parameters.

Even with a small number of compartments, PBPK-models require a substantial number of parameters [9]. These include physiological parameters such as blood flows, pulmonary ventilation, and organ volumes, as well as biochemical and physico-chemical parameters such as partition coefficients, tissue clearances, and the rates of metabolism [9, 10]. As they have a biological interpretation, most of them can be directly measured by experimental techniques. The remaining parameters have to be estimated. In empirical models all the parameters, as they lack a biological interpretation, have to be estimated from experimental data.

II.3.2 Tumor induction models

The models we presented so far were all deterministic. From here on they are either deterministic or stochastic. A deterministic model yields a single outcome, whereas a stochastic model yields multiple outcomes and assigns a probability to each of the different outcomes. Before going into the description of the models we briefly introduce a few basic concepts that crop-up in most of the stochastic models. Among these concepts are cumulative distribution function, survivor function and hazard rate. To introduce these concepts, we consider a relevant example.

Let T denote a variable representing the 'time to first tumor.' The random variable T, which may adopt any positive value, is exhaustively characterized by its cumulative distribution function $F_T(t) = prob\{T \leq t\}$. This expression reads 'the probability that the time to first tumor is less than or equal to t.' Ignoring mathematical exactness, this amounts to a prediction of the fraction of tumor bearing animals at time t. Closely related to F_T is the survivor function $G_T(t) = 1 - F_T(t) = prob\{T > t\}$ that provides 'the probability that an individual is tumor free at time t.' Finally, let h_T denote the hazard rate. Intuitively, the hazard rate concerns the probability per unit time that a tumor develops in a individual of age t, given that the individual is still tumor free. Mathematically, the hazard rate relates to the survivor function as follows:

$$G_T(t) = \mathrm{e}^{-\int_0^t h_T(s)\mathrm{d}s} \tag{II.3}$$

For further details on this expression, see Section III.5. As a consequence, if the hazard rate is known, the survivor function and the cumulative distribution function $F_T(t) = 1 - G_T(t)$ are also known, and vice-versa. Hence, the hazard rate constitutes an alternative way to exhaustively characterize a random variable. Most of the stochastic models described below provide expressions for the hazard rate.

The cumulative distribution function, the survivor function, and the hazard rate are denoted in the example above as F_T, G_T, and h_T respectively, where the subscript indicates the random variable. The same concepts can be defined in a more general sense for any random variable X (for further details see, for example, Cox and Oakes (1984)). For example, in the next section we will use F_U, where U is a random variable with the same dimension as the external dose. Finally, we notice that the biological and mathematical interpretations of survival only coincide if the random variable represents 'time to death of an individual.'

II.3.2.1 Tolerance distribution models

The models we present in this subsection are often motivated by the concept of tolerance distribution [91]. To introduce this concept, let us consider a group of mice that have been exposed to a chemical for a particular period of time. Any tolerance distribution model treats the group of mice as heterogeneous with respect to their susceptibility to the chemical: each individual has a different threshold-dose below which no response occurs. No hypothesis about possible mechanisms underlies such a threshold. The models treat the 'threshold-dose of an individual' (or tolerance, for short) as a random variable, say U.

For the given exposure time, let $P(d)$ denote the probability that an individual responds to a dose d (i.e., $P(d)$ amounts to a prediction of the fraction of tumor bearing animals). If the group of mice have been exposed to a dose d, only the animals with threshold dose below d will respond. Thus, the probability that an individual responds is $prob\{U \leq d\} = F_U(d)$, that is, in this context $P(d) = F_U(d)$. The actual expression for F_U depends on the distribution of U, the so-called tolerance distribution.

Any continuous statistical distribution can be used as tolerance distribution, the only constraint being that it covers only positive values ($d \geq 0$). Experimental results often show that a few animals have a very high tolerance. To account for this, skewed distributions are preferred. The choice for one or another distribution is further motivated by the desired simplicity of the expression for F_U. The log-normal, log-logistic and Weibull distributions offer the desired shape with relatively simple expressions. Therefore, these are the statistical distributions most frequently used in dose-response analysis. The log-normal, log-logistic and Weibull distributions give rise to the log-probit, log-logistic and dose-Weibull models, respectively.

The log-probit model (frequently abbreviated to probit) assumes the logarithm of the tolerance has a normal distribution [37]. The tolerance ($U = \mathrm{e}^W$, with W the logarithm of the tolerance) then has a so-called log-normal distribution. The resulting cumulative distribution function for U (see Figure II.4) is often expressed in terms of two parameters, θ_1 and θ_2, which relate to the mean and the variance of W as shown in Table II.1. The values of parameters θ_1 and θ_2, which have to be estimated by fitting experimental data, implicitly depend on the duration of the exposure. This follows from the fact that although time does not figure in the model, longer exposure times increase the chances of an animal developing a tumor.

The log-logistic model (usually called logit, on the analogy of probit) assumes that the tolerance U has a log-logistic distribution or, equivalently,

that the logarithm of the tolerance W has a logistic distribution. The resulting cumulative distribution function for U is often expressed in terms of two parameters, ϱ_1 and ϱ_2, which relate to the mean and the variance of W as shown in Table II.1. Like in the log-probit model, the values of the parameters implicitly depend on the duration of the exposure. It can be seen from Figure II.4 that the logit and log-probit models provide very similar predictions for the fraction of tumor bearing animals. The choice among them is therefore largely arbitrary. Motivations for the use of one or the other are rarely given. We suspect that the choice for a particular tolerance distribution is mainly due to habit.

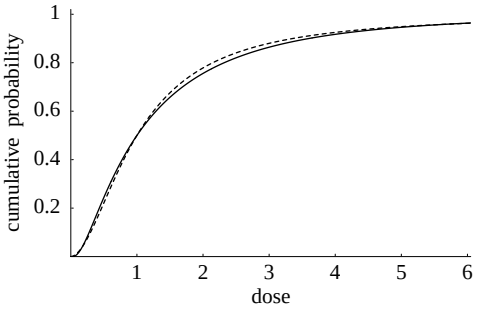

Figure II.4: Fraction of tumor bearing animals as a function of dose, $P(d)$. Solid line: prediction according to the log-probit model (W normally distributed). Dashed line: prediction according to the logit model (W logistically distributed). For both distributions the underlying stochast W has zero expectation and unit variance (W represents the logarithm of the tolerance).

Finally, the 'dose-Weibull model' assumes that the tolerance has a Weibull distribution. The resulting model is:

$$P(d) = 1 - \mathrm{e}^{-\lambda d^{\beta}} \tag{II.4}$$

where again the values of the parameters implicitly depend on the duration of the exposure. Although equation II.4 is the usual representation of the model, there is an alternative in which the exponent λd^{β} is replaced by $(d/d_*)^{\beta}$. The motivation for this alternative representation is that in equation II.4 the dimension of λ depends on the value of β. As the value of β derives from experimental data, the dimension of λ varies depending on the data considered, which renders the parameter λ uninterpretable. In contrast, the parameter d_* has always the same dimension as d, and has the interpretation of a reference dose. The reference dose must depend on the exposure time, as zero exposure time cannot result in a tumor. For a given exposure time, the corresponding d_* is the level of exposure at which the fraction of tumor bearing animals is $P(d_*) = 1 - \mathrm{e}^{-1} \approx 0.632$.

Table II.1: Log-probit and log-logistic models.

Let W denote the logarithm of the tolerance, $E[W]$ the mean, and $Var[W]$ the variance. Let us assume that W has a normal distribution and let us denote the mean and variance as μ and σ^2, respectively. For the log-probit model, F_U can then be written as below, with $\theta_1 = \mu/\sigma$ and $\theta_2 = 1/\sigma$. Thus, $F_U(d) = \phi(-\theta_1 + \theta_2 \ln d)$, where ϕ represents the cumulative distribution function of the standard normal distribution. Alternatively, let us assume that W has a logistic distribution and let us denote the mean and variance as μ and $\pi^2 z^2/3$, respectively. For the log-logistic model, F_U can then be written as below, with $\varrho_1 = \mu/z$ and $\varrho_2 = 1/z$. Thus, $F_U(d) = \psi(-\varrho_1 + \varrho_2 \ln d)$ where ψ represents the logistic function.

MODEL	W	$E[W]$	$Var[W]$	F_U
log-probit	normal	μ	σ^2	$F_U(d) = \int_{-\infty}^{-\frac{\mu}{\sigma}+\frac{1}{\sigma}\ln d} (2\pi)^{-\frac{1}{2}} \mathrm{e}^{\frac{-x^2}{2}} \mathrm{d}x$ $= \int_{-\infty}^{-\theta_1+\theta_2\ln d} (2\pi)^{\frac{-1}{2}} \mathrm{e}^{\frac{-x^2}{2}} \mathrm{d}x$ $= \phi(-\theta_1 + \theta_2 \ln d)$
log-logistic	logistic	μ	$\frac{\pi^2 z^2}{3}$	$F_U(d) = \left(1 + \exp\{\frac{\mu}{z} - \frac{1}{z}\ln d\}\right)^{-1}$ $= \left(1 + \mathrm{e}^{\{\varrho_1 - \varrho_2 \ln d\}}\right)^{-1}$ $= \psi(-\varrho_1 + \varrho_2 \ln d)$

II.3.2.2 Empirical 'time-to-tumor' models

Survival analysis is the branch of statistical modeling that deals with the analysis of failure time data. The failure time of an individual is the time until a particular event occurs. Any event that occurs at most once to each individual defines a failure time. Because the occurrence of a first tumor is such an event, survival analysis techniques can be applied to time-to-tumor data.

Any continuous statistical distribution can be used as failure time distribution, the only constraint being that it covers only positive values ($t \geq 0$). As for the tolerance models the log-normal, log-logistic and Weibull are the statistical distributions most frequently used in time-response analysis. This should not come as a surprise, as again the only motivation for their choice is in the shape and simplicity of the distributions. The Weibull distribution, for instance, is now given by:

$$F_T(t) = 1 - \mathrm{e}^{-at^b} \tag{II.5}$$

where the variable T represents the time-to-tumor. Time t (and not dose d) is now the independent variable. Therefore, we refer to this expression

as 'time-Weibull model' in order to avoid confusion with the dose-Weibull model above. The values of parameters a and b, which have to be estimated by fitting experimental data, implicitly depend on the level of exposure.

II.3.2.3 One-hit and multi-hit models

Let us again consider a group of mice that have been exposed to a chemical for a particular period of time. Contrary to the tolerance distribution models discussed above, the hit-models assume that the group of animals is homogeneous with regard to their susceptibility to a process generating 'hits.' One might think of a 'hit' as any of the changes discussed in Section II.2.2. Let us assume that an individual develops a tumor when a hit occurs, and that the occurrence of a hit is a random event. In this special case the random variables 'time to first hit' and 'time to first tumor' are thus interchangeable. As long as a mouse is still tumor free, it may develop a first tumor with a certain probability during the next (small) time unit. In the simplest scenario, this probability per time unit (hit-rate) remains constant; the variable 'time to first hit' then has an exponential distribution, and thus:

$$\begin{aligned} h_T(t) &= \mu \\ F_T(t) &= 1 - \mathrm{e}^{-\mu t} \end{aligned} \tag{II.6}$$

where T represents 'time to first hit (or tumor),' and μ the hit rate. The hazard rate h_T and the cumulative distribution function F_T relate to each other as explained in the introduction to Section II.3.2. Although equation II.6 is often referred to as the one-hit model in survival analysis, we refer to it as the one-hit failure-time model (OHFT-model) to avoid confusion with the one-hit dose-response model presented below. The OHFT-model is characterized by a constant hazard rate, μ. This implies that *susceptibility of developing* a tumor does not increase with time (age). Note, however, that the (cumulative) *chances of developing* a tumor do increase with time (age)!

A natural extension of the model above is to assume that more than one hit is required before a tumor develops, say k hits. In this special case the random variables 'time to the k-th hit' and 'time to first tumor' are interchangeable. With the occurrence of a first hit, the process generating hits does not change, so that the hit-rate μ still is the same. This assumption implies that the variable 'waiting time between the first and the second hit' also has an exponential distribution with hazard rate μ, and more generally, any waiting time between two successive hits has an exponential distribution

with hazard rate μ (see Figure II.5). In this context the parameter μ is the (mean waiting time)$^{-1}$.

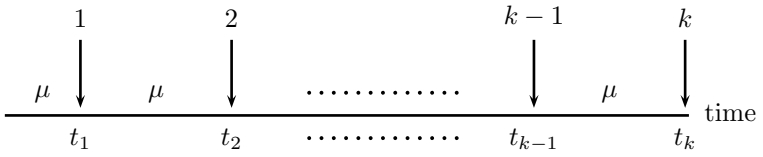

Figure II.5: The multi-hit failure-time model. It is assumed that the random variable 'waiting time between two successive hits' has an exponential distribution with parameter μ (k represents the number of hits required for tumor development; t_i represents the time until the i-th hit). Note that the hit-models are on the individual level, so μ is a probability of hit per time unit per individual.

The variable 'time to the k-th hit' now has a so-called Erlang distribution. For further details see Table II.2. Although this extension of the OHFT-model is often referred to as multi-hit model in survival analysis, we refer to it as multi-hit failure-time model (MHFT-model) to avoid confusion with the multi-hit dose-response model presented below.

The 'hit' models with dose-dependent parameters

The hit models described above do not yet account for the level of exposure, or dose. Obviously, the dose is an important determinant of the carcinogenic effect of the chemical, so it cannot be ignored. To account for the dose we have to specify its relationship with the hazard rate. Hanes and Wedel (1985) use the most simple approach to do this: they assume that the internal concentration is constant and proportional to the constant external dose (see Section II.3.1), and that the hit-rate is proportional to the chemical's internal concentration [80]. These assumptions lead to a constant hit-rate proportional to the external dose. The hazard rate, which equals the hit-rate in the one-hit failure-time model (equation II.6), then becomes αd. Substitution of the expression for the hazard rate in equation II.6 yields:

$$F_T(t, d) = 1 - \mathrm{e}^{-\alpha d t} \tag{II.7}$$

The probability that an animal exposed to a dose d develops a tumor before time t thus is a function of both exposure time and dose. Consequently, for a single fixed exposure time t^* it becomes a function of external dose alone. The fixed exposure time now plays the role of a model parameter with a known value. In sum, $F_T(t^*, d)$ provides a prediction of the fraction

Table II.2: Multi-hit models.

If any waiting time between two successive hits has an exponential distribution (with parameter μ), the variable 'number of hits in a fixed time interval' has a Poisson distribution (with parameter μt), and vice-versa. Let T denote the variable 'time to the k-th hit' (or 'time to first tumor') and let Z denote the variable 'number of hits in a time interval of length t'. The event in which Z is less than k is equivalent to the event in which T is greater than t. That is, $prob\{Z < k\} = prob\{T > t\} = G_T(t)$. Further, $F_T(t) = 1 - G_T(t) = 1 - prob\{Z < k\} = 1 - \sum_{i=0}^{k-1} \frac{e^{-\mu t}(\mu t)^i}{i!}$, because Z has a Poisson distribution. This expression can be written in the form shown below, where Γ represents the Gamma function.

$$F_T(t) = \int_0^t \frac{\mu^k s^{k-1} e^{-\mu s}}{\Gamma(k)} ds \tag{II.9}$$

For a fixed exposure time t^*, the MHFT-model gives rise to the multi-hit dose-response model:

$$P(d) = \int_0^d \frac{\lambda^k x^{k-1} e^{-\lambda x}}{\Gamma(k)} dx$$

with $\mu = \alpha d$ and $\lambda = \alpha t^*$.

of tumor bearing animals after an exposure period t^*, given an exposure to a dose d:

$$P(d) = 1 - e^{-\lambda d} \tag{II.8}$$

where $\lambda = \alpha t^*$ and $P(d) = F_T(t^*, d)$. Because the hit-rate μ has the interpretation of the inverse of mean waiting time, and $\mu t^* = \lambda d$, the product λd stands for the mean number of hits in a time interval of length t^*. Equation II.8 is referred to as one-hit model in dose-response analysis. Normally the one-hit model is only used because of its mathematical simplicity, and an interpretation of the model is rarely given.

Likewise, substitution of $\mu = \alpha d$ into the expression for the MHFT-model yields the so-called multi-hit dose-response model (see Table II.2). If the number of hits required for tumor development k is equal to one, the multi-hit model reduces to the one-hit model (equation II.8). Thus, the multi-hit model dose-response is an extension of the one-hit dose-response model.

Above it was assumed that the hit-rate is proportional to the dose, $\mu = \alpha d$. Substitution of this relation in equation II.6 gave rise to the one-hit dose-response model. Other assumptions are also possible. For instance, one might argue that the hit-rate is proportional to a power of dose, $\mu = \alpha d^{\beta}$. Substitution of this alternative expression for the hazard rate in equation II.6 gives rise to the same mathematical expression for $P(d)$ as the dose-Weibull model (equation II.4) with $\lambda = \alpha t^{*}$.

II.3.2.4 Multi-stage models

Many epidemiologic studies have revealed that age-specific cancer-incidence rates increase with age. Plots of the age-specific incidence rate against age yield straight lines when logarithmic axes are used. This suggests that age-specific incidence rates increase proportionally with a power of age. To explain this result, Nordling (1953) proposed that several mutations in the same cell are required to induce a tumor: "If three mutations were required, a cancer frequency proportional to the second power of age might be expected, with four mutations to the third power of age, and so on." In 1954, Armitage and Doll examined Nordling's work and presented a mathematical formulation of his hypothesis [11]. The resulting model is now widely known as the Armitage-Doll multi-stage model (AD-model), one of the first mathematical models for carcinogenesis.

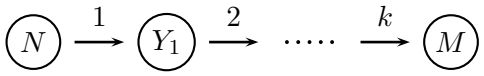

Figure II.6: Armitage-Doll model. A normal cell (N) goes through several intermediate stages before becoming a tumor cell (M). The transition from any state to the next is determined by the occurrence of a specific change. An intermediate cell type i (Y_i) is a cell that has incurred exactly i changes. k denotes the number of changes required to transform a normal cell into a tumor cell.

The AD-model assumes that several successive 'changes' in one cell are required to transform it into a tumor cell (see Figure II.6). Nordling maintains that the changes are mutations, but this specification is overly restrictive for the mathematical development of the AD-model [11]. The only constraint on the nature of the changes is that they must be irreversible and take place independently of each other. Let us assume that k changes are required for transformation of a normal cell into a malignant one. This implies that a

normal cell (N) goes through $k-1$ intermediate stages before becoming a tumor cell (M). For any $i < k$, an intermediate cell type i (Y_i) is a cell that has incurred exactly i changes. With regard to the time course, the AD-model postulates that the waiting time between any two successive changes is exponentially distributed with transition rate p_i (see Figure II.7). Finally, the AD-model posits that the changes must proceed in a unique order. None of the other multi-step models impose restrictions on the order of the steps and, therefore, the last assumption characterizes the AD-model.

One can translate the above assumptions into an expression for the probability that a certain cell becomes a tumor cell before time t (see, for example, reference [167]). One needs three additional assumptions to extrapolate this result from single cells to entire organisms. First, one has to assume that cells transform independently of each other. Table II.3 shows how this assumption is used. Second, one has to know which cells are susceptible to the changes. According to the so-called stem cell theory, only proliferative cells qualify for this. The effective number of normal cells thus equals the number of 'stem cells.' The third and final assumption maintains that the number of stem cells is constant. These assumptions, together with the other assumptions of the AD-model, lead to an expression for the probability that the time to first *tumor cell* is less than or equal to t. In general, this probability differs from the probability that the time to first *tumor* is less than or equal to t. However, on the assumption that a tumor cell constitutes a detectable tumor (for a further explanation on this assumption, see Section II.3.3), the same expression describes both probabilities. This expression, usually referred to as the AD exact formula, is a rather awkward page-filling equation (see, for example, reference [167]). Table II.3 provides a derivation of the exact formula for a two-stage model.

The original AD-model is an approximation of the AD exact formula. It holds if any transition rate is small in comparison with the organism's life span, and malignant transformation is a rare phenomenon. Table II.3 includes some explanatory information on these assumptions and their implications. The approximate expression for the AD-model is given by:

$$\begin{aligned} h_T(t) &\approx \mu t^{k-1} \\ F_T(t) &\approx 1 - \mathrm{e}^{-\frac{\mu}{k}t^k} \end{aligned} \tag{II.10}$$

where the parameter μ is proportional to the product of the transition rates p_i and proportional to the number of stem cells. According to this expression, an age-specific incidence proportional to a $(k-1)$-th power of age indicates that malignant transformation requires k steps, and vice-versa.

The mathematical expression for the survivor function (equation II.10) is a special form of the time-Weibull model (equation II.5), with $b = k$ an integer. Moreover, if the number of required changes to transform a normal cell into a tumor cell is one, the AD-model (equation II.10) reduces to the OHFT-model (equation II.6).

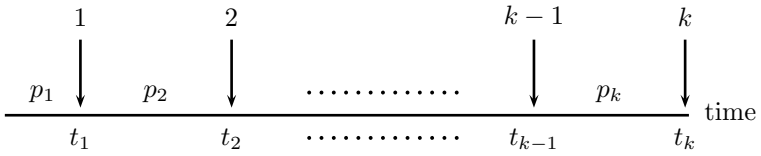

Figure II.7: Comparison of the AD-model with the MHFT-model. k, number of changes required for malignant transformation; p_i transition rate i; t_i time to occurrence of the i-th change. (a) The AD-model is a model on the cellular level, whereas the MHFT-model is a model on the individual level. Indeed, p_i is rate per time per cell, whereas μ is a rate per time per individual. (b) In the AD-model the waiting time for a cell to go from state i to state $i+1$ has an exponential distribution with parameter p_{i+1}, whereas in the MHFT-model any waiting time for an individual to go from any state to the next has a exponential distribution with the *same* parameter μ. (c) In the AD-model the changes must take place in a unique order, whereas in the MHFT-model no restriction is placed on the order of the hits.

The AD-model with dose dependent parameters

So far we have not mentioned the level of exposure. To use the AD-model in risk assessment, one needs to assume something about the relation between the hazard rate and the dose. For instance, one might argue that each transition rate is proportional to external dose, $p_i = \alpha_i d$. More frequently each transition rate is assumed to be a linear function of dose [41], $p_i = a_i + b_i d$, where the a_i have the interpretation of background transition rates (see Section II.3.2.6). F_T can then be viewed as a function of exposure time and dose. Moreover, the probability of tumor at a fixed exposure time t^* can be seen as a function of dose only:

$$P(d) = 1 - \mathrm{e}^{-\sum_{i=0}^{k} q_i d^i} \tag{II.11}$$

where any compound parameter q_i is a product of $(t^*)^k$, the number of normal cells, and a function of the coefficients a_j and b_j. Please note that this approach disregards the step from an external dose to an internal dose. This is only justified when these two quantities are constant and proportional to each other. The only kinetic models that satisfy this constraint are

linear compartment models (see Section II.3.1). Equation II.11 is known as the linearized multi-stage (LMS) dose-response model [141]. If the dose is low, the following approximation holds: $P(d) \approx 1 - \mathrm{e}^{-q_0 - q_1 d}$. An analogous expression can be obtained from the OHFT-model (equation II.6) by assuming that the hit rate is a linear function of dose. See also Section I.5.4 on low-dose extrapolation.

Table II.3: Multi-stage models.

Let N_0 denote the number of susceptible normal cells (stem cells) and J the random variable 'time until a certain cell gives rise to a tumor cell.' The probability that an organism is tumor free at time t equals the probability that not any cell transforms into a tumor cell before time t. Under the assumption that cells transform independently of each other, this implies that $G_T(t)$ equals the product of N_0 times $G_J(t)$ or, equivalently, $G_T(t) = G_J(t)^{N_0} = (1 - F_J(t))^{N_0}$. In terms of the hazard rates this means $h_T(t) = N_0 h_J(t)$.

Exact formula: If two changes are required to transform a certain cell, the time to transformation equals the sum of of the waiting time until the first change (K_1) and the waiting time between the first and the second change (K_2). The variables K_1 and K_2 follow an exponential distribution with parameters p_1 and p_2, respectively. F'_J can be expressed in terms of F'_{K_1} and F'_{K_2}, as follows: $F'_J(t) = \int_0^t F'_{K_1}(s) F'_{K_2}(t-s)\mathrm{d}s = \frac{p_1 p_2}{(p_2 - p_1)}(\mathrm{e}^{-p_1 t} - \mathrm{e}^{-p_2 t})$. Integration gives an exact expression for F_J and, thus, also for $G_T = (1 - F_J)^{N_0}$.

Approximate formula: From equation II.3: $G'_J(t) = -h_J(t) G_J(t)$. Because of the relation $F_J = 1 - G_J$, this is equivalent to $F'_J(t) = h_J(t)(1 - F_J(t))$. In this context, the assumption that transformation is a rare phenomenon means $(1 - F_J) \approx 1$ or, equivalently, $h_J(t) \approx F'_J(t)$. The hazard for T then yields: $h_T(t) = N_0 h_J(t) \approx N_0 F'_J(t) = \frac{p_1 p_2 N_0}{(p_2 - p_1)}(\mathrm{e}^{-p_1 t} - \mathrm{e}^{-p_2 t})$. Based on expansion in Taylor series about $t = 0$ and the assumption that p_1 and p_2 are small, this expression reduces to: $h_T(t) \approx p_1 p_2 N_0 t$. Thus, for the two stage model $\mu = p_1 p_2 N_0$ (equation II.10).

Some modifications of the AD-model

In the original AD-model, a single cell undergoes successive changes before becoming a tumor cell. That is, the model does not account for proliferation and death of intermediate cells. In 1957, Armitage and Doll proposed a two-stage model that incorporates cell kinetics [12]. This model assumes that once an intermediate cell is generated, it starts to proliferate at a constant rate. In 1993, Chen extended the two-stage model to account for age-dependent parameters [30]. Two years later, Little generalized the two-stage model to account for an arbitrary number of stages and time-varying parameters [138].

II.3.2.5 Multi-event models

In 1971 Knudson conducted a statistical study on hospital patients and concluded that two mutations must occur before retinoblastoma can develop [113]. He also proposed that the first mutation is germinal in the inherited form of the disease, whereas both mutations are somatic in the non-inherited form. It is now widely accepted that this childhood cancer is caused by the biallelic inactivation of the *RB* tumor suppressor gene [90, 95]. Thus, Knudson's two mutations correspond to mutational events at homologous loci of the *RB* gene. This result, generalized to the hypothesis that most tumors arise by mutation of recessive tumor suppressor genes, constitutes the basis of a two-event carcinogenesis model proposed by Moolgavkar, Venzon and Knudson [166, 170]. On the basis of the initials of the authors, this model is called the MVK-model.

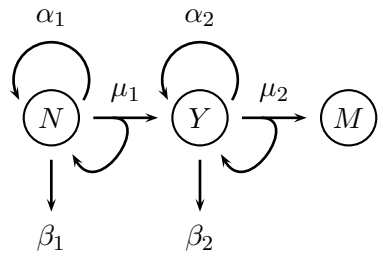

Figure II.8: Two-event model. Normal cells progress to intermediate and then to tumor cells (0, 1 and 2 mutations respectively). The mutational events are irreversible. N, normal susceptible cell (stem cell); Y, intermediate cell; M, malignant cell; α_1, rate (per cell per year) of cell division of normal cells; β_1, rate (per cell per year) of death or differentiation of normal cells; μ_1, rate (per cell per year) of division into one normal and one intermediate cell. α_2, β_2, and μ_2 are defined similarly for intermediate cells.

Like the Armitage-Doll model (AD-model), the MVK-model starts from the cellular level. It is for this reason that the models share some basic assumptions. For instance, both assume that only mutations in stem cells lead to cancer, and that cells transform independently of each other. However, in contrast to the AD-model, the MVK-model accounts for both cell proliferation and cell death. Indeed, cell kinetics plays a major role in the MVK-model. Clonal expansion of intermediate cells significantly affects the probability of tumor induction, because it increases the number of target cells for the second mutational event [161, 164]. Moreover, in the context of the MVK-model, a 'mutational event' is equivalent to a cell division pro-

ducing one mutant daughter cell. This interpretation of a mutational event was first suggested by Kendall (1960). It is based on the observation that fixation of a mutation requires at least one cycle of cell division [19, 88]. Hence, in the MVK-model an intermediate cell arises when a normal cell divides into one normal and one intermediate cell (such a division does not change the number of normal cells). In a similar way the genesis of a tumor cell occurs during the division of an intermediate cell. It should be noted that a mutational event in the MVK-model concerns the occurrence of an *effective* mutation for the tumor type of interest. That is, the model's mutation rates do not correspond to mutation rates measured by experimental techniques.

All tumor induction models described in the previous sections view tumor induction as a stochastic process. In the tolerance models, an individual has a probability to respond to a dose. In the multi-hit and multi-stage models, hits and changes may occur with a certain probability. The MVK-model also views tumor induction as a stochastic process. It incorporates stochasticity in a different manner, though. It assumes that the mutational events as well as cell division and cell death are random events. Hence, in any small time interval, normal cells may divide into two normal cells, die or differentiate, or divide into one normal cell and one intermediate cell. Likewise, intermediate cells may divide into two intermediate cells, die or differentiate, or divide into one intermediate cell and one tumor cell. Each of these events may occur with a certain probability. Further, the model assumes that the probability of more than one event occurring in the small time interval is negligibly small. Finally, the MVK-model assumes that a tumor cell constitutes an observable tumor. The AD-model also uses the terms tumor and tumor cell interchangeably. For a further explanation on this assumption, see Section II.3.3.

A model based on the assumptions above was considered difficult to apply. For this reason, an approximation has been used based on the assumption that the probability of malignant transformation is small (the resulting expression for the hazard rate is shown in Table II.4). The same assumption is also used in the AD-model to obtain an approximate expression. Such an approximation can be useful if the result does not deviate significantly from the full model. This appears not to hold for this approximation, though. Moolgavkar and Dewanji pointed out that the approximation is unlikely to be adequate when dealing with animal experiments in which the probability of tumor is high [165]. Furthermore, several studies have revealed that the approximate MVK-model can deviate significantly from the full model for certain parameter values [121, 167, 87, 86, 94]. To avoid misleading re-

sults, the use of the full model is recommended by these authors. Several studies exemplify how the full model can be applied to epidemiological and experimental data (for review, see [169, 167]).

One way to get closer to a workable expression for the full model is to make the additional assumption that the number of normal cells (N) is constant. This is approximately true if the number of normal cells is large. If, in addition, the rates of mutation, cell division and cell death remain constant in time, the model yields exact analytical expressions for the hazard rate and the survivor function [262, 123] (see Table II.4). Less restrictive is the assumption that the parameters are piece-wise constant. This means that the parameters are constant for a certain time interval; they then may change, after which they are again constant for some time. A closed form expression can be found for such a model [169, 87], but this expression is "not easy for nonmathematicians [94]." Because of this difficulty, Clewell *et al.* (1995) and Hoogeveen *et al.* (1999) developed an improved approximate model with arbitrarily time-varying parameters. For time-constant parameters, the derived expression is exact [94].

Above we used the MVK-model to obtain an expression for the hazard rate and the survivor function, which predict the fraction of tumor bearing animals. Interestingly, we can also use the model to obtain expressions regarding the size and number of intermediate clones (*foci*) [47, 144, 46]. This is relevant for those experiments in which information on the number of premalignant clones and their sizes is available. The proper way to analyze data on *foci* is currently topic of research [146, 77, 44, 73].

The MVK-model with dose-dependent parameters

If one wants to use the MVK-model in risk assessment, one needs to specify how the parameters of the model depend on the level of exposure. Two choices need to be made for this. One has to decide which parameters are affected by a particular chemical, and one must specify how they are affected. Thorslund *et al.* (1987) presented an overview of possible answers to the first question. However, in practice only two of the possibilities are considered: genotoxic carcinogens can act by altering the mutation rates, whereas non-genotoxic carcinogens can act by changing cell kinetics.

Before we explain how carcinogens can affect the parameters, we introduce some compound parameters. The effects of non-genotoxic carcinogens are most easily characterized in terms of these parameters. The compound parameters are simple functions of the basic parameters of the MVK-model, which are shown in Figure II.8. The first compound parameter is the mutation probability, m_1. If α_1 denotes the rate (per cell per year) of cell division

of normal cells and μ_1 the rate (per cell per year) of aberrant division into one normal and one intermediate cell, then the mutation probability at cell division is $m_1 = \frac{\mu_1}{\mu_1+\alpha_1}$. The second compound parameter characterizes the net proliferation of a normal cell. If β_1 denotes the rate (per cell per year) of death or differentiation of normal cells, then the net proliferation rate of a normal cell is $(\alpha_1 - \beta_1)$. The parameters α_2, β_2, μ_2, and m_2 describe the behavior of intermediate cells in a similar way.

In the context of the MVK-model, a genotoxic carcinogen increases the mutation rates (μ_1 and μ_2). Obviously, an increase in either of the mutation rates (or both of them) accelerates tumorigenesis. Theoretical interest in this possibility is limited, probably due to the trivial nature of the mechanism. In the last decade, modeling the effect of non-genotoxic carcinogens has received much more attention, due to the increasing interest in the role of cell proliferation in tumorigenesis (e.g., [7, 34, 205]). The architecture of the MVK-model suits the study of this problem, as it explicitly accounts for cell kinetics. A non-genotoxic carcinogen increases the parameters involved in cell kinetics, without changing the mutation probabilities m_1 and m_2. Note that such chemicals indirectly increase the mutation rates per cell per year. That is, if α_2 increases, μ_2 must increase for the probability $m_2 = \frac{\mu_2}{\mu_2+\alpha_2}$ to remain constant.

A non-genotoxic carcinogen may increase both cell division and death rates in such a way that the net proliferation rate of an intermediate cell does not change. Indeed, this occurs if the chemical increases α_2 and β_2 such that $(\alpha_2 - \beta_2)$ remains constant. This leads to a rather small effect on tumor incidence [162]. In contrast, even small changes in the net proliferation rate of intermediate cells $(\alpha_2 - \beta_2)$ lead to a rather profound effect on tumor incidence [162]. In this situation the non-genotoxic chemical affects tumor incidence by at least two mechanisms, namely increasing the mutation rates (μ_1 and μ_2) while simultaneously increasing the net change in the number of intermediate cells [164]. Moolgavkar (1986) suggested that the action of hormones exemplifies this phenomenon.

Some modifications of the MVK-model

Since its first publication, the MVK-model has received considerable attention (e.g., [21, 29, 31, 39, 122, 263]). Many investigators either sought to extend the model to incorporate further biological details, or to facilitate its practical use in cancer risk assessment. Several theoretical studies on the full MVK-model deal with improved implementation (e.g., [94, 43, 86]) and parameter identifiability (e.g., [81, 85, 87, 206]). Model extensions ac-

Table II.4: The MVK-model.

The following parameters figure in the MVK-model (see Figure II.8): N_0, initial number of normal susceptible cells (stem cells); α_1, rate of cell division of normal cells; β_1, rate of death or differentiation of normal cells; μ_1, rate of division into one normal and one intermediate cell; α_2, β_2, and μ_2 are defined similarly. For a detailed mathematical development of the model see, for example, references [166, 169]. For a description of the mathematical techniques see, for example, references [120, 216].

Approximate formula: It relies on the assumption that the probability of malignant transformation is small. In the particular case that the rates of mutation, cell division, and cell death remain constant in time, the following expression for the (approximate) hazard rate can be derived:

$$h_T(t) \approx \begin{cases} \frac{s_1}{s_2 - s_3}(\mathrm{e}^{s_2 t} - \mathrm{e}^{s_3 t}) & \text{for } s_2 - s_3 \neq 0 \\ s_1 t & \text{for } s_2 - s_3 = 0 \end{cases}$$

where $s_1 = \mu_1 \mu_2 N_0$, $s_2 = (\alpha_1 - \beta_1)$, and $s_3 = (\alpha_2 - \beta_2)$.

Exact formula: An exact analytical expression for the hazard rate can be derived when (i) the number of normal cells is constant, and (ii) the parameter values remain constant. The hazard rate is then given by [123, 262]:

$$h_T(t) = \frac{1}{2x_1} \frac{(x_3 - x_2^2)(\mathrm{e}^{\sqrt{x_3}t} - 1)}{(\sqrt{x_3} - x_2) + (\sqrt{x_3} + x_2)\mathrm{e}^{\sqrt{x_3}t}}$$

where $x_1 = \frac{\alpha_2}{\mu_1 N_0}$, $x_2 = (\beta_2 + \mu_2 - \alpha_2)$, and $x_3 = (\alpha_2 + \beta_2 + \mu_2)^2 - 4\alpha_2\beta_2$ are identifiable parameters (i.e., these compound-parameters can be uniquely estimated from experimental data) [81]. Note that the exact formula has the same number of parameters and can be implemented as easily as the approximate formula. Again, the hazard rate and the survivor function relate to each other as shown in equation II.3.

counting for tumor growth are treated in Sections II.3.3 and II.3.5. Other examples of model extensions are discussed below.

A first example of model extension is the three-event model proposed by Moolgavkar (1992). The motivation for this extension was the classic paper on colorectal cancer by Fearon and Vogelstein (1990). In the model the first two events correspond to mutations at homologous loci of the *DCC* gene, whereas the third is a mutation at one allele of the *p53* gene [163]. To account for the fact that different cancers may involve different numbers of mutations, Little (1995) has provided an expression for a multi-event model with an arbitrary number of steps. The practical interest of this expression is somewhat doubtful. With any additional step included, the number of parameters piles up, making practical application of the model impossible. For practical application the two-event model is used even if it is known that more than two steps are involved. This use is motivated by the casual assumption that only two steps are rate limiting.

Multiple-pathway models were first developed by Tan and Chen (1990). The motivation for such models was the observation that the same type of tumor might arise from different pathways. Multi-variate models account for the possibility that a single agent may induce two or more different types of tumors [216]. Mixed models allow for different individuals in the population either to start the process of carcinogenesis at different steps of the same pathway, or to involve different pathways [218]. For an exhaustive study on multiple-pathway, mixed and multi-variate models, see Tan (1991).

Attempts have also been made to describe in more detail the interaction between the carcinogen and the cell. For instance, a few models explicitly account for DNA repair. Among them are the damage-fixation model formulated by Portier and Kopp-Schneider (1991), and the model developed by Bois and Compton-Quintana (1992). Both models describe DNA repair as a random process. Alternatively, Conolly (1988) incorporated DNA repair in a deterministic way by describing the formation of DNA adducts. The adduct formation rate is assumed to be proportional to the amount of genotoxic carcinogen and to the amount of nucleotides, whereas the adduct repair rate is assumed to be proportional to the amount of adducts. The MVK mutation rates (μ_1 and μ_2) are then assumed to depend on the amount of adducts.

II.3.2.6 Background tumor incidence

The dose-response models we discussed above aim to relate tumor incidence to the dose the animals are exposed to. Experiments concerning this re-

lationship always include a control group of non-exposed animals ($d = 0$). Most of the dose-response models above predict absence of tumor incidence in this group, that is, no dose implies no response (i.e., $P(0) = 0$). This contradicts the observational evidence that tumors often develop in control animals. Background incidence can be easily incorporated into the models, however. It requires a choice between two assumptions [41, 92]. One assumption is frequently referred to as 'additive background assumption,' whereas the other is frequently referred to as 'independent background assumption.'

An additive background means that the same mechanism is responsible for both spontaneous and induced tumors. This assumption holds when the carcinogen acts by accelerating naturally occurring processes. To account for an additive background response, one often introduces a dummy dose d_0. So, one postulates an unknown background dose to be responsible for background tumor incidence. The fraction of animals bearing either a spontaneous or induced tumor at dose d is then $P^*(d) = P(d_0 + d)$, where P represents some dose-response model.

On the basis of a time-dependent model, whose parameters have an interpretation, a more realistic approach is possible. This approach requires two additional choices. First, one has to decide which parameters are affected by the chemical. We already addressed this topic for the hit, multi-stage, and multi-event models. Second, one has to specify how the parameters are affected. For instance, to use the Armitage-Doll model as dose-response model, the transition rates are assumed to depend linearly on dose, $p_i = a_i + b_i d$, where a_i has the interpretation of a background transition rate. Thus, a linear dose-dependence accounts for background incidence. Moreover, any dose-dependence of the form $p_i = a_i + g_i(d)$, where g_i is an arbitrary function satisfying $g_i(0) = 0$, accounts for an additive background incidence.

An independent background means that different mechanisms are responsible for spontaneous and induced tumors, and that both mechanisms take place independently of each other. In this context, one often uses what is know as Abbott's correction [1] to predict the fraction of animals bearing either a spontaneous or an induced tumor,

$$P^*(d) = P_0^* + (1 - P_0^*)P(d) \tag{II.12}$$

where P represents some dose-response model describing the occurrence of induced tumors; P_0^* is the tumor probability at dose zero. Table II.5 provides a derivation of this expression.

Table II.5: Independent background assumption.

Let R, I and T denote the random variables 'time to spontaneous tumor,' 'time to induced tumor,' and 'time to tumor' (as a consequence of the independence assumption, R does not depend on the level of exposure). At any point in time, the fraction of tumor-free animals is the fraction of animals that have neither a spontaneous nor an induced tumor. Under the independence assumption, this implies that $G_T^*(t,d)$ equals the product of $G_R(t)$ and $G_I(t,d)$. Expressed in terms of the cumulative tumor probabilities this translates into:

$$F_T^*(t,d) = F_R(t) + (1 - F_R(t))F_I(t,d)$$

For a fixed exposure time, this equation reduces to equation II.12 (Abbott's correction), with $P(d) = F_I(t,d)$. As the original dose-response model only accounts for induced tumors, it provides an expression for $F_I(t,d)$. In terms of the hazard rates the relation above implies $h_T = h_R + h_I$. Swanyer *et al.* (1984) relate h_I to h_R through a linear proportional hazard assumption, $h_I = \alpha d h_R$. In this particular situation, the survivor functions for R and T relate to each other as $G_T^* = G_R^{1+\alpha d}$.

II.3.3 Tumor growth models

Tumor induction models at the cellular level (such as the AD-model and the MVK-model) characterize the random variable 'time to first tumor cell.' As we showed above, they are used to analyze time-to-tumor data on the assumption that a single cell constitutes a detectable tumor. Such use is warranted if the tumor type fulfills two conditions. The first is that a tumor arises from a single cell; the observation that most tumors are monoclonal supports this. The second is that the time span a tumor cell requires to become a detectable tumor is negligibly small in comparison with the duration of tumor induction. The time to observing a tumor then roughly equals the time to developing a tumor, and the terms 'tumor cell' and 'tumor' become interchangeable.

For monoclonal fast growing tumors the growth period can thus be ignored. However, neglect of tumor growth is less realistic for slowly growing tumors as well as for rapidly induced tumors. If tumor growth cannot be neglected, the simplest way to account for it is to assume that the time it takes a tumor cell to reach a detectable size is constant, say t_g. The fraction of tumor bearing animals at time t is then the fraction of animals with a tumor cell at time $t - t_g$. A prediction for the latter fraction is provided by the original model. Iversen and Arley (1950) considered t_g, the time delay between the genesis of a tumor cell and the emergence of a detectable tumor,

but did not assume its value to be constant. In contrast, they assumed it to be a normally distributed random variable.

Disregard tumor growth rules out the possibility that a tumor regresses before reaching a detectable size [255]. In other words, it implies that once a tumor cell arises, it will certainly give rise to a detectable tumor. This also holds for the models above that incorporate growth as a time delay. Moreover, it also holds for any model that describes tumor growth in a deterministic way that does not account for a decrease in size. In the next sections we compare some deterministic growth models. As an alternative, some models for chemical carcinogenesis account for tumor growth in a stochastic way (e.g., [46, 145, 218, 207]). In such models tumor cells are subject to stochastic birth-and-death processes. That is, in any small time interval, tumor cells may divide or die with a certain probability. The actual probabilities depend on the tumor growth model.

Sherman and Portier (2000) modeled stochastic tumor growth on the basis of clones. So, the process of tumor growth starts when an intermediate cell gives rise to a malignant clone of size one. If the cell dies, the clone becomes extinct. If the cell divides, a clone of size two results. If then either cell dies the clone reverts to a single-cell clone, and so on. In summary, if an observable clone consists of $M_{\min}$ cells, to become observable a single-cell clone has to go through $M_{\min}$ stages of increasing size [207, 208]. The model assumes that once a clone reaches a detectable size, it can no longer regress in size.

II.3.3.1 Classic growth models

Several classic growth models from various disciplines have been used to describe tumor growth (see Adam and Bellomo (1997)). In this section we deal with four such models: exponential growth, Von Bertalanffy growth, Gompertz growth, and logistic growth. Mathematically these models share a common pattern: $V_u' = R(V_u)V_u$, where V_u denotes tumor volume, and $R(V_u)$ denotes the relative growth rate or the increase in volume per unit volume per unit time. The relative growth rate is thus some function of the size of the tumor; its actual expression differs among the different growth models. With the additional assumption that all cells within the tumor have the same volume, the equation above can be rewritten in terms of the total number of tumor cells. This is specially relevant for disseminated or dispersed tumors such as leukemias and lymphomas.

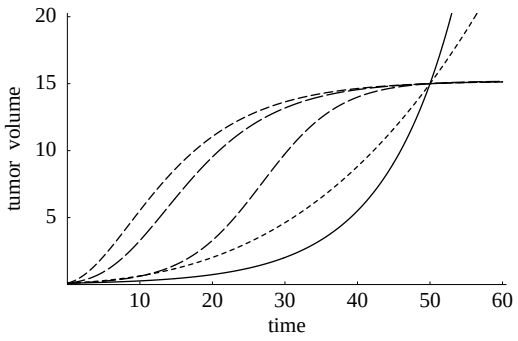

Figure II.9: Tumor volume as a function of time. Solid line: exponential growth. Dotted line: cube root growth. Broken lines from top down wards: Von Bertalanffy, Gompertz, and logistic growth. For all the models we chose parameters values such that $V_u(0) = 0.1$ and $V_u(50) = 15$ (and $V_{u\infty} = 15.20$ when relevant). The saturating curves reach half the maximum volume at time $\check{t} \approx 13.14$, $\check{t} \approx 16.68$ and $\check{t} \approx 26.87$, respectively. The model equations are shown in Tables II.6 and II.7.

The simplest growth model, the exponential growth model, results from the assumption that a constant fraction of tumor cells divide and die per time unit. If so, the relative growth rate is constant in time, and the tumor doubling time (T_2) is also constant. The tumor doubling time is $\frac{\ln 2}{z_u}$, with z_u the relative growth rate. Another relevant characteristic of the exponential growth model is that there is no maximum tumor volume (see Figure II.9).

The Von Bertalanffy growth model [15] defines growth as the net result of gains and losses in volume due to anabolic and catabolic processes, respectively. The gain in volume is proportional to tumor surface area, whereas volume loss is proportional to tumor volume. An additional assumption states that a tumor maintains the same shape during growth (isomorphic growth), so that its surface area is proportional to its $(\text{volume})^{\frac{2}{3}}$ [224]. Contrary to the exponential growth curve, the Von Bertalanffy curve is S-shaped with an asymptotic maximum tumor volume (see Figure II.9).

The model most widely used to describe tumor growth is the Gompertz growth model [72, 249] (see Figure II.9). As early as 1934, Casey used Gompertz curves to analyze experimental results on tumor transplantation [28]. Likewise, in 1964, Laird fitted the Gompertz growth model to tumor growth data with success [126]. It is intriguing that this model originally conceived as a 'law of human mortality' [72] gives such an accurate description of tumor growth.

Logistic growth arises from the assumption that the relative growth rate declines linearly with tumor volume. The resulting growth model is an S-shaped curve with an asymptotic maximum tumor volume (see Figure II.9). The logistic growth equation was originally used by Verhulst (1838) to describe the growth of biological populations. No biological mechanisms underly its formulation.

As long as tumor size remains small with respect to its maximum, the relative growth rate remains approximately constant for both the logistic and the Gompertz model. As a consequence, it may not be possible to discriminate between the exponential, logistic, and Gompertz models during the early growth period on the basis of experimental data.

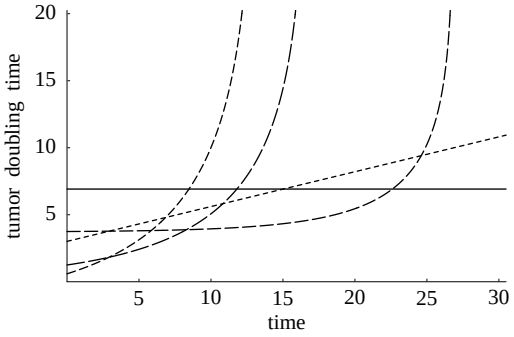

Figure II.10: Tumor doubling time (T_2) as a function of time. Exponential growth results in a constant tumor doubling time (solid line). Cube root growth results in a tumor doubling time that increases linearly with time (dotted line). The other growth models result in a tumor doubling time that increases more and more rapidly with time (broken lines). The model equations are shown in Tables II.6 and II.7.

There are at least two ways to compare growth models. A fit of the different models to the same data is useful to reveal similarities. Vaidya and Alexandro (1982) have carried out such an analysis for solid tumors, and Afenya and Calderón (2000) have done the same for disseminated tumors. As an alternative, in Figures II.9 and II.10, we sought to reveal the differences. To do this we forced the growth curves to include two values, $V_u(0) = 0.1$ and $V_u(50) = 15$. In addition, for the saturating curves, we chose a fixed asymptotic maximum volume, $V_{u\infty} = 15.20$. For the three S-shaped growth curves the doubling time becomes larger as the growth process continues. Laird (1964) observed that for the Gompertz model the doubling time increases slowly at the beginning of the growth process, but more and more

rapidly as the tumor becomes larger. This also applies to the logistic and Von Bertalanffy models. Another common characteristic of the S-shaped curves is that the doubling time becomes infinitely large when the tumor approaches half its maximum size. Figures II.9 and II.10 depict these results.

II.3.3.2 Living layer model

The living layer model, proposed by Mayneord (1932), is based on the experimental observation that solid tumors often have a dead kernel surrounded by a shell of viable tumor cells (see Figure II.11). The model is the first one that relates tumor growth to the tumor's structural heterogeneity. It involves three assumptions; first, the tumor is spherical in shape; second, there is a fixed maximum thickness (δ_m) for the living outer layer; and third, the cell population within the living layer grows exponentially [152].

Interestingly, the living layer model predicts three growth phases. During the first phase tumor radius is smaller than or equal to δ_m. As a consequence of the third assumption, the tumor grows exponentially. The second phase starts when tumor radius becomes larger than δ_m, giving rise to the development of a dead core. Finally, when the ratio of δ_m to tumor radius becames very small, tumor growth tends to follow the cube root law (that is, the cube root of tumor volume increases linearly with time; see Figure II.9). For a mathematical formulation of the model, see Chapter V (Appendix C).

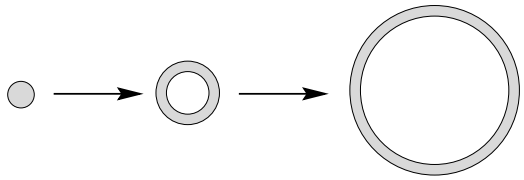

Figure II.11: Living layer model. (*1*) Early tumor without a dead kernel (radius smaller than or equal to the maximum thickness of the living layer). The whole tumor grows exponentially. (*2*) The tumor's radius has exceeded the maximum thickness of the living layer and, consequently, the tumor has developed a dead core (inner white sphere). (*3*) Advanced tumor. The tumor has increased in size, whereas the thickness of the living layer has remained constant.

Table II.6: Classic non-S-shaped tumor-growth models (without a point of inflexion). The exponential and cube-root growth model do not account for an asymptotic maximum tumor-size. The exponential growth model is characterized by a constant tumor doubling time (T_2). In the cube-root mode, for any parameter values, the time derivate of T_2 is $2^{\frac{1}{3}} - 1$. The monomolecular growth model is defined by a growth rate that declines linearly with tumor size. For the monomolecular model, the tumor doubling time is defined in the time interval $[0, \check{t})$, where $\check{t}$ is the time at which the tumor reaches a size of $V_{u\infty}/2$. The symbol V_{ui} denotes initial tumor volume, $V_{ui} = V_u(0)$. Table not included in the original paper I.M.M. van Leeuwen and C. Zonneveld (2001).

Model	**Growth equations**	**Tumor doubling time**
Exponential	$\frac{dV_u}{dt} = z_u V_u$ $V_u(t) = V_{ui} e^{z_u t}$	$T_2 = \frac{\ln 2}{z_u}$
Cube root	$\frac{dV_u}{dt} = 3 r_u V_u^{\frac{2}{3}}$ $V_u(t) = (r_u t + V_{ui}^{\frac{1}{3}})^3$	$T_2(t) = (2^{\frac{1}{3}} - 1)\left(t + \frac{V_{ui}^{\frac{1}{3}}}{r_u}\right)$
Monomolecular	$\frac{dV_u}{dt} = z_u(V_{u\infty} - V_u)$ $V_u(t) = V_{u\infty} - (V_{u\infty} - V_{ui}) e^{-z_u t}$	$T_2(t) = -\frac{1}{z_u} \ln\left(2 - \frac{V_{u\infty}}{V_{u\infty} - V_{ui}} e^{z_u t}\right)$ $\check{t} = \frac{1}{z_u} \ln\left(\frac{2(V_{u\infty} - V_{ui})}{V_{u\infty}}\right)$

Table II.7: Classic S-shaped tumor-growth models (with an inflexion point). For any model, the tumor doubling time is defined in the time interval $[0, \check{t})$, where $\check{t}$ is the time at which the tumor reaches a size of $V_{u\infty}/2$. In the Von Bertalanffy growth-model, the asymptotic maximum tumor-volume is given by $V_{u\infty} = (r_u/z_u)^3$. The corresponding growth-curve has a point of inflexion at $V_u = 8V_{u\infty}/27$, where the growth rate reaches its maximum value, $4z_uV_{u\infty}/9$. The logistic curve has a point of inflexion at $V_u = V_{u\infty}/2$, where the growth-rate reaches its maximum value, $z_uV_{u\infty}/4$. In the Gompertz growth-model, the maximum asymptotic maximum tumor-volume is given by $V_{u\infty} = V_{ui}\exp(z_u/\beta_u)$. The Gompertz curve has a point of inflexion at $V_u = V_{u\infty}/\mathrm{e}$, where the growth rate reaches its maximum value, $\beta_uV_{u\infty}/\mathrm{e}$. The symbol V_{ui} denotes initial tumor volume, $V_{ui} = V_u(0)$. Table not included in the original paper I.M.M. van Leeuwen and C. Zonneveld (2001).

Model	**Growth equations**	**Tumor doubling time**
Von Bertalanffy	$\frac{\mathrm{d}V_u}{\mathrm{d}t} = 3(r_uV_u^{\frac{2}{3}} - z_uV_u)$ $V_u(t) = \left(\frac{r_u}{z_u} - (\frac{r_u}{z_u} - V_{ui}^{\frac{1}{3}})\mathrm{e}^{-z_ut}\right)^3$	$\mathrm{T}_2(t) = -\frac{1}{z_u}\ln\left(\frac{r_u(1-2^{\frac{1}{3}})}{r_u - z_uV_{ui}^{\frac{1}{3}}}\mathrm{e}^{z_ut} + 2^{\frac{1}{3}}\right)$ $\check{t} = \frac{1}{z_u}\ln\left(\frac{2^{\frac{1}{3}}(r_u - z_uV_{ui}^{\frac{1}{3}})}{r_u(2^{\frac{1}{3}}-1)}\right)$
Logistic	$\frac{\mathrm{d}V_u}{\mathrm{d}t} = z_uV_u\left(1 - \frac{V_u}{V_{u\infty}}\right)$ $V_u(t) = \frac{V_{ui}V_{u\infty}}{V_{ui} + (V_{u\infty} - V_{ui})\mathrm{e}^{-z_ut}}$	$\mathrm{T}_2(t) = -\frac{1}{z_u}\ln\left(1 - \frac{V_{ui}}{V_{u\infty} - V_{ui}}\mathrm{e}^{z_ut}\right) + \frac{1}{z_u}\ln 2$ $\check{t} = \frac{1}{z_u}\ln\left(\frac{V_{u\infty} - V_{ui}}{V_{ui}}\right)$
Gompertz	$\frac{\mathrm{d}V_u}{\mathrm{d}t} = z_uV_u\mathrm{e}^{-\beta_ut}$ $V_u(t) = V_{ui}\exp\left(\frac{z_u}{\beta_u}(1 - \mathrm{e}^{-\beta_ut})\right)$	$T_2(t) = -\frac{1}{\beta_u}\ln\left(1 - \frac{\beta_u\ln 2}{z_u - \beta_u\ln\frac{V_u}{V_{ui}}}\right)$ $\check{t} = \frac{1}{\beta_u}\ln\left(\frac{z_u}{\beta_u\ln 2}\right)$

II.3.3.3 Complex tumor growth models

For clinical studies growth of tumors is of prime relevance. With the motivation to improve understanding and treatment of cancer, several complex models for tumor growth have been developed. Most of them are diffusion-limited growth-models. These models describe the growth of avascular tumors (or tumor-spheroids), assuming that nutrients must be taken up across the surface of the tumor. Uptake of nutrients at the surface together with their use by the tumor tissue creates a nutrient gradient within the tumor. The diffusion-reaction theory allows one to predict this gradient [75, 241]. Along the gradient, both proliferation and death of cells vary, according to availability of the nutrient. Most models assume that cells grow exponentially if the concentration of nutrients is above some critical level. When the tumor becomes larger, this approach predicts a structurally heterogeneous tumor with a outer living layer that remains constant in thickness and a necrotic core [223]. Basic diffusion-models have been extented to account for more realistic biological details such as presence of growth inhibitors [74], non-uniform nutrient consumption [153], and tumor-immune system interactions [2].

The complex growth models have the potential to increase our understanding. For practical applications such as the description of experimental data on chemical carcinogenesis they are less suited, due to the complexity of the mathematics they use. For this reason we only briefly mention these models.

II.3.4 Effects

In carcinogenicity studies on skin tumors the time to tumor onset (i.e., time to detectable tumor) is directly observable. This is the exception rather than the rule, however. In most carcinogenicity tests the time to tumor onset cannot be observed and, therefore, the presence of a tumor can only be detected after the death (or sacrifice) of the animal. Consequently, there is a need to make inferences about the actual time to tumor occurrence T, using the time to death caused by the tumor, $\dagger_u$. As tumor bearing animals have a certain probability to die from the tumor, such inferences concern tumor lethality.

Sawyer *et al.* (1984) assume that the tumor of interest is instantly lethal. This implies that time of death with tumor equals time to tumor onset. This method is appropriate for highly aggressive tumors, because they cause death shortly after their onset. However, many carcinogenicity tests involve

tumors that do not significantly affect survival. The use of the time to death from tumor as a surrogate for time to tumor occurrence is then unrealistic.

Data including cause-of-death information usually distinguish between five outcomes for the cause of death, only one of which is death from tumor of interest. The possible competing causes are natural death with incidental tumor, natural death without tumor, sacrifice with tumor, and sacrifice without tumor. Modelers usually cluster these outcomes into (1) death from tumor; (2) death from competing risk, with tumor present; and (3) death from competing risk, with no tumor present.

Some authors have sought to use cause-of-death information (e.g., [56, 62]). However, because cause-of-death determinations are frequently unreliable, other authors have sought to carry out the required inferences without using cause-of-death information (e.g., [4, 13, 48, 155]). Both approaches mainly have resulted in purely statistical (non-parametric) methods that do not rely on any conceptual model. A few authors assume a mathematical model for the time to tumor onset, whereas they use non-parametric estimates for both the time to death from tumor and time to death from a competing risk.

Dewanji *et al.* (1993) proposed a model-based approach that accounts for the three types of death. The use of cause-of-death data is possible but not necessary. They relate time to tumor onset and time to death from tumor through a lethality parameter ρ lying between zero (incidental tumor) and one (rapidly fatal tumor). They assume that the hazard rate for $\dagger_u$ is proportional to the hazard rate for T, with proportionality coefficient ρ. Consequently, the corresponding survivor functions relate to each other as $G_{\dagger_u}(t) = G_T(t)^\rho$. If ρ =0, there are no deaths from tumor ($G_{\dagger_u} = 1$), whereas if $\rho = 1$, the tumor is instantly lethal ($G_{\dagger_u} = G_T$).

II.3.5 Combined models

Models for chemical carcinogenesis aim to characterize the relation between tumor incidence and level of exposure to a certain (pro)carcinogen. The first model for chemical carcinogenesis, which was proposed by Iversen and Arley in the early 1950s, includes kinetics, tumor induction and tumor growth [101]. However, most of the models that are currently used focus on tumor induction only. That is, they use fairly elaborate assumptions on the induction process, whereas they use shallow 'default assumptions' for the remaining phases. Only a few models embrace more than one phase in similar detail. In this subsection we deal with these models.

II.3.5.1 Kinetics + Induction

All dose-response models in Section II.3.2 rely on the default assumption for kinetics, which states that the internal concentration is constant and proportional to the external dose. As discussed in Section II.3.1, this only holds for linear kinetics and constant external dose. A more realistic alternative is estimate the internal concentration with the aid of a kinetic model. Such an approach combines kinetics and induction in one model.

To illustrate how a kinetic and an induction model can be combined, we consider the one-compartment model (Section II.3.1) and the one-hit failure-time model (Section II.3.2.3). If we assume that the hit-rate is proportional to internal concentration ($\mu = \omega C$), it is no longer constant in time. The hazard rate, which equals the hit-rate in the one-hit model, now becomes:

$$h_T(t, d) = \frac{\nu\omega}{\eta}(1 - \mathrm{e}^{-\eta t})d$$

Because the hazard rate is not constant, the variable time-to-tumor T is no longer exponentially distributed. If after some time the internal concentration reaches steady-state conditions, the hazard rate becomes constant. The model then reduces to the one-hit dose-response model (equation II.7), with $\alpha = \frac{\nu\omega}{\eta}$.

Van Ryzin and Rai (1987) developed a combined model that embraces the phases of kinetics and induction. They described the internal concentration in the target organ by assuming Michaelis-Menten kinetics for both the incoming and outgoing processes. To solve the resulting mass balance equation, they assumed the external dose and internal concentration to be constant (steady-state conditions). Consequently, the internal concentration depends hyperbolically on the external dose. The model relates induction to internal concentration through a Weibull equation, $P(d) = 1 - \mathrm{e}^{-\gamma-\omega C(d)^\beta}$, where γ is a parameter that accounts for background incidence.

Still other combinations between kinetic models and induction models have been explored. For instance, to analyze the effect of metabolic transformation on tumor induction, Tan and Singh (1987) combined Michaelis-Menten kinetics with the MVK-model. Conolly *et al.* (1988) also used the MVK-model, but combined it with a PBPK-model. In this model the internal amount of active metabolite affect the MVK-parameters, according to the two types of carcinogens discussed in Section II.3.2.5. Bogen (1990) used approximate multi-event models to study tumor induction associated with exposure to chlorinated methanes. To predict the effective liver concentration, he used a PBPK-model. Reitz *et al.* (1996) combined a PBPK-model

with the linearized multi-stage (LMS) dose-response model, in an attempt to predict liver angiosarcoma incidence due to vinyl chloride exposure. Some of these attempts are difficult to evaluate, because they do not present either the model structure or the model equations. Indeed, most of the articles cited above focus on model results, rather than on model descriptions.

II.3.5.2 Induction + Growth

Multi-stage models and multi-event models (Sections II.3.2.4 and II.3.2.5) characterize the random variable 'time to tumor cell.' These models are directly used to analyze carcinogenicity tests on the assumption that the terms 'time to tumor cell' and 'time to tumor' are interchangeable. This constitutes the default assumption for tumor growth. As argued in Section II.3.3, it only holds for monoclonal fast growing tumors (see Section II.3.3).

A few attempts have been made to combine tumor induction and tumor growth in one model. For instance, Iversen and Arley (1950) define time to tumor onset as the sum of an 'excitation-time' and a 'growth-time.' Excitation involves the interaction of the chemical with a cell. The model describes excitation-time (i.e., time to tumor cell) on the basis of the one-hit theory (Section II.3.2.3). The growth-time plays the role of a stochastic delay between developing and observing a tumor. Alternatively, Yang (1991) combined a multi-event model with a tumor growth model. More recently, Sherman *et al.* (1994) extended the MVK-model to incorporate tumor growth [208, 207]. The model describes tumor growth on the basis of stochastic division and death of tumor cells. Like Yang's model, it treats the size of a detectable tumor as a constant (see Section II.3.3). Luebeck and Moolgavkar (1994) consider a threshold tumor size for which the probability of extinction is negligibly small. Beyond this threshold, the tumor can be assumed to grow deterministically. The difference between the detection threshold and the viability threshold is that the latter changes with the parameter values.

Models that combine induction and growth where both are treated as a stochastic process tend rapidly to become complicated. This might be one of the reasons that so few of these models have been formulated. Although models that combine kinetics and induction are slightly more common, in general, the combined models are far outnumbered by models that focus on induction alone.

II.4 Conclusions

In this Chapter we gave an overview of models describing any part of the chemical carcinogenesis process. We structured the overview according to a division of the entire process, from exposure to effect, into four consecutive phases. An alternative criterion to classify the models is whether a model is descriptive or mechanistic. This hardly is an all-or-none criterion; rather it defines a continuum with descriptive and mechanistic as endpoints. Tolerance distribution models, empirical time-to-tumor models, and classic growth models obviously cluster at the descriptive end of the continuum, whereas PBPK-models and multi-event models move some distance towards the mechanistic endpoint.

All descriptive models or, as we argued in the introduction to Section II.3.2, mathematical descriptions, have in common that they are rather simple mathematical expressions with a small number of parameters. They are useful to neatly summarize results of experiments in a few numbers, the parameter estimates. The summarizing parameter estimates lack a biological interpretation, however. This is different for mechanistically oriented models that rely on a set of assumptions on biological aspects of the process. Their parameter estimates provide quantitative information on the rates of processes and the factors that affect them [189].

Tests to determine the carcinogenic potency of a chemical aim to reveal the relationship between exposure to the chemical and occurrence of a carcinogenic response. This response may involve appearance of unusual tumors, increase in incidence of normal tumors, earlier occurrence of normal tumors, or increase in multiplicity of normal tumors. As we stated in the Introduction, models may facilitate the analysis of the sought relationship. Here we will evaluate to what extent current models actually contribute to this aim. But let us first briefly consider the data that have to be described.

In a standardized long-term carcinogenicity test several groups of animals are administered different levels of the chemical. Besides these dose-groups, the test includes an unexposed control group. The experiment has a fixed duration; those animals still alive at the end of the experiment are sacrificed to determine whether they bear tumors. The observed carcinogenic response, or data, vary from one study to another. If the tumor of interest is directly observable, tumor-onset times are recorded. In contrast, if the tumor is not directly observable, time to death (or sacrifice) and tumor pathology at the time of death (or sacrifice) are recorded.

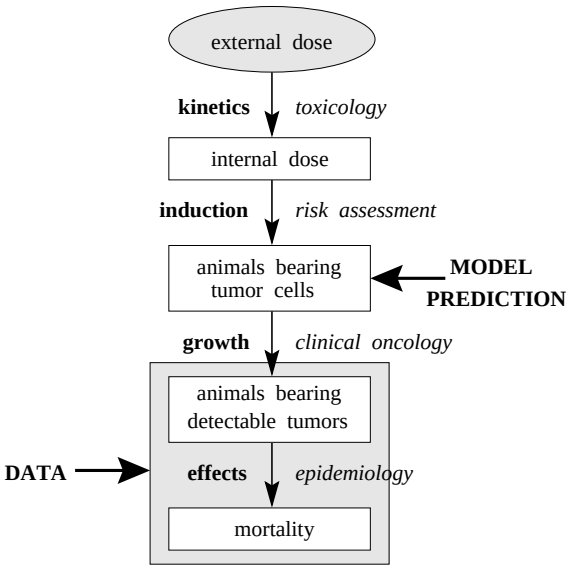

Figure II.12: Chemically induced carcinogenesis as a four-phase process. Kinetics concerns the relationship between exposure and effective internal dose. Tumor induction comprises the chemically induced transformation of normal cells into tumor cells. Tumor growth relates to the clonal expansion of a tumor. Effects involves the consequences of tumor development for the organism. As indicated in italics, models devised for the different phases derive from different disciplines. The large arrows indicate that tumor induction models make predictions concerning tumor cells, whereas one can only detect tumors of a certain minimum size. Even worse, one may not be able to detect tumors till the animal dies.

Between exposure and effect is a chain of processes, summarized in Figure II.12. In short, everything starts with the presence of a (pro)carcinogen. Kinetic processes lead to a certain internal concentration, which may induce the appearance of a tumor cell. This cell may become a detectable tumor in due time. The presence of this tumor may eventually result in the death of the animal.

In Section II.3 we gave an overview of models describing any part of chemical carcinogenesis. As shown in Figure II.12, models for the different phases derive from different disciplines. Kinetic models are mainly in the domain of toxicology; cancer risk assessment deals with tumor induction models; models for tumor growth are in the realm of clinical oncology; and effect models are the topic of epidemiology. Moreover, much of the work on different phases apparently proceeds in isolation of each other, as can be inferred from the paucity of cross references.

Models for chemical carcinogenesis aim to characterize the relation between dose and carcinogenic response. It seems desirable that such models deal with the entire process, from exposure to effect. Ideally, the models for the four phases should form a chain, in which the output of one model serves as the input for the next. Indeed, the very first model for chemical carcinogenesis by Iversen and Arley (1950) started to do just this (the model accounts for kinetics, induction, and growth). Current modeling is apparently not motivated by such a desire, though. Models for chemical carcinogenesis, with exception of the few combined models, focus on the tumor induction phase. This situation has some undesirable consequences.

One consequence is that most models for chemical carcinogenesis suffer from an imbalance between depth and width. For instance, a model for chemical carcinogenesis that covers tumor induction aspects in depth may shallowly treat, or even virtually ignore, kinetic aspects. Much new work tends to aggravate this imbalance, as it expands existing models by adding more biological details on tumor induction only. Biological details are probably added to increase the realism of the model. To judge whether a model has indeed become more realistic after addition of some new elements, it has to be confronted with data. Here we stumble upon another undesirable consequence. The predictions of an induction model concern tumor cells, whereas the data concern detectable tumors. In other words, the model predictions do not directly bear on the data! (This is also indicated in Figure II.12). This makes the interpretation of parameter estimates rather uncertain. It also hampers a straightforward interpretation of the realism of the models involved.

Let us now return to the original question: do current models contribute to the aim to relate exposure to carcinogenic response? Although sweeping generalizations over heterogeneous collections are always difficult to make, we think the answer is at best 'to some extent.' The models used are not overly realistic for the purpose of data description, because they ignore essential processes. An increase in realism should be sought in accounting for these processes in the first place. This may bridge the gap between model predictions and data. Other prospect for improvement is offered by the use of alternative information, especially on *foci*, as end-point in carcinogenicity testing. If the data concern *foci* rather than tumors or mortality, the gap between data and prediction could be eliminated. The model then only needs to cover kinetics and development of *foci*; there is no need to pay attention to tumor growth and the impact of the tumor on the animal. With such improvements the models may become much more useful for the purpose of estimation of cancer risk from carcinogenicity tests.

Acknowledgements

We should like to take this opportunity to thank Bas Kooijman, head of the Department of Theoretical Biology, for his support. Our thanks are also due to Jacques Bedaux, Bernd Brandt, Jan Kooter, Henk van Kranen, Wout Slob and two anonymous referees for their insightful comments on an earlier draft of this Chapter. The work presented in this Chapter was part of the research project VBI-4692, financially supported by the Netherlands Technology Foundation (STW) and DSM.

III

ANALYSIS OF TUMOR INCIDENCE DATA

> "*As well as formulating theories in precise mathematical form, and studying them – deducing consequences and analyzing behavior – there is an important requirement to put them to empirical test,*" **D. Brown & P. Rothery**

What do long-term studies tell us about the tumor-induction potential of chemical agents?

I.M.M. van Leeuwen (2003)

III.1 Introduction

As explained in Chapter I (Section I.3), long-term carcinogenicity bioassays play an important role in cancer risk assessment. A fundamental objective of such bioassays is to reveal the ability of the test agent to cause an increase in tumor occurrence rates as compared with those in unexposed controls. The aim of this Chapter is to examine how various interpretations of the results from carcinogenicity bioassays affect the chance to achieve this objective.

The remainder of this Chapter is organized in six sections. Section III.2 introduces two representative long-term carcinogenicity tests. Section III.3 outlines the impact of censoring on the outcome of a carcinogenicity bioassay. Section III.4 discusses the well-known Kaplan-Meier (KM) method and proposes two alternative formulations. Two uncertainties about the KM-method are pointed out. Section III.5 extends the information provided in Chapter II (Section II.3.2) on the hazard and survivor functions. Section III.6 gives a brief introduction to the maximum likelihood (ML) principle. Finally, Section III.7 shows the results obtained with computer-simulated carcinogenicity tests. It explores the capability of both the KM-method and the ML-approach to recover the 'real' time-to-tumor distribution from 'observed' events.

III.2 Examples of carcinogenicity studies

Throughout this thesis, two studies are repeatedly used as examples of long-term carcinogenicity bioassays. They concern the chemical compounds 1,3-butadiene and benzo[a]pyrene.

III.2.1 1,3-Butadiene

As can be seen from Table I.5, the industrial chemical 1,3-butadiene (CAS 106-99-0) has recently been classified in Category A (known human car-

cinogens). The compound is primarily used in the manufacture of synthetic rubber and thermoplastic resins [175]. The corresponding NTP study includes a 2-year inhalation bioassay, in which groups of 70 male and 70 female B6C3F$_1$ mice were administered 0, 6.25, 20, 62.5, and 200 ppm 1,3-butadiene for 6 hours a day, 5 days a week; groups of 90 male and 90 female mice were administered 625 ppm 1,3-butadiene on the same schedule [174]. After 9 months (287 days) and again after 15 months (462 days), up to 10 male and 10 female mice were randomly withdrawn from each dose-group for interim evaluations. I refer to this long-term carcinogenicity study as BUT-NTP. For each mouse, the following information is available:

Table III.1: BUT-NTP data.

Carcass identification number
Sex
Dose level
Number of days on study
Cause of withdrawn from study (spontaneous death, interim evaluation, terminal sacrifice, or missing)
Presence of tumors (e.g., lymphoma, lung neoplasm, and heart hemangiosarcoma)

III.2.2 Benzo[*a*]pyrene

Benzo[a]pyrene (CAS 50-32-8), a polycyclic aromatic hydrocarbon, has been reasonably anticipated to be a human carcinogen [175]. This chemical agent forms as a result of incomplete combustion of organic compounds. It is found, for instance, in gasoline and diesel exhaust, cigarette smoke, and coal tar. The RIVM recently carried out a 2-year gavage bioassay, in which groups of 52 male and 52 female rats (SPF Riv:TOX Wistar strain) were exposed to 0, 3, 10, 30 mg B[a]P/kg for 5 days a week [125]. I refer to this long-term carcinogenicity study as B[a]P-RIVM.

III.3 Censored data

During the analysis of the information shown in Table III.1, the interest is often focussed on the evaluation of two variables, namely time to death and time to death with tumor. Both variables constitute examples of so-called failure times. A difficulty in the interpretation of failure-time data is that often some individuals are not observed for the full time to failure [38]. In the BUT-NTP study, for instance, some mice remained failure-free till the end

of the bioassay. Moreover, up to 20 mice were randomly withdrawn from each group for interim evaluations. Incomplete observation of the failure time is called censoring [38].

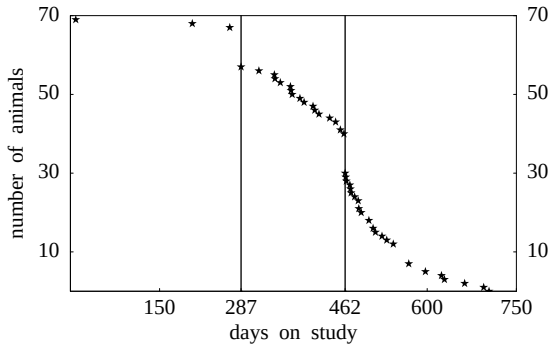

Figure III.1: Number of female mice present in the dose-group exposed to 200 ppm 1,3-butadiene. The initial number of animals in this group was 70. At day 287 and again at day 462, 10 animals were randomly withdrawn for interim evaluations. The vertical lines indicate these censoring events. Data from the BUT-NTP study (Section III.2.1).

Figure III.1 illustrates the change in the number of animals in the group of females exposed to 200 ppm 1,3-butadiene. The occurrence of two main censoring events results in a step-shaped pattern. Obviously, as spontaneous death is not the only cause underlying withdrawn from study, dividing the data shown in Figure III.1 by the initial number of animals does not provide an accurate estimate of the survivor probability. Below I explain how to estimate failure probabilities from censored data.

III.4 Kaplan-Meier estimators

Throughout this thesis, I use Kaplan-Meier (KM) estimators for both mortality and tumor incidence, to adjust them for censoring [14, 104]. To facilitate the definition of these estimators, I introduce some terminology and notation. By *event* I understand the departure of a single animal from the study. As explained in the previous section, two types of events can be distinguished, namely failure events and censoring events. The definitions of failure and censoring depend on the variable of interest. For instance, concerning mortality, any natural death is a failure event, whereas interim evaluations, terminal sacrifices and missing animals constitute censoring events.

In contrast, concerning tumor incidence, any death without the tumor of interest constitutes a censoring event. The interpretation of failure event in tumor incidence analysis is the main topic of Section III.4.2.

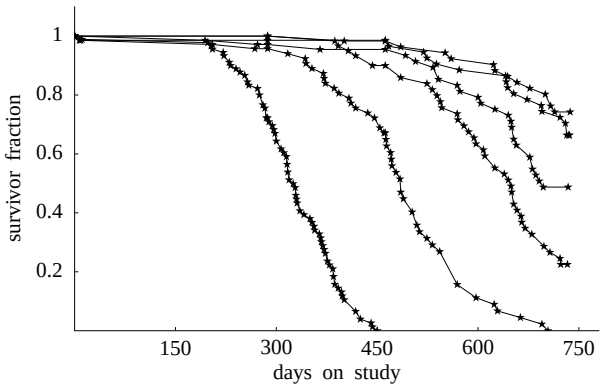

Figure III.2: Kaplan-Meier adjusted female mice survival data (i.e., data corrected for interim evaluations, accidental deaths and missing animals). KM-estimates ($\star$) have been joined to distinguish the 6 dose-groups. For curves from right to left, the administered 1,3-butadiene dose is 0, 6.25, 20, 62.5, 200 and 625 ppm, respectively. Data from the BUT-NTP study (Section III.2.1).

Let $t_1, t_2, \ldots, t_r$ denote the times at which the number of events and the remaining number of animals are recorded. For any given time interval $(t_{j-1}, t_j]$, let n_{cj} be the number of censoring events within that interval, n_{xj} the number of failure events, and $n_j = n_{cj} + n_{xj}$ the total number of events. The experimental observations can then be summarized as:

$$\{(t_1, n_{x1}, n_{c1}), (t_2, n_{x2}, n_{c2}), \ldots, (t_r, n_{xr}, n_{cr})\} \tag{III.1}$$

If the failure event is uncommon, most n_{xj} elements will be zero. Notice that, if N_{j-1} is the number of animals in the bioassay at t_{j-1}, the remaining number at t_j is given by $N_j = N_{j-1} - n_j$. The KM-estimates can be iteratively calculated as follows:

$$\begin{aligned} &\mathrm{KM}(t_0) = 1 \\ &\mathrm{KM}(t_i) = \hat{\theta}(t_i)\ \mathrm{KM}(t_{i-1}) \quad \text{for } i = 1, \ldots, r \end{aligned} \tag{III.2}$$

where $\mathrm{KM}(t_j)$ is the KM-estimate of the failure-free probability, that is, the probability that the failure event *does not* occur before time t_j. The

function $\hat{\theta}(t_j)$ provides an estimate of the probability that the failure event does not take place within the interval $(t_{j-1}, t_j]$ given that it did not take place before time t_{j-1}. I distinguish between two possible expressions for this estimator, the first one being:

$$\hat{\theta}_F(t_i) = \frac{N_{i-1} - n_{xi}}{N_{i-1}} \tag{III.3}$$

Substitution of this expression into equation III.2 leads to the classical KM-estimator, which I will refer to as *forward* KM-estimator. Figure III.2 shows the forward KM-adjusted female mice survival data from the BUT-NTP study [174].

Alternatively, I define:

$$\hat{\theta}_B(t_i) = \begin{cases} \frac{N_i}{N_{i-1} - n_{ci}} & \text{if } N_{i-1} \neq n_{ci} \\ 1 & \text{if } N_{i-1} = n_{ci} \end{cases} \tag{III.4}$$

which leads to what I will refer to as *backward* KM-estimator.

III.4.1 The role of interval size

The KM approach provides good estimates of the failure probability, in the sense that the estimates converge to the true probabilities as the sample size gets larger and larger [235]. However, in practice the KM-estimates may present some problems when failure and censoring events happen in the same interval. For instance, KM-estimates using equation III.3 differ from those using equation III.4 unless $n_{xj} = 0$ or $n_{cj} = 0$ for any j. Indeed, using the forward KM-estimator, an underestimation of the failure probability may be expected because equation III.3 presumes that (in each time interval) failure events precede censoring; in contrast, using the backward KM-estimator, an overestimation of the failure probability may be expected. These statements are supported by the KM-estimates shown in Figure III.3.

III.4.2 Influence of cause-of-death assumptions

In most long-term carcinogenicity tests, the presence of a tumor can only be diagnosed after the death of the animal. Therefore, as explained in Chapter II (e.g., Section II.4), the analysis of tumor incidence data usually involves inferences regarding tumor growth and cause of death (tumor lethality). The assumptions made in order to carry out these inferences may significantly affect both the KM-estimates and the fitting procedures and, consequently, also the eventual risk estimates.

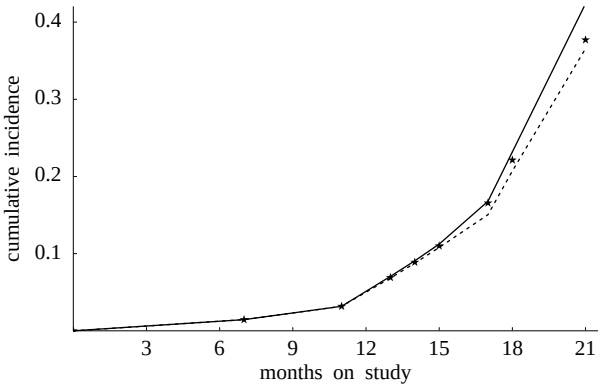

Figure III.3: Cumulative incidence of spontaneous deaths with malignant lymphoma in female mice exposed to 200 ppm 1,3-butadiene. Stars ($\star$) represent the KM-estimates obtained when the events are recorded per day. As only on day 454 both a censoring and a failure event take place, forward and backward estimates are almost identical (indeed, they are indistinguishable in this figure). However, if the events are recorded once a month, the backward KM-estimates (solid line) and forward KM-estimates (broken line) clearly differ. Data from the BUT-NTP study (Section III.2.1).

The expression for the KM-estimator (Equation III.2) depends on two choices: (*i*) variable of interest; (*ii*) criterion to classify the observed events into two groups, namely censoring events and failure events (occurrences of the variable of interest). For survival data, the variable of interest is 'time to death' and the classification of events consists in distinguishing spontaneous from non-spontaneous deaths. For tumor incidence data, however, the settings are less obvious. Using the variable 'time to death from tumor,' I will now discuss the implications of choosing different classification criteria.

The KM-estimates of lymphoma incidence shown in Figures I.1 and III.3 are based on the following assumption. If a lymphoma is found in an animal that died spontaneously, the cause of death can be attributed to this tumor. As malignant lymphoma has a high lethality, it is expected that Figure I.1 reflects well the behavior of the variable 'time to death from lymphoma.' This does not necessarily imply that Figure I.1 illustrates accurately the overall lymphoma incidence. Indeed, lymphomas found in sacrificed animals are not taken into account.

The influence of cause-of-death assumptions on the KM-estimates is exemplified in Figure III.4, which shows the cumulative lung cancer incidence

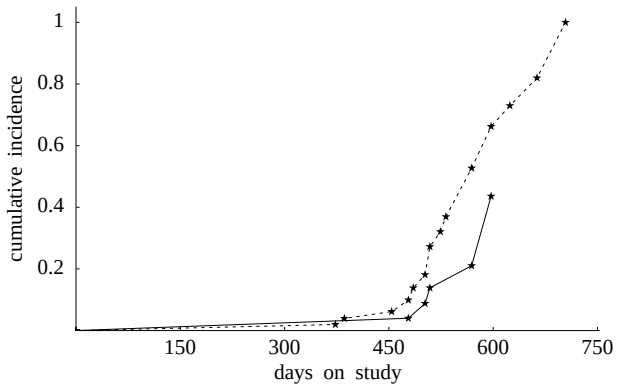

Figure III.4: Influence of cause-of-death assumptions on the KM-estimates. Cumulative incidence of lung cancer in female mice exposed to 200 ppm 1,3-butadiene. Solid line: natural deaths with two tumors, including lung cancer, are viewed as censoring events. Broken line: any natural death with a lung tumor is viewed as a failure event. Data from the BUT-NTP study (Section III.2.1).

according to two different criteria. The broken line assumes that the cause of any natural death bearing a lung tumor can be attributed to this neoplastic lesion. The solid line, instead, assumes that natural deaths with two tumors (lung cancer and lymphoma or lung cancer and heart tumor) are not due to lung cancer. That is, according to the second criterion, such events are additional censoring events. Both criteria consider any non-spontaneous death as a censoring event, independently of the presence or absence of lung tumors. As can be seen from Figure III.4, the incidences predicted by the two criteria differ considerably.

III.5 Hazard rates and survivor functions

Most failure-time models (e.g., tumor induction and survival models) are expressed in terms of hazard rates. In Chapter II (Section II.3.2), we briefly introduced the concepts of random variable, cumulative distribution function, survivor function and hazard rate. In this section, I provide a more detailed mathematical definition of these concepts. For any failure-time random variable X, its cumulative distribution function $F_X(t)$ is defined as $prob\{X \leq t\}$ and its survivor function as $G_X(t) = 1 - F_X(t)$. The latter corresponds to the probability that the variable X takes a value larger than t.

The hazard rate is given by [38, 253]:

$$h_X(t) = \lim_{\triangle t \to 0} \frac{prob\{t < X \leq t + \triangle t | X > t\}}{\triangle t} \tag{III.5}$$

The relationship between the hazard rate and the survivor function (equation II.3) can be directly deduced from these definitions. From the relation between G_X and F_X:

$$-\frac{\mathrm{d}}{\mathrm{d}t} G_X = \frac{\mathrm{d}}{\mathrm{d}t} F_X = f_X(t) \tag{III.6}$$

where f_X, the derivative of F_X, is called the probability density function of X. Figure III.5 depicts the probability density functions of two Gamma distributions. The expression for the hazard rate can be re-written as follows:

$$\begin{aligned} h_X(t) &= \lim_{\triangle t \to 0} \frac{prob\{t < X \leq t + \triangle t\}}{prob\{X > t\} \triangle t} \\ &= \frac{1}{prob\{X > t\}} \lim_{\triangle t \to 0} \frac{prob\{t < X \leq t + \triangle t\}}{\triangle t} \\ &= \frac{1}{G_X(t)} \lim_{\triangle t \to 0} \frac{F_X(t + \triangle t) - F_X(t)}{\triangle t} = \frac{1}{G_X(t)} \frac{\mathrm{d}}{\mathrm{d}t} F_X \end{aligned}$$

Thus, from equation III.6:

$$h_X = \frac{f_X}{G_X} = -\frac{1}{G_X} \frac{\mathrm{d}}{\mathrm{d}t} G_X = -\frac{\mathrm{d}}{\mathrm{d}t} \ln G_X \tag{III.7}$$

which leads to $\frac{\mathrm{d}}{\mathrm{d}t} G_X = -h_X G_X$. The analytical solution of this differential equation is:

$$G_X(t) = \mathrm{e}^{-\int_0^t h_X(s) \mathrm{d}s}, \qquad t \geq 0 \tag{III.8}$$

which is analogous to the expression shown in equations II.3 and IV.7.

III.6 Maximum likelihood principle

In Section III.4, I discussed how mortality and tumor incidence data can be adjusted to account for censoring events. In this section, I explain a way to deal with censoring during the model fitting procedure. For this purpose, let me consider an arbitrary failure-time model describing the probability

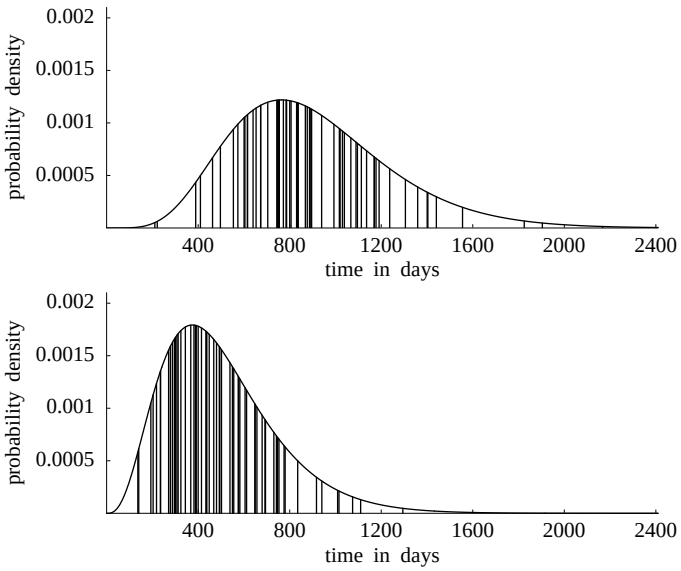

Figure III.5: Examples of probability density functions. *Upper plot:* Gamma distribution with mean $m = 900$ days and standard deviation $\sigma = 350$ days. *Lower plot:* Gamma distribution with $m = 500$ days and $\sigma = 250$ days. The vertical lines in each plot represent 60 randomly generated tumor-induction times.

distribution of a random variable X. The model is defined by a particular hazard rate h_X that depends on a parameter vector θ.

The intuitive idea underlying the maximum likelihood method is to take as estimates of the parameters those values for which the observations (equation III.1) are most likely to have occurred [38]. A failure event recorded at t_i corresponds to an observation of $t_{i-1} < X \leq t_i$. In contrast, a censoring event recorded at t_j is an observation of $X > t_{j-1}$. The observed failure event thus contributes a term $F_X(t_i|\theta) - F_X(t_{i-1}|\theta)$ to the likelihood, whereas the observed censoring-event contributes $G_X(t_{j-1}|\theta)$. If all events are assumed to occur independently of each other, the probability of observing the whole set of observations can be expressed as a function of the parameter vector θ:

$$\mathcal{L}(\theta) = \prod_{i=1}^{r} (F_X(t_i|\theta) - F_X(t_{i-1}|\theta))^{n_{xi}} \prod_{j=1}^{r} G_X(t_{j-1}|\theta)^{n_{cj}}$$

which is called the *likelihood function*. According to the maximum likelihood principle, the best parameter estimate of θ is the value at which the

likelihood function reaches its maximum.

If the time intervals $(t_{j-1}, t_j]$ are small or if the observations (equation III.1) correspond to the instants at which events took place, the likelihood function is defined instead as:

$$\mathcal{L}(\theta) = \prod_{i=1}^{r} f_X(t_i|\theta)^{n_{xi}} \prod_{j=1}^{r} G_X(t_j|\theta)^{n_{cj}} \tag{III.9}$$

The *log-likelihood function* is defined as the logarithm of the likelihood:

$$\mathcal{LL}(\theta) = \sum_{i=1}^{r} n_{xi} \ln f_X(t_i|\theta) + \sum_{j=1}^{r} n_{cj} \ln G_X(t_j|\theta)$$

Instead of finding the maximum of $\mathcal{L}$, one often finds the maximum of $\mathcal{LL}$, which is mathematically equivalent but computationally more convenient. According to equation III.7, the probability density function can be expressed as: $f_X = h_X G_X$. Substitution of this expression into the equation above leads to:

$$\mathcal{LL}(\theta) = \sum_{i=1}^{r} n_{xi} \ln h_X(t_i|\theta) + \sum_{j=1}^{r} n_j \ln G_X(t_j|\theta)$$

where $n_j = n_{xj} + n_{cj}$. Finally, from equation III.8:

$$\mathcal{LL}(\theta) = \sum_{i=1}^{r} n_{xi} \ln h_X(t_i|\theta) - \sum_{j=1}^{r} n_j \int_0^{t_j} h_X(s|\theta) \mathrm{d}s \tag{III.10}$$

This expression is frequently used because it expresses the log-likelihood function in simple terms of the hazard rate. Equation III.10 was used, for instance, to get the model fit shown in Section III.7. Moreover, a generalized version of this expression will be used in Chapter IV (equation IV.16) to fit three mortality data sets simultaneously.

When fitting a model to experimental data, parameter values are estimated by minimizing the function $-\mathcal{LL}(\theta)$. For this purpose, different function minimization algorithms can be used. Throughout this thesis, I use the *Mathematica* `FindMinimum` function, which is based on a modification of Powell's method when the number of parameters exceeds one [252].

III.7 Computer-simulation studies

The two studies described in Section III.2 concern standard carcinogenicity bioassays and are therefore adequate to test some of the methodology

available to analyze tumor incidence data. In this Section, I confront the Kaplan-Meier method and the maximum likelihood (ML) approach with computer-simulated data. Compared with the experiments that they mimic, computer simulations possess the advantage that the differences between estimated and 'real' tumor incidences can be calculated.

III.7.1 Randomly generated data

Two hypothetical rat populations of $N_0 = 60$ individuals are exposed to a chemical carcinogen $\mathcal{R}_{\mathcal{A}}$ for their lifespan. The doses administered to the populations are denoted as d_L and d_H, with $d_L < d_H$. In response to the exposure, the animals develop an unusual tumor, type $\mathcal{A}$, which has a negligible incidence in untreated controls. The random variable $T =$ 'time to tumor' follows the Gamma distribution defined by the following cumulative distribution function:

$$F_T(t) = \frac{1}{\Gamma(m^2/\sigma^2)} \int_0^{mt/\sigma^2} s^{-1+(m/\sigma)^2} \mathrm{e}^{-s} \mathrm{d}s, \qquad t \geq 0 \qquad \text{(III.11)}$$

where Γ denotes the Gamma function and m and σ represent the mean and standard deviation of the distribution, respectively. In the particular case that $k = (m/\sigma)^2$ is an integer, equation III.11 corresponds to a multi-hit model (equation II.9) with k the number of hits and $\mu = m/\sigma^2$ the hit rate. I assume that both the mean time-to-tumor and the standard deviation decrease with increasing exposure levels. In the multi-hit model this happens, for instance, if the hit-rate is proportional to the dose. For the time-to-tumor distribution in the d_L-group, I take a mean of 900 days and a standard deviation of 350 days, whereas for the d_H-group I assume $m = 500$ and $\sigma = 250$ days. Figure III.6 depicts both cumulative distribution functions. As can be seen from this figure, the distributions defined by the chosen parameter values are in agreement with the results from experimental carcinogenicity studies. I further assume that type $\mathcal{A}$ tumors are immediately lethal. Consequently, the variables $\dagger_u =$ 'time to death from tumor' and $T =$ 'time to tumor' are identical.

As can be seen from Figure III.6, the probability that an animal develops a tumor before time t tends to one when t becomes large. That is, like any standard failure-time model, the Gamma distribution presumes that, in absence of a competing cause of death, any individual will eventually fail (develop a tumor). Because the animals are exposed for a long period, however, natural deaths take place due to the aging process. To account for this competing cause of death, I assume that the random variable $\dagger_\alpha =$ 'time

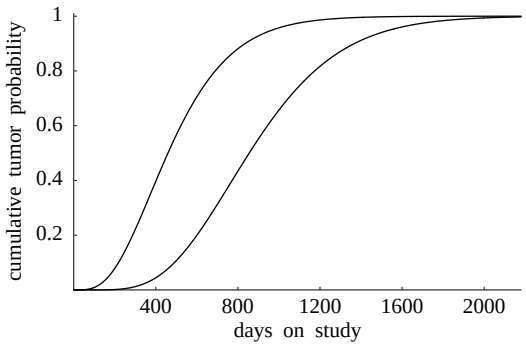

Figure III.6: Cumulative distribution functions of the variable 'time to type $\mathcal{A}$ tumor.' *Left curve*: Gamma distribution (equation III.11) with m and σ equal to 500 and 250 days, respectively (dose d_H). The cumulative tumor incidence after 730 days is: $F_T(730|d_L) \approx 0.35$. *Rigth curve*: Gamma distribution with $m = 900$ days and $\sigma = 350$ days (dose $d_L < d_H$). Figure III.5 shows the corresponding probability density functions. The cumulative tumor incidence after 730 days is: $F_T(730|d_H) \approx 0.834$.

to aging-mediated death' is Weibull distributed (equation II.5) with mean 800 days and standard deviation 250 days.

Assuming that the variables $\dagger_\alpha$ and $\dagger_u$ are independent, the distribution of the variable $\dagger$ = 'time to death' is given by the following survivor function:

$$G_\dagger(t) = G_{\dagger_\alpha}(t) G_{\dagger_u}(t) \tag{III.12}$$

For type $\mathcal{A}$ tumors, as the variables $\dagger_u$ and T are the same, this expression leads to $G_\dagger(t) = G_{\dagger_\alpha}(t)(1 - F_T(t))$. Finally, to imitate experimental situations reliably, I randomly remove 10 individuals after 200 days and another 10 after 400 days. Moreover, I assume that all remaining animals are sacrificed after 730 days. As animals may leave the study before they developed a tumor, the observed tumor incidence may differ from the incidence shown in Figure III.6. overview of all randomly generated events in the d_L-group is provided in Figure III.7.

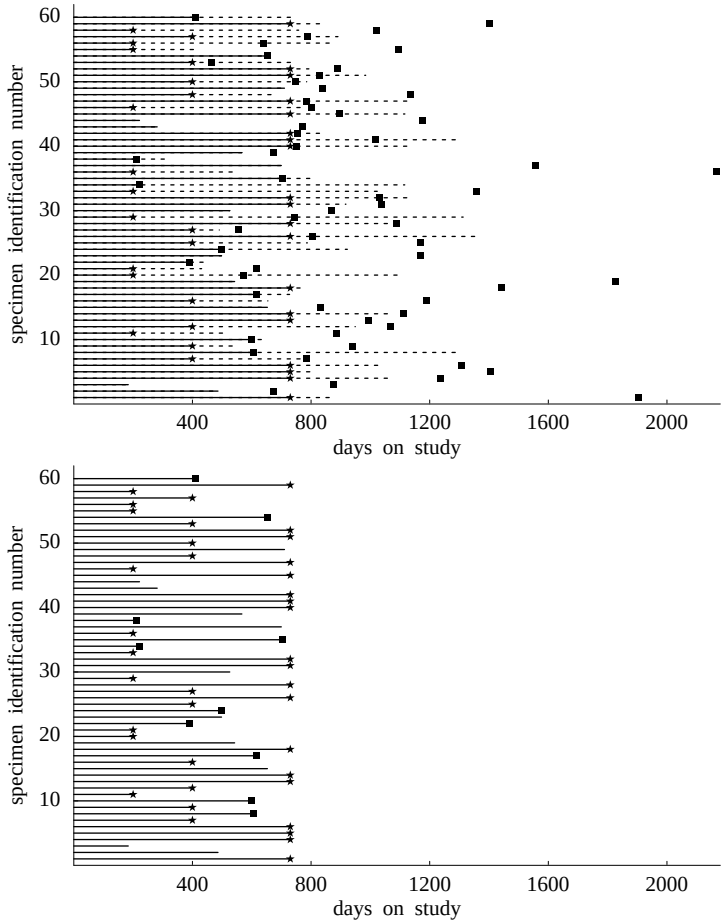

Figure III.7: Randomly generated events in a rat population exposed to dose d_L of compound $\mathcal{R}_\mathcal{A}$. Each horizontal line represents a single specimen. Lines are solid as long as the corresponding specimens are still alive. *Upper panel:* Specimens leave the study because of aging-related death, tumor-mediated death, or sacrifice. Filled boxes represent time of death from tumor. Dotted lines indicate the lifespans expected when aging is the only cause of death. After 200 days and again after 400 days, up to 10 specimens ($\star$) are removed from the study. Moreover, all remaining animals are sacrificed after 730 days. *Lower panel:* Observed events. In both panels, the solid lines ending with a box are specimens that died from a tumor.

III.7.2 Error measures

To evaluate the quality of tumor incidence estimates, I use two error functions:

$$\begin{aligned} D_{\text{KM}}(t) &= 1 - \text{KM}(t) - F_T(t|m,\sigma) \\ D_{\text{fit}}(t) &= F_T(t|\bar{m},\bar{\sigma}) - F_T(t|m,\sigma) \end{aligned} \tag{III.13}$$

where $\text{KM}(t)$ is the KM-estimation of the tumor-free probability (equation III.2), F_T is defined as in equation III.11, and $\bar{m}$ and $\bar{\sigma}$ are the estimates of m and σ obtained by the maximum likelihood (ML) approach. The error functions express the difference between the estimated cumulative tumor incidence and 'real' cumulative tumor probability. Using these functions, I define the following error measure: $\mathcal{E}_{\text{fit}}^{\max} = D_{\text{fit}}(t_{\#})$, where $t_{\#}$ is the instant at which the function $|D_{\text{fit}}|$ reaches its maximum value. If $\mathcal{E}_{\text{fit}}^{\max} < 0.05$, the ML-estimate of the cumulative tumor incidence deviates less than 5% from the real cumulative tumor probability. As the estimate of the cumulative tumor incidence at the end of the study is often used for risk assessment, I also introduce: $\mathcal{E}_{\text{fit}}^{730} = D_{\text{fit}}(730)$ and $\mathcal{E}_{\text{KM}}^{730} = D_{\text{KM}}(730)$.

Figure III.8 exemplifies the use of the error measures defined above. It concerns the effect of censoring on a given set of randomly generated tumor-induction times. In Figure III.8.*a*, as no censoring takes place, the KM-estimates equal the cumulative incidences of randomly generated events. As can be seen from this Figure, the randomly generated events (bullets) are close to the corresponding real distributions (solid lines). Moreover, the real (solid lines) and fitted (broken lines) cumulative incidences only differ slightly. The values of the corresponding error measures also reveal this: $\mathcal{E}_{\text{fit}}^{\max}(d_L) = -0.038$ and $\mathcal{E}_{\text{fit}}^{\max}(d_H) = -0.060$, which reflect the largest discrepancies between estimated and real incidences. Figure III.8.*b* shows the real and estimated tumor incidences when aging-related death is the only competing cause of death. Finally, Figure III.8.*c* shows the outcome of the bioassay when all censoring events described in Section III.7.1 are included.

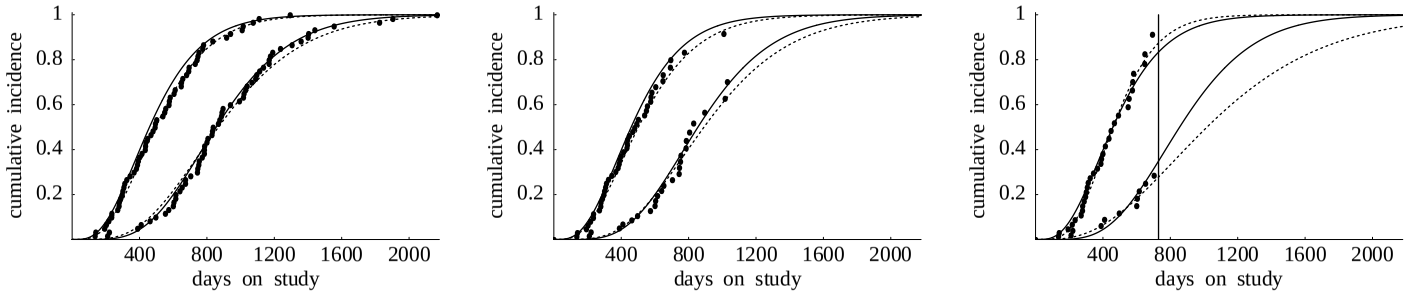

Figure III.8: Effect of censoring on the estimated tumor incidence. The three figures concern the same randomly generated tumor-induction times. Bullets represent the KM-estimated tumor incidences. The solid lines are the same as in Figure III.6 ('real' cumulative tumor incidences). The broken lines are model fits (equation III.11).
(a) Type $\mathcal{A}$ tumors are the only cause of death. ML-estimated parameter values: $\bar{m} = 925.52$ and $\bar{\sigma} = 402.12$ days (d_L-group); and $\bar{m} = 537.37$ and $\bar{\sigma} = 260.68$ days (d_H-group). Error measures: $\mathcal{E}^{\max}_{\text{fit}}(d_L) = -0.038$, $\mathcal{E}^{730}_{\text{KM}}(d_L) = -0.0657$, $\mathcal{E}^{\max}_{\text{fit}}(d_H) = -0.060$, and $\mathcal{E}^{730}_{\text{KM}}(d_H) = -0.0673$.
(b) Type $\mathcal{A}$ tumors and aging are the only causes of death. ML-estimated parameter values: $\bar{m} = 947.94$ and $\bar{\sigma} = 404.3$ days (d_L-group); and $\bar{m} = 548.91$ and $\bar{\sigma} = 280.86$ days (d_H-group). Error measures: $\mathcal{E}^{\max}_{\text{fit}}(d_L) = -0.0551$, $\mathcal{E}^{730}_{\text{KM}}(d_L) = -0.0827$, $\mathcal{E}^{\max}_{\text{fit}}(d_H) = -0.071$, and $\mathcal{E}^{730}_{\text{KM}}(d_H) = -0.0338$.
(c) Specimens leave the study because of tumor-mediated death, aging-mediated death, or sacrifice. For the d_L-group, same data as in Figure III.7. The vertical line indicates day 730 (terminal sacrifices). ML-estimated parameter values: $\bar{m} = 1114.36$ and $\bar{\sigma} = 574.05$ days (d_L-group); and $\bar{m} = 489.17$ and $\bar{\sigma} = 207.62$ days (d_H-group). Error measures: $\mathcal{E}^{\max}_{\text{fit}}(d_L) = -0.192$, $\mathcal{E}^{730}_{\text{fit}}(d_L) = -0.0711$, $\mathcal{E}^{730}_{\text{KM}}(d_L) = -0.0631$, $\mathcal{E}^{\max}_{\text{fit}}(d_H) = -0.0429$, $\mathcal{E}^{730}_{\text{fit}}(d_H) = 0.0405$, and $\mathcal{E}^{730}_{\text{KM}}(d_H) = 0.0793$.

III.7.3 Divergences among bioassays

Long-term carcinogenicity tests are time and money consuming bioassays. Therefore, cancer risk assessment is generally based on the results of one single long-term rodent test. But, what is the chance that the outcome of a single test accurately reveals the relation between exposure and incidence of tumors? This question can be addressed with the aid of computer-simulated bioassays.

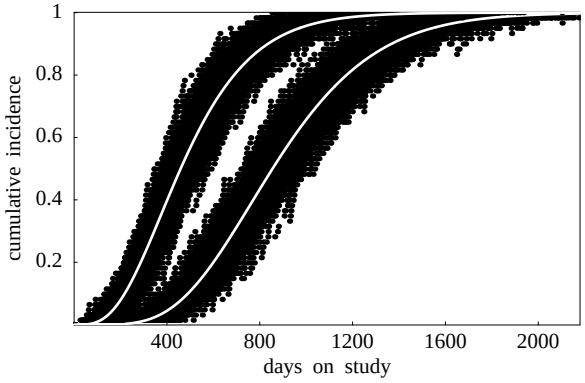

Figure III.9: Variation in tumor incidence among bioassays. Cumulative incidence of type $\mathcal{A}$ tumors in absence of competing causes of death. Data from 500 independent computer-simulated bioassays. The solid lines are the real cumulative tumor probabilities shown in Figure III.6.

Figure III.9 shows that, indeed, the observed tumor incidence can differ dramatically among bioassays, even in absence of competing causes of death. Consequently, the model fits depicted in Figure III.8 may not be representative, as they concern one single bioassay. I therefore simulated the $\mathcal{R}_{\mathcal{A}}$-bioassay 10,000 times and analyzed the capability of both the maximum likelihood approach (equation III.10) and the Kaplan-Meier method (equation III.2) to recover the real time-to-tumor distributions shown in Figure III.6. For this simulation study, I utilized the bioassay design illustrated in Figure III.8.*c*. The results of the simulations are summarized in Figures III.10 and III.11.

Figure III.10 shows the frequency of errors in the estimation of tumor-incidence among the 10,000 d_L-groups. The error range $[-1, 1]$ has been divided into 250 intervals of length 0.008. The histogram bars show the percentage of error values located within each interval for a sample of 10,000

variates. The three histograms, from top downwards, illustrate the distribution of $\mathcal{E}_{\text{fit}}^{\max}(d_L)$, $\mathcal{E}_{\text{fit}}^{730}(d_L)$, and $\mathcal{E}_{\text{KM}}^{730}(d_L)$ values, respectively. Figure III.11 shows the results for a similar simulation concerning 10,000 d_H-groups.

Figures III.10.*b* and III.10.*c* show that the distributions of the maximum likelihood and Kaplan-Meier estimation errors at day 730 are similar in shape. This means that for the d_L-group both methods provide equally good estimates of the final cumulative tumor incidence (FCTI), $F_T(730|d_L)$. In the d_H-group, however, the maximum likelihood (ML) approach behaves better than the KM-method. Compared to the KM-method, the ML-approach has a 12.15% higher chance to get an FCTI estimation that differs less than 5% from the real value.

In the example shown in Figure III.8.*c*, the $\mathcal{E}_{\text{fit}}^{\max}(d_H)$ value is much lower than the $\mathcal{E}_{\text{fit}}^{\max}(d_L)$ value. That is, the maximum likelihood prediction of the d_H time-to-tumor distribution is more accurate. This is in agreement with the shape of the corresponding error value distributions (Figures III.10.*a* and III.11.*a*). Indeed, the mean of both distributions is close to zero, but the standard deviation of $\mathcal{E}_{\text{fit}}^{\max}(d_H)$ is smaller than that of $\mathcal{E}_{\text{fit}}^{\max}(d_L)$. Consequently, the chance to get a maximum likehood estimate of F_T that differs less than 5% from F_T is 19.26% and 37.97% for the d_L- and d_H-group, respectively.

In Figure III.11.*c*, an isolated bar clearly stands out from the body of the $\mathcal{E}_{\text{KM}}^{730}(d_H)$ distribution. It is mainly due to the frequency of the error value 0.166. This maximum overestimation occurs when the last specimen dies with a tumor before day 730, which implies $\text{KM}(730) = 0$ (equation III.2) so that $D_{\text{KM}}(730) = 1 - 0.834 = 0.166$ (equation III.13). This observation suggests that the number of animals left after 730 days is important for the Kaplan-Meier FCTI-estimation. I explored this further in Figure III.12, which shows the relation between the $\mathcal{E}_{\text{KM}}^{730}(d_H)$ value and the number of animals alive after 730 days.

Figure III.12 displays $\mathcal{E}_{\text{KM}}^{730}(d_H)$ against the number of animals that are still alive at the end of the bioassay, N_{730}. In the boxplot, each box shows the median (50th percentile) error value as a line and the first (25th percentile) and third quartile (75th percentile) of the error value distribution as the lower and upper parts of the box. The area in the box thus represents the middle 50% of the values. The mean values are indicated with bullets. The 'whiskers' shown above and below the boxes represent the largest and smallest observed error values.

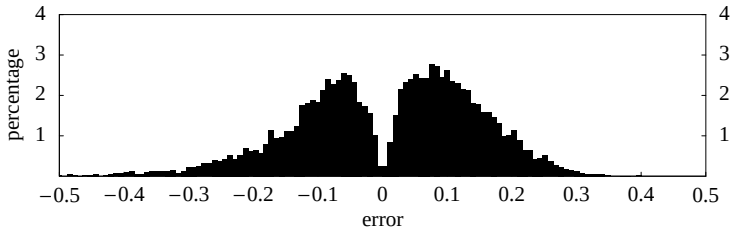

(a)

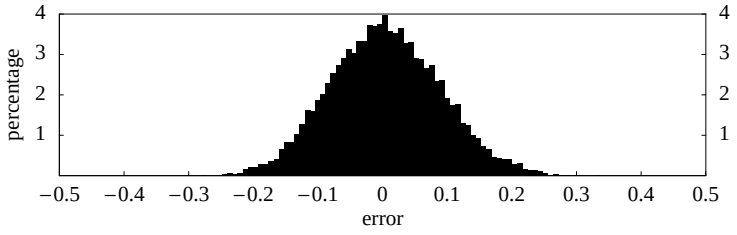

(b)

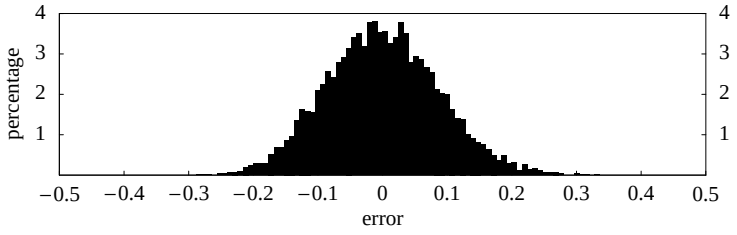

(c)

Figure III.10: Frequency of tumor-incidence estimation-errors among 10,000 randomly-generated bioassays (60 rats exposed to a dose d_L of $\mathcal{R}_{\mathcal{A}}$). The bars show the percentage of error values located within intervals of length 0.008. (**a**) Frequency of $\mathcal{E}_{\text{fit}}^{\max}(d_L)$ values. Mean value = 0.0071 and standard deviation = 0.138. The percentage of error values that lie between −0.05 and 0.05 is 19.26%. (**b**) Frequency of $\mathcal{E}_{\text{fit}}^{730}(d_L)$ values. Mean value = 0.00475 and standard deviation = 0.085. Percentage between −0.05 and 0.05: 43.67%. (**c**) Frequency of $\mathcal{E}_{\text{KM}}^{730}(d_L)$ values. Mean value = −0.000047 and standard deviation = 0.087. Percentage between −0.05 and 0.05: 42.93%.

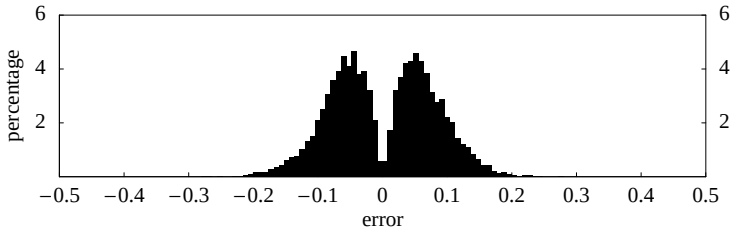

(a)

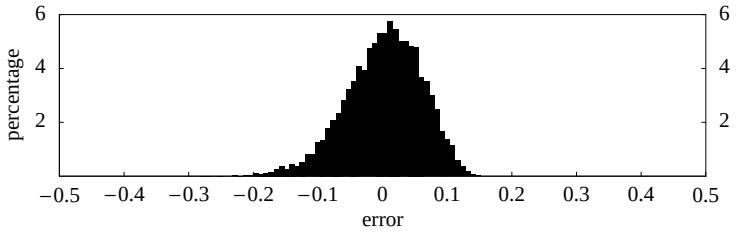

(b)

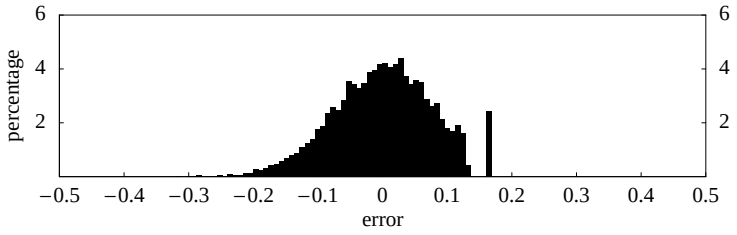

(c)

Figure III.11: Frequency of tumor-incidence estimation-errors among 10,000 randomly-generated bioassays (60 rats exposed to a dose d_H of $\mathcal{R}_{\mathcal{A}}$). The bars show the percentage of error values located within intervals of length 0.008. (**a**) Frequency of $\mathcal{E}_{\rm fit}^{\rm max}(d_H)$ values. Mean value = 0.00104 and standard deviation = 0.0779. The percentage of error values that lie between −0.05 and 0.05 is 37.97%. (**b**) $\mathcal{E}_{\rm fit}^{730}(d_H)$ values. Mean value = 0.0019 and standard deviation = 0.0585. Percentage between −0.05 and 0.05: 59.91%. (**c**) $\mathcal{E}_{\rm KM}^{730}(d_H)$ values. Mean value = −0.00066 and standard deviation = 0.076. Percentage between −0.05 and 0.05: 47.76%. For an explanation on the isolated bar, see text.

Figure III.12 suggests that there is a linear relation between $\mathcal{E}^{730}_{\rm KM}(d_H)$ and N_{730}. For a d_H-group of 60 rats (upper panel), according to the least-squares line obtained from 10,000 bioassays, the $\mathcal{E}^{730}_{\rm KM}(d_H)$ value is approximately zero if $N_{730} \approx 3.175$. In contrast, if $N_{730} > 3.175$, its value is negative. Below I argue that 3.175 concerns the expected number of animals alive at day 730 according to the real failure-time distributions.

A specimen is still alive after 730 days only if it does not die spontaneously before day 730 and it is not sacrificed at day 200 nor at day 400. The expected number of specimens that are still present in the study at day 730 can thus be calculated as:

$$E[N_{730}] = N_0 G_\dagger(730)(1 - P_{c200})(1 - P_{c400})$$

where N_0 is the initial number of animals, $G_\dagger(730)$ is given by equation III.12. P_{c200} and P_{c400} are the probabilities that a specimen is censored at day 200 and at day 400, which are given by:

$$P_{c200} = \frac{n_{c200}}{N_0 G_\dagger(200)}$$
$$P_{c400} = \frac{n_{c400}}{N_0 G_\dagger(400)(1 - P_{c200})}$$

with n_{c200} and n_{c400} the number of animals sacrificed at day 200 and at day 400, respectively. Substitution of the equations above into the expression for $E[N_{730}]$ leads to:

$$E[N_{730}] = G_\dagger(730)\left(N_0 - \frac{n_{c200}}{G_\dagger(200)} - \frac{n_{c400}}{G_\dagger(400)}\right) \qquad \text{(III.14)}$$

In the d_H-group, for $N_0 = 60$, $n_{c200} = 10$, and $n_{c400} = 10$, the expected number of remaining animals at day 730 is $E[N_{730}] = 3.178$, whereas for $N_0 = 100$, $n_{c200} = 10$, and $n_{c400} = 10$, the expected number of remaining animals at day 730 is $E[N_{730}] = 7.215$. These $E[N_{730}]$ values are in agreement with the roots of the straight lines depicted in Figure III.12. Thus, for N_{730} values larger than $E[N_{730}]$, the KM-method has a clear tendency to underestimate the FCTI.

Acknowledgements

The author thanks José Ferreira and Cor Zonneveld for their insightful suggestions.

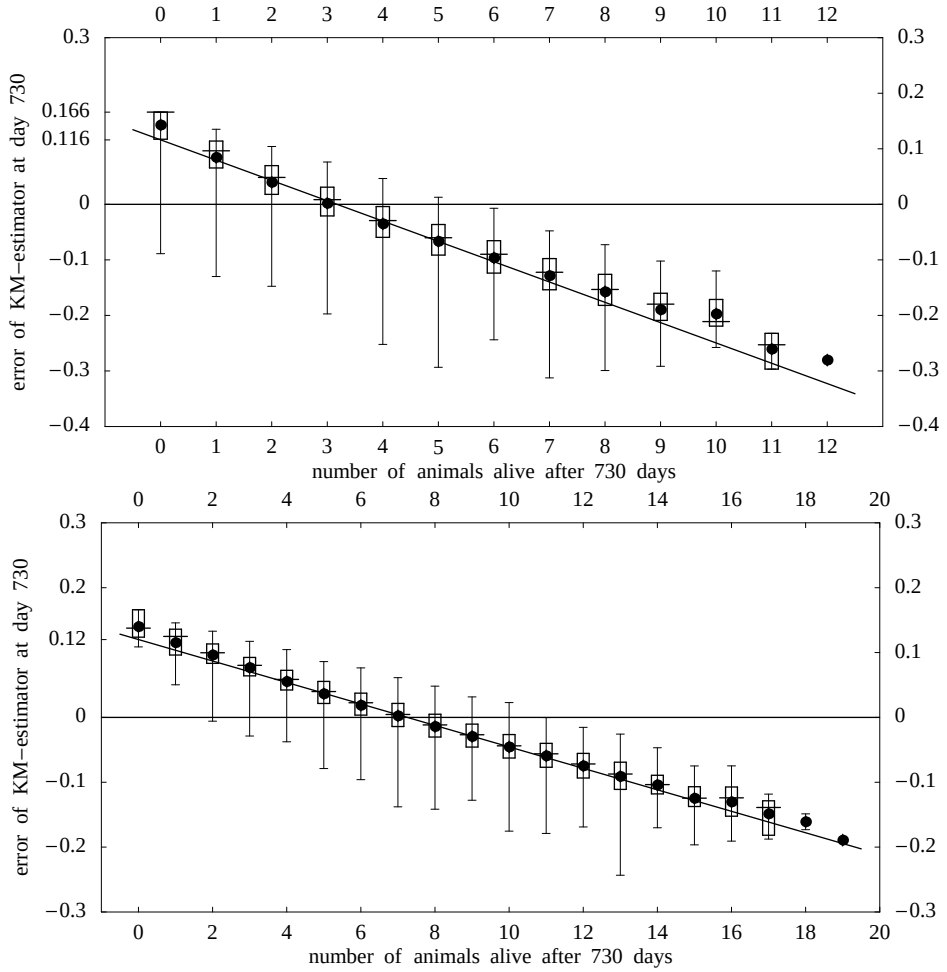

Figure III.12: Boxplot summarizing the relation between the $\mathcal{E}_{\mathrm{KM}}^{730}(d_H)$ values and the number of animals that are still alive at day 730. Data from 10,000 randomly-generated bioassays. Each box shows the median as a line and the first and third quartile of the error value distribution as the lower and upper parts of the box. The mean values are indicated with bullets (•). The whiskers shown above and below the boxes represent the largest and smallest observed error values. *Upper panel:* $N_0 = 60$. Same $\mathcal{E}_{\mathrm{KM}}^{730}(d_H)$ values as in Figure III.11.*c*. Least-squares fitting of a straight line gives: $y_1(x) = 0.116 - 0.0365x$, which satisfies $y_1(0) = 0.116$ and $y_1(3.175) = 0$. *Lower panel:* $N_0 = 100$. Least-squares fitting of a straight line gives: $y_2(x) = 0.12 - 0.0165x$, which satisfies $y_2(0) = 0.12$ and $y_2(7.25) = 0$.

IV

MODELING OXIDATIVE DAMAGE AND AGING

"*The secret to all the chemistry of oxygen, whether we think of it as* 'good' *or* 'bad,' *is the formation of free radicals,*" **N. Lane**

"*With a little luck, there's no reason why you can't live to be one hundred. Once you've done that, you've got it made, because very few people die over one hundred,*" **G. Burns**

A mathematical model that accounts for the effects of caloric restriction on body weight and longevity

Adapted from:
I.M.M. van Leeuwen, F.D.L. Kelpin, and S.A.L.M. Kooijman (2002)
Biogerontology, 3(6): 373–381

Abstract
Several aspects of energy dynamics, such as energy expenditure and caloric intake, are known to affect the aging process. In this Chapter, we therefore model the aging process within a mathematical framework describing the energy dynamics of an organism. The resulting model comprises food intake, body growth and survival. The equation for the mortality rate accounts for food consumption and is suited to describe caloric restriction data. For non-growing animals, the expression for the mortality rate reduces to the well-known Gompertz equation. We successfully applied our model to growth and survival data on mice exposed to different food levels.
Keywords
Dietary restriction; Dynamic Energy Budget theory; free radicals; metabolic rate; mitochondrial aging theory; senescence.

IV.1 Introduction

Energy dynamics and aging seem to be strongly correlated. This is best illustrated by the effects of caloric restriction. Studies on caloric restriction carried out with different organisms, ranging from rotifers to rhesus monkeys [183, 198, 260], have revealed that calorically-restricted animals not only live longer but also have fewer age-associated diseases. The aim of this Chapter is to formulate a simple mathematical model that quantitatively links aging to food consumption and body growth.

The model we present consists of two parts, a general mathematical framework describing energy dynamics and a module dealing with aging. The former provides quantitative expressions for characteristics and processes such as food consumption, fat content, body growth, and metabolic

rate. It is a slightly adapted version of the Dynamic Energy Budget (DEB) theory as developed by Kooijman [116, 117]. The aging module of the model is based on the free radical theory, which argues that senescence is the result of intracellular damage inflicted by free radicals [82, 61]. Oxidative damage to mitochondria [130, 159], which results in an increase in the generation rate of free radicals, plays an important role in this module as it entails an acceleration of the whole aging process.

An important link between the general framework and the aging model is the concept of 'rate of living' [181, 247]. This link is supported by the observation that intracellular generation of free radicals is predominantly a function of metabolic rate [61, 209, 211]. In the context of the DEB-theory, the rate of living is best characterized by the so-called utilization rate, or catabolic rate, i.e., the total energy expenditure per time unit. As the catabolic rate is a function of food consumption, we obtain a quantitative expression for the relationship between life expectancy and food consumption.

The remainder of this Chapter is organized as follows. We first briefly explain the general framework, comprising food consumption, body growth and catabolic rate. Thereafter we present our mathematical model for aging. We show that our approach leads to a biologically-based interpretation of the widely used Gompertz model. Finally we confront our model with experimental data [246] on growth and survival of mice kept on various levels of caloric restriction.

IV.2 DEB-based model for energy dynamics

The aim of this Chapter is to model the aging process within a general framework describing the energy dynamics of an individual. A set of rules to characterize intake and use of energy, which qualifies for our purposes, is provided by the Dynamic Energy Budget (DEB) theory. It is based on fundamental mechanisms that all organisms seem to have in common. The basic structure of the DEB-theory is depicted in Figure IV.1. It assumes that the body consists of two components: reserve materials (stored energy) and structural biomass. The model for an individual therefore comprises a set of two differential equations. The total weight of an animal at a certain time (age) is given by the sum of the weights of its structure and reserves at that time (age). For an introduction to the wide range of applications of the DEB-theory, we refer the reader to reference [118] and for an exhaustive description to [117].

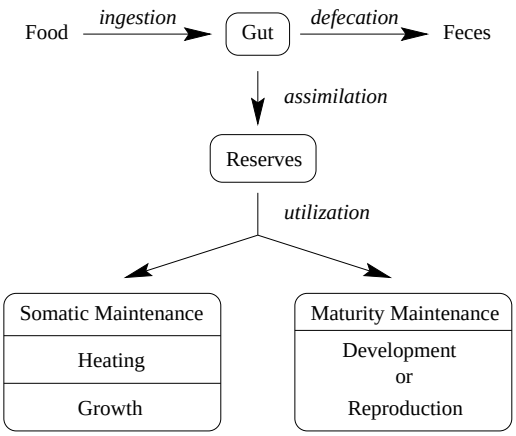

Figure IV.1: Energy fluxes according to the DEB-theory. Food is conceived as material bearing energy. Part of this energy is taken up via the blood and delivered to the reserves. Energy required to carry out the various physiological processes is obtained from these reserves. A fixed proportion of the utilized energy is spent on growth plus somatic maintenance plus heating, whereas the remainder proportion is spent on maturity maintenance plus development (embryos and juveniles) or reproduction (adults). According to the DEB-theory, the body consists of two components, namely structure and reserve materials (stored energy). This decomposition is useful for the quantification of maintenance costs, as these costs are assumed to be paid for structural biomass only. Constant chemical composition is assumed for both structure and reserves.

In this Chapter we focus on the effects of caloric-restriction (CR) on the body weight and life expectancy of laboratory rodents. Mice and rats as experimental animals have the advantage that a lot is known about their physiology and, in particular, about their diet requirements. This substantially increases the probability that during a CR-study the condition 'undernutrition without malnutrition' is fulfilled.

Several long-term studies with mice and rats have shown that *ad libitum* food consumption is approximately constant during the study period [96, 112, 125]. As the animals usually grow during the study period (e.g., Figure IV.2), this observation implies that food consumption in laboratory rodents is independent of body size. This is in conflict with the finding that the feeding-rate of wild animals increases with body size [111, 250]. Since the DEB-theory assumes an increase in the ingestion rate with body size, a first step in modeling the physiology of laboratory rodents is to adapt the DEB theory to account for constant food consumption.

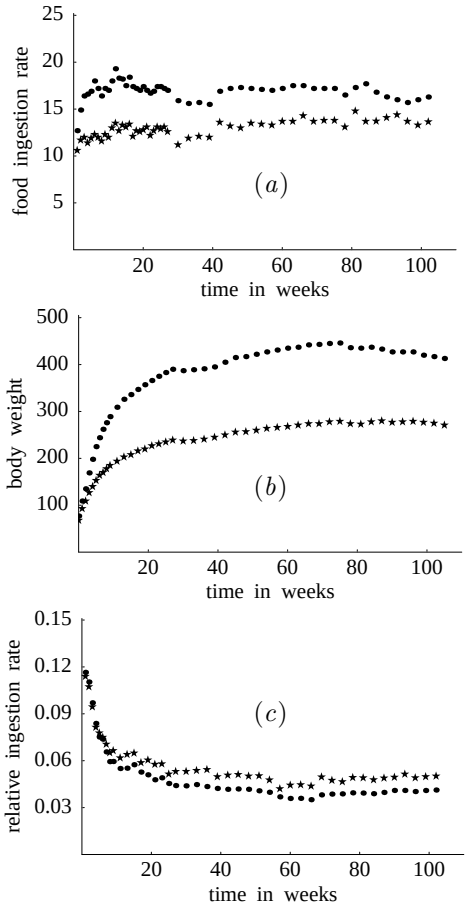

Figure IV.2: Food consumption and body growth of male (•) and female (⋆) control rats. Food and tapwater were supplied *ad libitum*. Data from B[a]P-RIVM study (Section III.2.2). The animals were approximately 6 weeks of age at study initiation [125]. (a) Average food consumption rate (gram per day); (b) Body weight (gram) as a function of time; and (c) Average food consumption per body weigth per day. Female rats have a higher relative ingestion rate than male rats.

Most caloric-restriction studies share a common experimental design. Animals are organized in different diet-groups that either have food available *ad libitum* or receive a fixed fraction ϱ of *ad libitum* food consumption. In mathematical terms this means that, for any diet-group, the constant food ingestion rate I can be written as:

$$I = \varrho I_m \tag{IV.1}$$

where I_m is the (diet-composition specific) maximum food consumption rate and ϱ is a coefficient satisfying $0 < \varrho \leq 1$. If an animal receives *ad libitum* feeding, $\varrho = 1$ and $I = I_m$. If it instead receives 75% of *ad libitum* food consumption, $\varrho = 0.75$ and $I = 0.75 I_m$.

The expression for the ingestion rate (equation IV.1) can be incorporated into the DEB model to obtain expressions for the change in the amount of

reserves and structure. The resulting set of differential equations is shown in Table IV.1 (equations IV.2 and IV.3), whereas the mathematical model development is summarized in Appendix A. In Table IV.1 the variable V represents structural volume, whereas e represents the so-called scaled reserve-density. The presence of the coefficient ϱ in equation IV.2 indicates that food intake directly influences reserve density. It can be shown that a lower food availability results in a lower reserve density. Equation IV.4 shows how total body weight $W(t)$ depends on structural volume and scaled reserve density. Below we will use this expression to estimate model parameters from observed body weights. Finally, equation IV.5 provides the expression for the scaled catabolic-rate $c(t)$, which is defined as the catabolic rate $C(t)$ divided by the maximum reserve density.

IV.3 A simple model for aging

As we said in Section IV.1, our aging model is based on the assumption that oxidative damage is responsible for age-associated physiological decline. At any time (age) the amount of accumulated oxidative damage determines the chance to survive. This idea is incorporated into the model by taking the hazard rate proportional to the amount of oxidative damage per unit structural volume:

$$h(t) = \beta \frac{D(t)}{V(t)} \tag{IV.6}$$

$$S(t) = \mathrm{e}^{-\int_0^t h(s)\mathrm{d}s}, \qquad t \geq 0 \tag{IV.7}$$

where h is the mortality rate or hazard rate, D the amount of oxidative damage, and V the structural volume. We will refer to the fraction $\frac{D}{V}$ as damage density. The coefficient β is the damage-specific killing rate, which is assumed to be independent of time (age). Equation IV.7 is the mathematical relation between the hazard rate and the survivor function; $S(t)$ denotes the probability that an animal is still alive at time (age) t. For further details on the hazard and survivor functions, see Chapter III (Section III.5).

In the previous section we obtained an expression for V, which depends on food availability (equation IV.3). Yet a characterization of the hazard rate (equation IV.6) also requires an expression for D. To deduce an expression for D, in this section we give a step-by-step explanation of the processes summarized in Figure IV.3, starting from the generation of free radicals.

The main source of oxidative damage are Reactive Oxygen Species (ROS), with some additional contributions by reactive nitrogen species [251]. Reac-

Table IV.1: Equations for energy dynamics. Dimensions: − no dimension; L length; M mass; T time; # amount.

$$\frac{\mathrm{d}e}{\mathrm{d}t} = \frac{v}{V^{\frac{1}{3}}}\left(\varrho\frac{V_{1\infty}^{\frac{2}{3}}}{V^{\frac{2}{3}}} - e\right) \tag{IV.2}$$

$$\frac{\mathrm{d}V}{\mathrm{d}t} = \frac{v}{e+g}\left\{\left(e - \frac{V_h^{\frac{1}{3}}}{V_m^{\frac{1}{3}}}\right)V^{\frac{2}{3}} - \frac{V}{V_m^{\frac{1}{3}}}\right\} \tag{IV.3}$$

$$W = d_V\left(1+\xi e\right)V \tag{IV.4}$$

$$c = e\left(vV^{\frac{2}{3}} - \frac{\mathrm{d}V}{\mathrm{d}t}\right) \tag{IV.5}$$

Parameter	Dimension	Interpretation
d_V	ML^{-3}	Structural-volume specific weight
g	-	Growth energy-investment ratio
v	LT^{-1}	Energy conductance
V_h	L^3	Volume reduction due to heating
V_m	L^3	Ectothermic maximum volume
$V_{1\infty}$	L^3	Maximum structural volume
ξ	-	Scaled reserve specific weight
ϱ	-	Food-supply coefficient
Variable	**Dimension**	**Interpretation**
e	-	Scaled reserve-density
V	L^3	Structural volume
W	M	Total body weight
c	L^3T^{-1}	Scaled catabolic-rate

tive species are continuously generated in cells as a consequence of reactions involved in, for instance, the respiratory chain, in phagocytosis, and in the P-450 system [83]. However, it is known that most intracellular ROS are produced by the mitochondria. Mitochondria consume more than 90% of cellular oxygen and, *in vitro*, transform 1–2% of the consumed molecules into superoxide anions [61]. The generation of ROS is thus directly related to the rate of oxygen consumption and indirectly to the rate of living. Our first assumption states that the intracellular ROS-generation rate is proportional to the catabolic rate:

$$J_+(t) = \alpha(t)C(t) \tag{IV.8}$$

where $J_+(t)$ is the ROS-production rate at time (age) t, $C(t)$ the catabolic rate at that time, and $\alpha(t)$ stands for the amount ROS produced per utilized reserve-unit. Below we will argue that the value of α varies in time because it depends on the amount of accumulated oxidative damage.

The reactivity of ROS is so great that the time delay between generation and interaction with a cellular component is very small [149]. We assume that the lifespan of ROS is negligibly short. Consequently, the rate of ROS production (J_+) immediately translates into a rate of ROS reaction (J_r). Further we assume that a fixed fraction of the produced ROS is inactivated by antioxidant defense systems, whereas the remaining fraction γJ_+ actually interacts with cellular components. The balance between ROS production and elimination thus determines the level of oxidative damage:

$$J_r(t) = J_+(t) - J_-(t) = \gamma J_+(t) \tag{IV.9}$$

with $J_-(t)$ the ROS-elimination rate at time (age) t.

The change in the amount of oxidized macromolecules is not only determined by the rate of ROS reaction and the ability of the interacting ROS to cause damage, but also by rate of repair or degradation of damaged cell components. In addition, we assume that an amplification of damage occurs as a consequence of existing damaged macromolecules. The change in the amount of oxidized macromolecules is given by:

$$\frac{\mathrm{d}D}{\mathrm{d}t} = zJ_r + xD - yD \tag{IV.10}$$

where the first term stands for the ROS-mediated oxidation rate, the second for the rate of damage production due to amplification, and the third for the rate of repair (or degradation) of oxidized macromolecules. The coefficient z depends on the ability of the reacting ROS to cause oxidative damage relevant to the aging process.

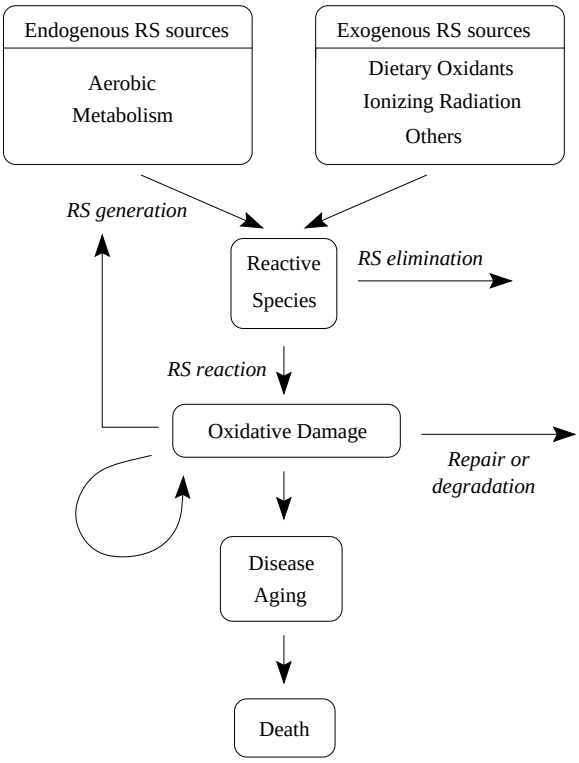

Figure IV.3: Basic structure of the aging module. Reactive species (RS) are generated during normal aerobic metabolism. Additional RS can come from exogenous sources. A fraction of the generated RS is eliminated, whereas the remainder fraction reacts with cellular components causing oxidative damage. Oxidized macromolecules can be either repaired or degraded. Oxidative damage accelerates the aging process via two 'feedback' mechanisms. Accumulated oxidative damage is responsible for physiological decline eventually resulting in the death of the organism.

Reactive species have been shown to attack most cellular components, including nuclear DNA, lipids, and mitochondria [78, 222]. Oxidative damage to mitochondria is of special interest as it engenders an increase in ROS generation, thereby accelerating the whole aging process (see Figure IV.3). Indeed, damage in the mitochondrial DNA has been shown to inhibit the initial and middle segments of the respiratory chain, leading to massive production of superoxide radicals [179]. Moreover, proteins of the electron transport system are preferentially targeted for oxidation [222], which may result in a less accurate activity. In mathematical terms, the occurrence of damage-mediated amplification of ROS generation means that the coefficient α (equation IV.8) is an increasing function of the amount of accumulated oxidative damage. We assume that this function is linear in D, so that the ROS-production rate is given by $J_+(t) = [\alpha_0 + \alpha_1 D(t)]C(t)$. This expression, together with equations IV.9 and IV.10, leads to:

$$\frac{\mathrm{d}D}{\mathrm{d}t} = [(x-y) + \alpha_1 z\,\gamma\,C]D + \alpha_0 z\,\gamma\,C$$

This equation can be rewritten as follows:

$$\frac{\mathrm{d}D}{\mathrm{d}t} = [\psi + \phi\,c]D + \varphi\,c \tag{IV.11}$$

with c the scaled catabolic rate (equation IV.5). The compound parameter ψ is defined as $x-y$, the compound parameter ϕ is the product of $\alpha_1 z\,\gamma$ and the maximum reserve density, and φ is the product of $\alpha_0 z\,\gamma$ and the maximum reserve density. Equation IV.6 together with equation IV.11 constitute our model for aging.

Before confronting the model with experimental data, we want to compare our approach with the model most frequently used to describe survival data: the Gompertz model [60, 72]. When body size remains constant, according to equations IV.2 and IV.5, reserve density and catabolic rate also remain constant in time. Let c_* denote the constant scaled catabolic-rate of a fully grown animal. If in addition the parameter φ has value zero, integration of equation IV.11 provides a simple expression for the scaled oxidative damage: $D(t) = D(0)\mathrm{e}^{(\psi+\phi\,c_*)t}$. Substitution of this expression into the mortality rate (equation IV.6), leads to $h(t) = \beta\frac{D(0)}{V(0)}\mathrm{e}^{(\psi+\phi\,c_*)t}$. This can be rewritten as:

$$h(t) = h_0\mathrm{e}^{\eta t}, \qquad t \geq 0 \tag{IV.12}$$

with $h_0 = \beta \frac{D(0)}{V(0)}$ the initial or baseline mortality rate, and $\eta = \psi + \phi\, c_*$ the exponential mortality-rate coefficient. This is the well-known Gompertz equation, which quantifies the observation that the mortality rate usually increases exponentially with age. Interestingly, we now have obtained a biological interpretation of the Gompertz parameters. The initial mortality h_0 is the product of the damage-density at $t = 0$ and the constant scaled killing rate. Obviously the initial damage density depends on the amount ROS produced until the beginning of the study, but it is independent of what happens thereafter. The exponential mortality-rate coefficient η is a linear function of the catabolic rate. It thus depends on the food level and varies among species. Different species not only differ in their catabolic rates, but also in the values for ψ and ϕ because these parameters depend on processes such as elimination of ROS and repair of oxidative damage.

IV.4 Results and discussion

In 1996, Sohal and Weindruch claimed that any causal hypothesis for senescence should explain at least the following three observations:

(*i*) organisms undergo progressive physiological decline with age;

(*ii*) caloric-restriction (CR) extends the average and maximum lifespan of organisms;

(*iii*) life expectancy varies within and among species.

Although such causal hypotheses are usually stated verbally, they can also be cast in the form of a mathematical model. Senescence then appears as a mortality rate that increases with age. Such an approach has the added benefit of quantitative testability.

The model we present in this Chapter is based on the free radical theory for aging, which attributes age-associated physiological decline to intracellular oxidative damage. Several authors, including Sohal and Weindruch themselves, have claimed that the free radical theory satisfactorily justifies the first observation. In the previous Section we showed that a simple version of our model reduces to the Gompertz model. Indeed, our model can be seen as a biologically-based generalization of the Gompertz model that accounts for body growth and level of food availability. Even the reduced version (Gompertz model) describes survival data well and, thus, succeeds in explaining the age-associated increase in mortality rate in a quantitative sense.

Both a decreased energy expenditure and a retarded increase in the level of oxidative stress have been reported in calorically-restricted animals [193, 258, 259]. The hypothesis for aging illustrated in Figure IV.3 therefore suggests that CR affects the mortality rate by decreasing the catabolic rate and, thus, by decreasing the level of oxidative damage. To test if the model satisfies the second condition in a quantitative sense, we confronted it with CR data from Weindruch *et al.* (1986). The study includes three groups of mice that are exposed to three different food levels: *ad libitum*, 85 kcal/week (25% restriction), and 50 kcal/week (56% restriction). According to the terminology introduced in Section IV.2, this means that ϱ has values 1, 0.75, and 0.44, respectively. We fitted the three body-weight data sets simultaneously (see Appendix B). The growth curves corresponding to the estimated parameter values are depicted in Figure IV.4.

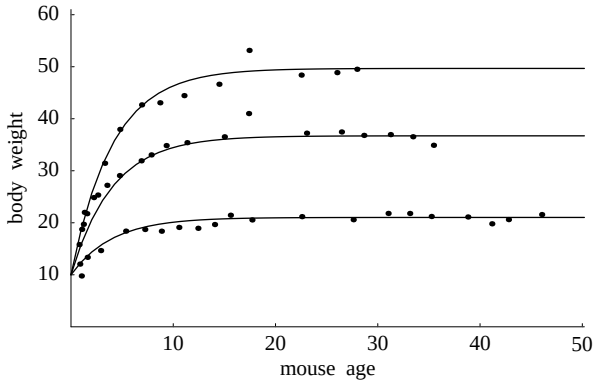

Figure IV.4: Average body weight $W(t)$ as a function of time (age). Data from Weindruch *et al.* (1986). From the top downwards the relative food level ϱ equals 1, 0.75, and 0.44, respectively. We fitted the three body-weight data sets simultaneously. Details on the fitting procedure and on the estimated parameter values are provided in Appendix B.

Once values for all the DEB-parameters (Table IV.1) have been estimated, we are able to calculate the corresponding scaled catabolic-rate. Figure IV.5 shows the scaled catabolic-rate per structural biomass. We predict a clear difference in scaled catabolic-rate per structural biomass among the diet-groups at the beginning of the study. However, this difference eventually disappears with the passage of time. This is in agreement with the experimental observations: "In general, whole-body studies have reported an

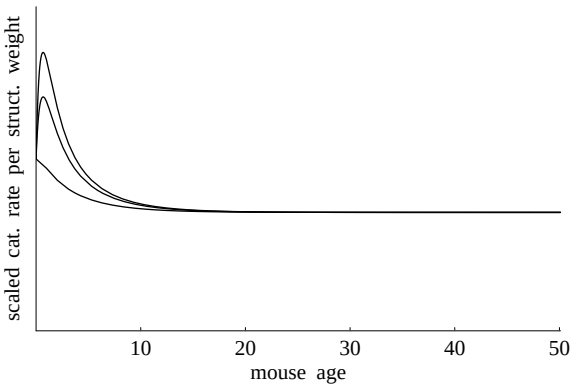

Figure IV.5: Model simulation of the scaled catabolic-rate per structural body weight, $\frac{1}{d_V}\frac{c(t)}{V(t)}$ where $V(t)$ is given by equation IV.3 and c by equation IV.5. Parameter values as in Figure IV.4. From the top downwards the relative food level ϱ equals 1, 0.75, and 0.44, respectively. Initially, caloric-restriction results in a decrease in the catabolic rate per structural biomass. However, later on this difference disappears. This is in agreement with the experimental observations on energy expenditure.

acute decrease in mass-adjusted energy expenditure that disappears with long-term energy restriction [193]."

With the parameter values obtained above, the state variables $c(t)$ and $V(t)$ in the aging module (equations IV.6 and IV.11) are known. Food consumption indirectly influences survival through these two quantities. That is, the model predicts differences in longevity on the basis of differences in energy dynamics. We fitted the three survival data sets simultaneously (see Appendix B). As can be seen from Figure IV.6, our model is able to explain differences in survival on the basis of the differences in food consumption and, therefore, satisfies Sohal and Weindruch's second condition.

To describe the survival data shown in Figure IV.6, the Gompertz model can be used. However, because it does not account for the food level, the survival data of the three diet-groups can only be fitted independently of each other. This means that a total of 4 parameter values are required (three values for η and one value for h_0). Notice that the number of parameters depends on the number of diet-groups considered. So, for four diet-groups, 5 parameter values have to be estimated. Figure IV.7 depicts the result of fitting three independent Gompertz curves (broken lines) as well as the result of fitting simultaneously the three data sets with our model. As can be seen from this figure, the quality of the fits is almost the same. Our

model has the advantage that the number of parameters does not depend on the number of diet-groups considered. Moreover, it has the additional advantage that predictions can be made on the body weight and longevity of animals exposed to alternative feeding-conditions.

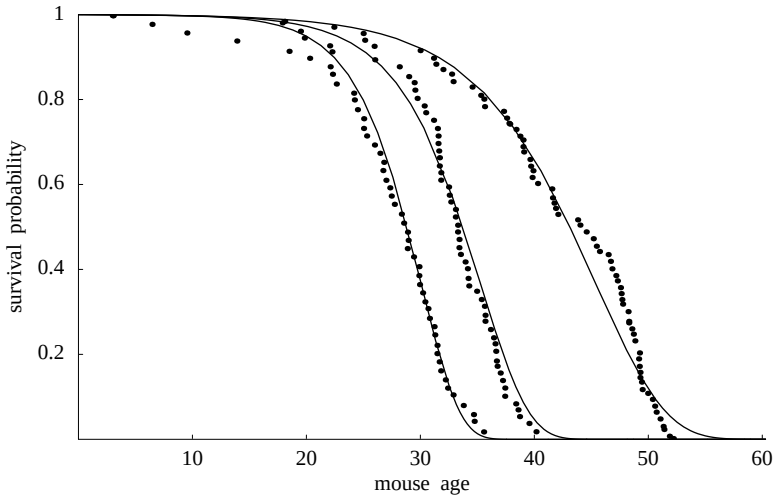

Figure IV.6: Survival probability $S(t)$ as a function of time (age). Data from Weindruch *et al.* (1986). From left to right ϱ equals 1, 0.75, and 0.44, respectively. DEB-parameter values as in Figure IV.4. We fitted the three survival data sets simultaneously. Details on the fitting procedure and on the estimated parameter values are provided in Appendix B.

The third of Sohal and Weindruch's conditions concerns intra and inter-species differences in mortality rates. In the present Chapter, we focus on growth and mortality of animals with constant food consumption, such as laboratory rodents. The aging module, however, is based on fundamental mechanisms that are not species-specific. If it is combined with the DEB-model as presented in Kooijman (2000), the resulting model can be used to describe the growth and mortality of animals with alternative food intake behavior. To fulfill the third condition, differences in parameter values should account for the differences in mortality rates. The DEB theory includes rules to compare energy dynamics among species. The so-called primary scaling relationships link differences in body size to differences in parameter values. The primary scaling relationships allow the derivation of body-size scaling relationships for a variety of eco-physiological features such as food ingestion, respiration, catabolic rate, and body growth. Further research is

needed to extend this approach to obtain body-size scaling relationships for the aging process.

It has been argued that, in addition to Sohal and Weindruch's general observations, a hypothesis for aging should also explain some more specific features of mortality kinetics. Gavrilov and Gavrilova (2001), for instance, argued that it should explain the exponential increase in mortality rates with age observed in many adult species (Gompertz law) and the occurrence of late-life mortality deceleration. With regard to the former, in the previous section we showed that, for adult non-growing animals, our model reduces to the Gompertz equation. Mortality deceleration at older ages can be described in the context of our model as the consequence of the selection of a special subpopulation. Late-life plateaus thus occur because animals that reach advanced ages are genetically different.

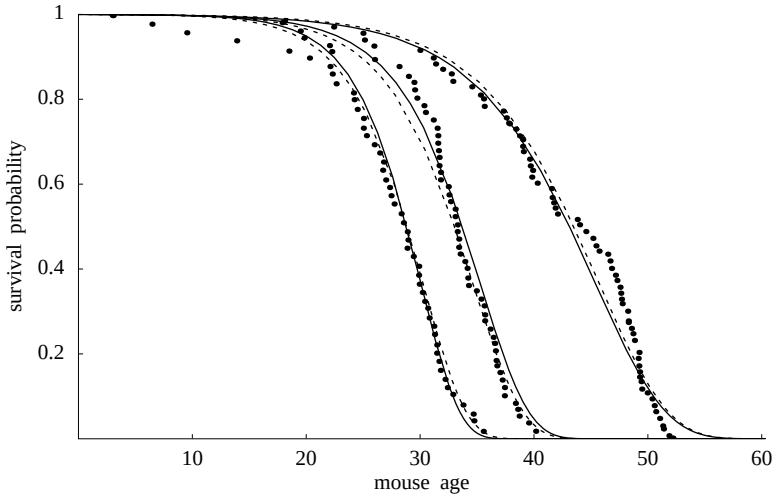

Figure IV.7: Comparison with the Gompertz model. Broken lines: Gompertz curves. Solid lines: same curves as in Figure IV.6. Data from Weindruch *et al.* (1986). As the Gompertz model (equation IV.12) does not account for food consumption, three different values for the exponential mortality-rate coefficient η have been estimated. In contrast, our aging model (equation IV.6) naturally accounts for food consumption and the three data sets have, thus, been fitted simultaneously. Details on the fitting procedure and on the estimated parameter values are provided in Appendix B.

Many biogerontologists have argued that aging is a multicausal process. The model we present reflects this. It integrates elements of three major theories for aging, namely the free radical theory, the rate of living theory and the mitochondrial theory for aging. Further research is needed to explore the relationship between our model and other theories for aging, such as the disposable soma theory [109, 110] and the telomere loss theory [5, 178]. The former states that longevity is determined by optimizing the investments in somatic maintenance and reproduction. As the DEB-theory provides quantitative expressions for the costs of both somatic maintenance and reproduction, analysis of the trade-off between mortality and reproduction is possible within the context of our model. The telomere loss theory argues that mitosis-associated progressive telomere shortening is responsible for cellular (replicative) senescence. It has been observed that the rate of telomere loss depends on the level of oxidative stress [264]. The consequences of this observation can be studied quantitatively with aid of our model. These subjects are, however, beyond the scope of the present Chapter.

As explained above, our model can be used to explore proposed hypotheses for aging. It can also be used to elucidate the effects of external factors that may influence the aging process. In this Chapter, for example, we studied the influence on longevity of long-term caloric restriction. Moreover, Figure IV.3 shows how exposure to dietary oxidants can be incorporated into the model. Other factors whose effect can be quantified are upregulation of antioxidant defenses and exposure to stress. A response to such events can be modeled as a change in DEB-parameters or in aging parameters.

Finally, we conclude by summarizing the most salient features of the model presented in this Chapter: (1) we developed a physiologically-based model for aging that is rather simple from a mathematical point of view. This is illustrated by the possibility to estimate the required parameter values from growth and survival data only; (2) the model is able to predict differences in survival on the basis of differences in food consumption. As can be seen from Figure IV.6, the model not only predicts CR-animals to live longer, but also provides CR-survival curves that are consistent with the experimental observations; (3) we obtained an interpretation of the Gompertz-parameters in terms of DEB-parameters. We deduced that the exponential mortality-rate coefficient η is a function of the catabolic rate and, thus, depends on food supply; (4) the aging module is based on fundamental mechanisms that are not species-specific; and (5) as explained above, the model can be extended to incorporate other mechanisms of aging or to

elucidate the consequences of several influential factors. In sum, the model presented in this Chapter constitutes a useful tool for modeling aspects of aging.

Acknowledgements

The authors thank Jacques Bedaux, Bernd Brandt, Bob Kooi, Cor Zonneveld, and two anonymous referees for advice. The work presented in this Chapter is part of the research project DEBtum (VBI-4692), financially supported by the Netherlands Technology Foundation (STW) and DSM.

Appendix

A. DEB model with constant food consumption

According to the DEB-model, the assimilation efficiency is independent of the ingestion rate and, consequently, the assimilation rate relates to the ingestion rate as $A/A_m = I/I_m$, with A_m the (diet-composition specific) maximum assimilation rate. The term 'assimilated energy' refers to the energy content of the ingested food minus the energy content of the feces and minus all energy losses during the digestion process. As can be seen from equation IV.1, we assume that I/I_m equals ϱ, which implies $A/A_m = \varrho$. Let us define the surface-area specific maximum assimilation rate as $\{A_m\} = A_m V_{1\infty}^{-2/3}$, with $V_{1\infty}$ the *ad libitum* maximum structural volume. The assimilation rate is then given by:

$$A = \varrho\{A_m\}V_{1\infty}^{\frac{2}{3}} \tag{IV.13}$$

As can be seen from Figure IV.1, the change in the amount of reserves is given by the difference between the assimilation and utilization rates, i.e., $\frac{\mathrm{d}E}{\mathrm{d}t} = A - C$. The change in scaled reserve density ($e = \frac{E}{[E_m]V}$) is then:

$$\frac{\mathrm{d}e}{\mathrm{d}t} = \frac{1}{[E_m]}\frac{\mathrm{d}}{\mathrm{d}t}\frac{E}{V} = \frac{1}{[E_m]}\left(\frac{A-C}{V} - \frac{E}{V^2}\frac{\mathrm{d}V}{\mathrm{d}t}\right) \tag{IV.14}$$

where $[E_m]$ represents the maximum reserve density of the fully grown adult and $V(t)$ the structural volume of the organism at time t. According to the DEB-model, the utilization rate (catabolic rate) is:

$$C = \frac{E}{V}\left(vV^{\frac{2}{3}} - \frac{\mathrm{d}V}{\mathrm{d}t}\right) \tag{IV.15}$$

with $v = \{A_m\}/[E_m]$ the energy conductance. An important property of $C(t)$ is that it only depends on the structural volume of the organism and its reserve density. The scaled catabolic rate (equation IV.5) is defined as $c = C/[E_m]$.

Substitution of the expressions for A (equation IV.13) and C (equation IV.15) into equation IV.14, leads to equation IV.2. According to the DEB-model [117],

the change in structural body volume is given by equation IV.3. Food availability indirectly influences growth via the reserve density. For $\varrho = 1$, the scaled reserve density (equation IV.2) tends to 1 and growth (equation IV.3) ceases when the structural volume approaches its maximum value $V_{1\infty} = (V_m^{1/3} - V_h^{1/3})^3$.

The total body weight of an organism is the sum of the weights of the two body components: $W(t) = W_V(t) + W_E(t) = d_V V(t) + d_E \frac{E(t)}{r_E}$, with r_E defined as $\frac{\text{amount reserves}}{\text{volume reserves}}$. The coefficients d_V and d_E represent the volume-specific weights of structure and reserves, respectively. The expression above can be rewritten as shown in equation IV.4, where $\xi = \frac{d_E}{d_V} \frac{[E_m]}{r_E}$.

B. Fitting procedures

At the beginning of the caloric-restriction CR-study, a population of mice is split into three groups after weaning [246]. This entails that the three diet-groups share the same initial conditions at $t = 0$ or, equivalently, the parameter values $W(0)$, $e(0)$ and $D(0)$ are equal for all groups. The same holds for the Gompertz parameter h_0.

Body-weight data (Figure IV.4)

At the start of the study ($t = 0$) the animals have an average weight of 10 g [246]. We therefore took $W(0) = 10$ g for any diet-group. In addition, we fixed d_V on a value of 1 g/cm^3 [117]. Because all mice received *ad libitum* feeding until the beginning of the CR-study, the assumption that $e(0) = 1$ is appropriate [117]. We fitted our growth model (equation IV.4) to the three body-weight data sets simultaneously to obtain values for v, g, ξ, V_h, and V_m (5 parameters). Please note that because $V_{1\infty}$ can be expressed in terms of V_m and V_h (see Appendix A), only values for the latter two parameters need to be obtained during the least-square fitting procedure. The estimated DEB-parameter values are: $\bar{g} = 6.43$, $\bar{v} = 5.71$ cm month^{-1}, $\bar{V}_h = 1.4\ 10^{-7}$cm^3, $\bar{V}_m = 42.05$ cm^3, and $\bar{\xi} = 0.19$. The corresponding growth curves are depicted in Figure IV.4.

Survival data (Figures IV.6 and IV.7)

Because we do not have data on the amount of oxidative damage, $D(t)$, not all five aging-parameters (ψ, ϕ, φ, β, and $D(0)$) can be estimated. The parameters φ, β and $D(0)$ are linked: multiplying φ and $D(0)$ with a constant and dividing β by the same constant does not change the hazard rate. This means that one of the three parameters can be chosen freely. Therefore we took $D(0) = 0.1$. We fitted the three survival data sets simultaneously, using the maximum likelihood principle (Section III.6). That is, we obtained $\bar{\theta}$ that maximizes the log-likelihood function $\mathcal{LL}(\theta)$:

$$\mathcal{LL}(\theta) = \sum_{i=1}^{3} \sum_{j=1}^{n_i} \ln h_{\varrho_i}(t_{ij} \mid \theta) - \sum_{i=1}^{3} \sum_{j=1}^{n_i} \int_0^{t_{ij}} h_{\varrho_i}(s \mid \theta) \mathrm{d}s \qquad \text{(IV.16)}$$

where θ is the 4-dimensional parameter $(\psi, \phi, \varphi, \beta)$ and t_{ij} is the time at which the j-th mouse dies in diet-group i (see equation III.10). The hazard rate for diet-group i is denoted by h_{ϱ_i}. The food supply coefficient has values $\varrho_1 = 1$, $\varrho_2 = 0.75$, and $\varrho_3 = 0.44$. The initial number of mice in each diet-group are $n_1 = 49$, $n_2 = 57$, and $n_3 = 71$.

The estimated parameter values are shown in Table IV.2, whereas the corresponding survival curves are depicted in Figure IV.6. We also fitted three Gompertz curves to the same data (Figure IV.7). Because the Gompertz model does not account for food consumption, the value of the exponential mortality-rate coefficient η differs among the diet-groups. The estimated Gompertz-parameter values are included in Table IV.2. Since the Gompertz model and our model have the same number of parameters, they can be compared using the difference between the corresponding log-likelihood values. A difference lower than one, according to the Akaike information criterion [24], indicates that both models describe the data equally well.

Table IV.2: Estimated aging-parameters.

Our model (equation IV.6) $\bar{\theta} = (\bar{\psi}, \bar{\phi}, \bar{\varphi}, \bar{\beta})$	Gompertz model (equation IV.12) $\bar{\theta}_G = (\bar{h}_0, \bar{\eta}_1, \bar{\eta}_2, \bar{\eta}_3)$
$\bar{\psi} = 0.058$ month^{-1}	$\bar{h}_0 = 8.4\ 10^{-5}$ month^{-1}
$\bar{\phi} = 0.0034$ cm^{-3}	$\bar{\eta}_1 = 0.27$ month^{-1} for $\varrho_1 = 1$
$\bar{\varphi} = 1.7\ 10^{-5}$ # cm^{-3}	$\bar{\eta}_2 = 0.23$ month^{-1} for $\varrho_2 = 0.75$
$\bar{\beta} = 0.018$ cm^3 #$^{-1}$ month^{-1}	$\bar{\eta}_3 = 0.17$ month^{-1} for $\varrho_3 = 0.44$
$\mathcal{LL}_G(\bar{\theta}_G) - \mathcal{LL}(\bar{\theta}) = 0.16$	

V

MODELING TUMOR GROWTH

> "*The tumor cell population has to be viewed within the cell community that constitutes the organism,*" **P.A. Lazo**

The embedded tumor: host physiology is important for the evaluation of tumor growth

Adapted from:
I.M.M. van Leeuwen, C. Zonneveld and S.A.L.M. Kooijman (2003)
British Journal of Cancer, to appear

Abstract
The growth potential of a tumor can significantly depend on host features such as age, cell proliferation rates and caloric intake. Although this is widely known, existing mathematical models for tumor growth do not account for it. We therefore developed a new model for tumor growth, starting from a mathematical framework that describes the host's physiology. The resulting tumor-in-host model allowed us to study the implications of various specific interactions between the energetics of tumor and host. The model accounts for the influence of both age and feeding regimen of the host organism on the behavior of a tumor. Concerning the effects of a tumor on its host, it explains why tumor-mediated body-weight loss is often more dramatic than expected from the energy demands of the tumor. We also show how the model can be applied to study enhanced body-weight loss in presence of cachectic factors. Our tumor-in-host model thus appears a proper tool to unite a wide range of phenomena in tumor host interactions.
Keywords
Tumor growth rate; Cancer cachexia; DEB theory; Energy expenditure; Calorie restriction; Tumor doubling time.

V.1 Introduction

Mathematical models for tumor growth have been widely used in different sub-disciplines, such as cancer risk assessment [46, 207], cancer biology [126, 242], cancer treatment [2, 223], and oncological decision making [66]. Since the first models for tumor growth were published [15, 152, 249], they have become more detailed and, consequently, more complex [75, 241]. Most classic and modern approaches share at least one feature, though: both

describe the increase in size of an independent 'entity.' The models are therefore adequate to analyze, for instance, data on tumor spheroids growing *in vitro*. Their use to describe data on tumors growing *in vivo* may be less warranted because of interactions between tumor and host. The aim of this Chapter is to develop a mathematical model to explore such interactions between the growth of a tumor and the physiology of the host organism.

We based our model on well-recognized interactions between tumor growth, energy homeostasis, utilization of stored energy by tumor and host, and cancer cachexia. The formulation in terms of a mathematical model has several benefits. First, it forces us to specify quantitative formulations about the interactions, which improves testability of the hypotheses involved. Second, because the model asks for an overall view of a number of processes and their interrelationships, it can offer insights that complement those arising from individual experimental studies. Finally, model simulations allow to switch on or off particular hypothetical mechanisms easily, so that we can evaluate their impact on and relevance for the expected outcome.

The Chapter is organized as follows. First, we introduce the Dynamic Energy Budget (DEB) theory [117, 118], which provides quantitative expressions for fundamental physiological features and processes, such as food consumption, body growth, metabolic rate, and aging. We then extend this theory to account for tumor growth. Second, with the aid of computer simulations, we show that tumor growth can significantly depend on host physiology and *vice versa*. Regarding the influence of the host on tumor behavior, we focus on the implications for the tumor of differences in host energetics associated with host age and host caloric intake. Thereafter, we study the decrease in body weight associated with the increase in size of a tumor. Finally, we discuss several implications of the results obtained. The Appendix contains additional information on the mathematical formulation of the model as well as on the fitting procedures and parameter values.

V.2 Material and methods

V.2.1 Introduction to the DEB-theory

To model the interaction between tumor and host, we need a general framework describing the physiology of the host organism. Such a framework is provided by the DEB-theory. The theory starts with a set of rules to characterize an individual organism, based on fundamental mechanisms that all organisms seem to have in common. From these rules the theory derives quantitative expressions for sundry physiological processes. In this Chap-

ter, we explain only those aspects of the theory indispensable to understand our model for tumor growth. A more complete, though still qualitative, introduction to the theory can be found in [118], while [117] provides an exhaustive formulation.

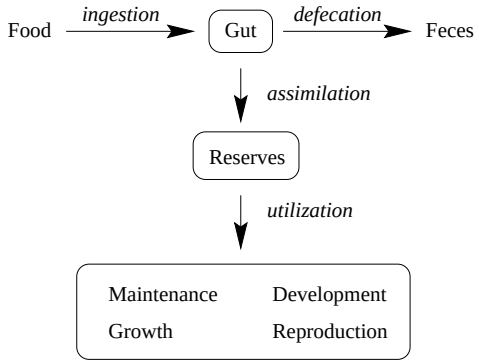

Figure V.1: Energy fluxes in an individual organism, according to the DEB-theory. Food is conceived as material that bears energy. Part of this energy is taken up via the blood and delivered to the reserves. Energy required to carry out the various physiological processes is obtained from these reserves.

Figure V.1 shows the basic outline of the DEB-framework. According to this framework, the body consists of two components, namely structural biomass and reserve compounds. The latter pool comprises compounds characterized by a high mobility. The reserve dynamics follows from the supply and demand of the available resources. Structural biomass can be conceived as volume, hence it is denoted by $V(t)$. Both body components have, by assumption, a constant, but not necessarily identical, chemical composition. As the relative amount of reserves and structure can vary, the composition of the total body can vary. For instance, during fasting the body loses predominantly reserves, so that the overall composition of the body changes.

V.2.2 The κ-rule

Maintenance costs play a key role in our model. Maintenance comprises a range of different processes, among which are protein turnover, heating, maintenance of membrane concentration gradients and muscle tension levels. The costs of such processes should be distinguished from the costs of growth, development and reproduction, as was already concluded in 1898 by Duclaux. Since then, the importance of maintenance processes has become widely accepted [27, 180, 186]. The DEB-theory assumes that maintenance costs per unit structural volume per time unit, $[M]$, are constant, which implies that total maintenance costs amount to $M(t) = [M]V(t)$ per time

unit. This assumption leads to a relationship between body size and respiration that accounts for both growth and maintenance. This prediction is well supported by experimental data concerning the scaling of respiration with body size [117].

The DEB-theory assumes that somatic processes (growth and maintenance) and reproductive processes (development and reproduction) take place in parallel. This is supported by the observation that some species start reproduction while they are still growing; others start reproduction well after reaching adult size. Yet in both species growth levels off in the same way. This implies that the onset of reproduction cannot be the cause of the cessation of growth.

According to the so-called κ-rule, an individual spends a fixed fraction κ of the available energy on somatic processes (growth and maintenance) whereas it spends the remainder fraction on reproductive processes (development, maintaining the degree of differentiation, and reproduction). The part of the κ-rule concerning growth can be written as:

$$\textit{energy available for growth} = \kappa C(t) - \textit{maintenance costs} \tag{V.1}$$

with $C(t)$ the utilization rate at time t; the utilization rate is the rate at which energy is mobilized from the reserves and is made available for physiological processes (see Figure V.1). All the quantities in equation V.1 are expressed per time unit. Thus equation V.1 is an energy *rate* balance, rather than an energy balance. This applies to all similar equations in this Chapter.

To stay alive, an animal has to give maintenance priority over growth. Increase in size consequently ceases when all energy available for maintenance and growth is spent on maintenance only. Maintenance thus determines the ultimate size an organism can reach. The costs of growth are the same for each unit increase in size. Thus, costs of growth per time unit are proportional to the increase in structural volume: $G(t) = [G]\frac{\mathrm{d}V}{\mathrm{d}t}$, with $[G]$ a constant. With the energy available for growth (equation V.1), the organism's size thus changes according to:

$$\frac{\mathrm{d}V}{\mathrm{d}t} = \frac{\kappa C(t) - [M]V(t)}{[G]} \tag{V.2}$$

The DEB-model provides a quantitative expression for the utilization rate $C(t)$ (see Appendix A). When food availability remains constant and food intake is proportional to a body surface area, equation V.2 reduces to the well-known Von Bertalanffy growth equation [15]. This equation fits growth curves of a wide variety of animal species that do not change in shape during growth [115].

V.2.3 Generalized κ-rule

In the introduction to the κ-rule (Section V.2.2), we treated the animal's structure as a single variable. Since we want to describe tumor growth within the DEB-framework, we have to expand the basic formulation. Suppose we zoom in on a cell that changes into a tumor cell. From an energetic point of view several things may happen. First, because tumor tissue is generally less differentiated than other tissues, tumor growth and maintenance costs per tumor volume may be lower allowing tumor cells to proliferate faster than normal cells. But because a tumor is a part of the body that has run out of control, a second energetic aspect may also change: a tumor cell may consume more than its share of the available energy, at the expense of other tissues. In other words, tumor cells may become gluttonous, taking what they want, and leaving the left-over available to the body proper. Thus, in our approach to tumor growth, mutations can lead to hyperplasia by decreasing the costs of somatic processes (maintenance or growth) or by increasing the energy supply per cell.

To model tumor growth dynamics, we need some additional variables and parameters. In addition to body size V, we consider tumor size V_u. Obviously, to survive and proliferate, the tumor has to obtain nutrients from the host. We characterize the gluttony of the tumor by a coefficient μ_u. If $\mu_u = 1$, each tumor cells demands the same amount of energy as an average normal cell; if $\mu_u > 1$, then a tumor cell takes more than an average body cell. Below we will argue that the gluttony coefficient μ_u plays an important role in determining the aggressiveness of a tumor.

The growth rate of a tumor is not only determined by the ability of the tumor to exploit the host's resources, but also by the tumor's maintenance and growth investments. We assume that the tumor appropriates a fraction $\kappa_u(t)$ of the energy that the host has available for somatic processes. This assumption implies that tumors have priority for the resources over the host, which is supported by experimental evidence [26]. The κ-rule above (equation V.1) can now be extended to account for the energetics of the developing tumor:

$$\begin{aligned} \textit{energy available for tumor growth} &= \kappa\kappa_u(t)C(t) - \textit{tumor maint. costs} \\ \textit{energy available for body growth} &= \kappa(1-\kappa_u(t))C(t) - \textit{body maint. costs} \end{aligned} \tag{V.3}$$

where C is the rate of energy mobilization from the reserves. Like in equation V.1, all quantities are expressed per time unit.

Experimental observations support that the tumor's energy demand increases with tumor size. This means that κ_u is a function of tumor size. We assume that

$$\kappa_u(t) = \frac{\mu_u V_u(t)}{V(t) + \mu_u V_u(t)} \tag{V.4}$$

so that κ_u, like κ, takes values between zero and one. Our assumption implies that at small tumor size the fraction of the resources appropriated by the tumor is approximately proportional to tumor size. As the tumor becomes larger, the fraction still increases, but at a diminishing pace. The energy-allocation rules above (equations V.3 and V.4), together with the expressions for the tumor's maintenance and growth costs, completely specify the growth of a tumor. Appendix A outlines further details on the model equations.

V.3 Results

In this section, we analyze the implications of our approach with the aid of computer simulations. For this purpose, we first need to have a set of values for the physiological parameters. These values differ between species, so we had to choose a particular species. As our target species we chose the rat, because many data relevant to our study pertain to rodents. Moreover, since the rat is a typical model species in cancer research, this choice may facilitate testing of our predictions.

As explained in Chapter IV, for tumor-free laboratory rodents after weaning it is warranted to assume constant food consumption. In our approach, this experimental observation replaces the DEB-based assumption that food uptake increases with body size. To obtain the required host parameter values, we fitted the resulting model to data on male rat body growth from a study by Hubert *et al.* (2000). This study includes three groups of 60 male rats exposed to *ad libitum* feeding, 25% caloric restriction, and 55% caloric restriction. Figure V.2 shows the growth curves corresponding to the estimated parameter values. Information on the fitting procedure can be found in Appendix B.

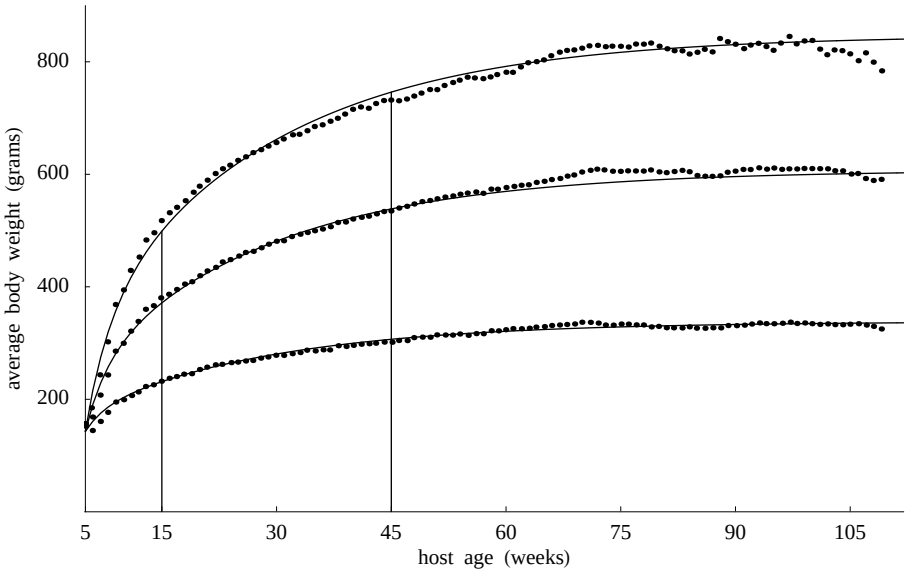

Figure V.2: Growth of Sprague-Dawley male rats. From top downwards: food available *ad libitum*, 25% caloric restriction, and 55% caloric restriction. Dots represent data from Hubert *et al.* (2000). The animals were 5 weeks old at study initiation. We fitted the three data sets simultaneously, varying only food supply among the diet groups. For information on the fitting procedure and the five estimated parameter values, see Appendix. Tumorigenesis may occur, for instance, at age $t_{i1} = 15$ or at age $t_{i2} = 45$ weeks. The vertical lines indicate these moments.

Once values for the parameters characterizing the organism are known, we are able to predict the behavior of the utilization rate as a function of age. In this Chapter, we will show that the utilization rate per structural volume ($[C] = \frac{C}{V}$), rather than the utilization rate itself, is important for tumor growth. As can be seen from Figure V.3, caloric intake significantly affects $[C]$ at the beginning. After some time, however, the body adapts to low food availability and the difference in $[C]$ with food availability disappears. This is in agreement with the experimental observation that differences in energy expenditure per lean body mass disappear with long-term caloric restriction [193].

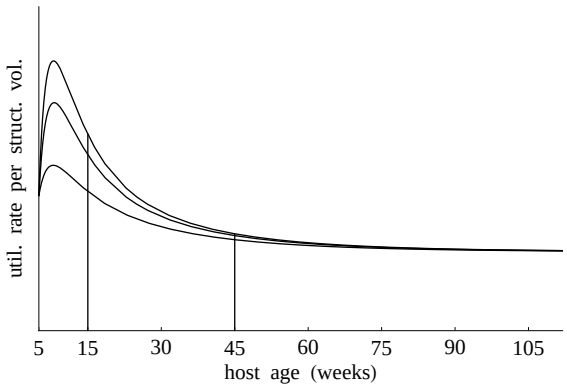

Figure V.3: Model simulation of the energy-expenditure rate per structural volume, $[C] = \frac{C}{V}$. From top downwards: food available *ad libitum*, 25% caloric restriction, and 55% caloric restriction. Tumorigenesis may occur, for instance, at age $t_{i1} = 15$ or at age $t_{i2} = 45$ weeks. The vertical lines indicate these moments.

V.3.1 Tumor growth

In addition to the choice of the rat physiological parameter values, we also need to characterize the tumor by choosing appropriate parameter values. Because of the lack of adequate tumor growth data, we choose these values with an eye on host parameter values. Basically, three parameters characterize the tumor: its coefficient of gluttony μ_u, its growth costs $[G_u]$ and its maintenance costs $[M_u]$. It is the values of these parameters that determine the ability of a tumor to outgrow host tissues. Tumor cells, for instance, may be more successful extracting nutrients from the blood than normal cells (i.e., $\mu_u > 1$). Moreover, because tumor cells have no fine-tuned morphology, it seems likely that tumor growth costs are less than host growth costs (i.e., $[G_u] < [G]$). The same logic applies to tumor maintenance costs (i.e., $[M_u] < [M]$).

To obtain the expressions above (equations V.3 and V.4), we did not make *a priori* assumptions on the shape of the tumor growth curve. Our simulations show that both saturating and non-saturating growth patterns are possible (see Figure V.4). The relevant quantities that determine the growth pattern are the maintenance costs of tumor cells compared to that of host cells and the coefficient of gluttony. Hence, it turns out that a tumor can only grow if $[M_u]$ is smaller or equal to $\mu_u[M]$. Moreover, only if $[M_u] = \mu_u[M]$ holds, it has an S-shaped growth curve. In contrast, if $[M_u] > \mu_u[M]$, the tumor dies off.

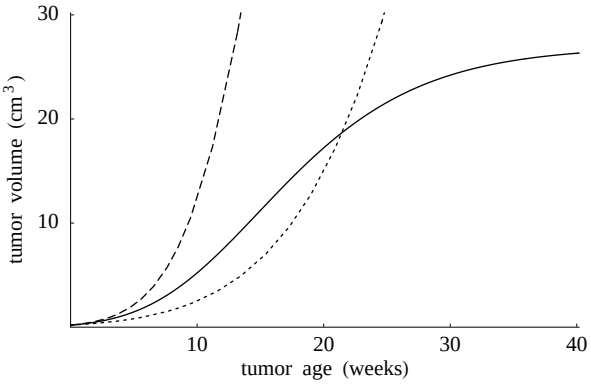

Figure V.4: The shape of the tumor growth curve depends on the relative values of the tumor and host parameters. For any curve: $[G_u] < [G]$. Solid line: $\mu_u > 1$ and $[M_u] = \mu_u[M]$. Dotted line: $\mu_u = 1$ and $[M_u] < [M]$. Broken line: $\mu_u > 1$ and $[M_u] = [M]$. Tumorigenesis at age $t_{i1} = 15$ weeks in an *ad libitum* fed host (see Figure V.2). For further information on the parameter values, see Appendix B.

V.3.2 Influence of host on tumor

Effect of host age on tumor growth

Cancer incidence rates clearly vary with age. Yet, the influence of host age is not restricted to the tumorigenesis phase. Several studies indicate that tumor growth rates also depend on host age. For example, Peer *et al.* (1993) found that breast cancers grow slower in old than in young human females. Pili *et al.* (1994) inoculated Engleberth-Holm-Swarm (EHS) carcinoma cells into mice of different ages. They reported that EHS tumors develop faster in young than in old mice [185]. Moreover, rapid tumor growth resumed upon transfer of tumor tissue from old animals into young animals. Likewise, Donin *et al.* (1997) found a decreased growth potential of B16 melanomas in middle-aged *versus* young mice. Besides reduced growth rates, a less aggressive behavior of tumors has been reported in old as compared to young hosts [93].

To study the effect of host age on tumor progression with our modeling approach, we considered two *ad libitum* fed male rats of ages 15 and 45 weeks, respectively (see Figure V.2). We simulated the implantation of a tumor cell clone ($V_{ui} = 0.2$ cm^3; 10 million cells approximately) of the same type of tumor in both animals. The resulting tumor growth patterns are shown in Figure V.5. The behavior of the tumors differs significantly. As

we did not incorporate in our model any phenomena related to the aging process *per se*, the predicted age-related differences in tumor growth can be attributed to changes in the energetic state of the host during its lifespan. Figure V.3 shows that the host energy expenditure per structural volume diminishes with age. This results in a lower energy availability for the tumor in old *versus* young host, leading to slower tumor growth in the older hosts.

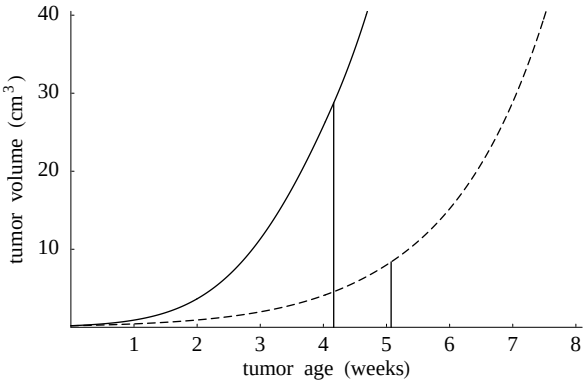

Figure V.5: Tumor growth is influenced by changes in energetics during the host's lifespan. Solid line: growth of a tumor early in the host's life (transplantation at age $t_{i1} = 15$ weeks). Broken line: growth of the same tumor later in life (transplantation at age $t_{i2} = 45$ weeks). Tumor parameters values: $\mu_u > 1$, $[M_u] < [M]$, and $[G_u] < [G]$. Whereas Figure V.4 depicts the change in size of three slowly growing tumors, this Figure corresponds to a more aggressive tumor. The interpretation of the vertical lines will be clarified later on. For further information on the parameter values, see Appendix B.

Effect of caloric restriction on tumor growth

Another aspect of tumor-host interactions is the effect of host nutrition on tumor growth. In the context of the DEB-theory, physiological processes such as energy expenditure, body growth and aging, depend on food intake [132]. As we developed our model for tumor growth within this framework, our approach naturally accounts for food consumption. The model is thus suited to study quantitatively, for example, the influence of host caloric intake on the behavior of a tumor.

Figure V.6 shows the growth of a tumor in hosts exposed to the same levels of caloric restriction that underly the different growth curves depicted in Figure V.2. Solid lines represent the growth of the tumor in three hosts that

have been exposed to the feeding regimen for only 10 weeks; the broken lines correspond to tumorigenesis after 40 weeks exposure. There are thus two variables in this simulation. First, age at tumor transplantation, and second, duration of the exposure to caloric restriction before tumor transplantation. The effect of age was already discussed in Figure V.5. Figure V.6 adds to his the impact of the different levels of caloric restriction. Based on differences in the disparity of the three curves for each age of transplantation, we conclude that short-term caloric restriction has far greater influence on tumor development than long-term caloric restriction. As explained above,

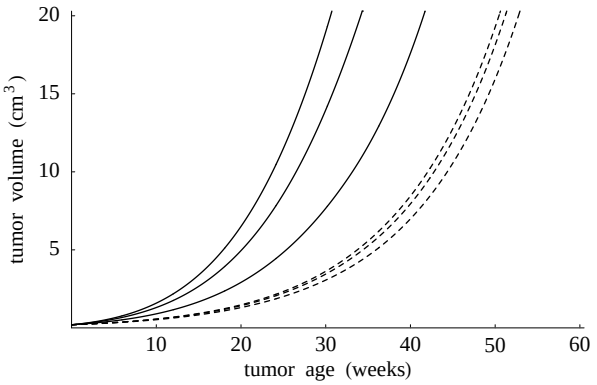

Figure V.6: Food consumption affects tumor growth. Solid lines: tumor implantation after a short exposure to caloric restriction ($t_{i1} = 15$ weeks). Dotted lines: implantation of the same tumors after long time exposure to the same levels of caloric restriction ($t_{i2} = 45$ weeks). Same tumors as in Figure V.5. For each set of three curves, from left to right, food available *ad libitum*, 25% caloric restriction, and 55% caloric restriction.

in our model the growth capacity of a tumor depends on the host's rate of energy-expenditure per structural volume, $[C]$. Figure V.3 shows that food restriction results in a diminished $[C]$. We therefore predict that a tumor grows slower in calorically restricted animals than in *ad libitum* fed ones. However, as can also be seen from Figure V.3, the body adapts to low food availability and the differences in $[C]$ become smaller after exposure to long-term caloric restriction. Consequently, the effect of caloric restriction on tumor growth fades away during long-term caloric restriction. For this reason, the broken lines in Figure V.6 are closer to each other than the solid lines.

V.3.3 Influence of tumor on host

Effect of tumor growth on body weight

We now pay attention to the implications of tumor growth for host physiology. As the tumor exploits the resources of the host organism, the latter disposes of less energy to carry out normal physiological processes. Because maintenance always has priority over growth, the energy spending-cut initially results in a decrease of the host growth rate. If it decreases to zero and tumor size still increases, the host has two ways to survive while satisfying the tumor's energy demand: (a) reduce its own maintenance investment and (b) degrade structural biomass. The former entails that not all required maintenance processes are carried out, which may lead to serious physiological problems and predispose for disease. The latter results in loss of, for instance, skeletal muscle, which may ultimately lead to death.

Although the generalized κ-rule (equations V.3) allows for body-weight loss, there are two reasons why it would be inappropriate to use these equations to describe tissue degradation. First, if these equations were used, all energy originally invested in "building" a unit biomass would be regained, which is thermodynamically impossible. Second, equations V.3 imply that the host re-utilizes all energy released from tissue degradation to pay its own maintenance costs. This contradicts accepted knowledge, indicating that both host and tumor benefit from the released resources. We therefore have to explicitly account for tumor-mediated body-weight loss.

The generalized κ-rule (equation V.3) can easily be extended to account for the loss of body weight often observed in tumor-bearing organisms. Above we argued that a tumor has priority over the available resources. This implies that it also demands a fraction κ_u of the energy obtained from the loss of structural biomass. The host re-utilizes the remainder to pay its own maintenance costs. When no energy is available for body growth, equations V.3 can be written as:

$$\begin{aligned} \textit{energy for tumor growth} &= \kappa_u(\kappa C + \mathcal{S}) - \textit{tumor maint. costs} \\ 0 &= (1-\kappa_u)(\kappa C + \mathcal{S}) - \textit{body maint. costs} \end{aligned} \tag{V.5}$$

where $\mathcal{S}$ represents the rate at which energy is regained from the degradation of structural biomass. We assume that $\mathcal{S}(t) = -\omega[G]\frac{\mathrm{d}V}{\mathrm{d}t}$, which means that the amount of energy that becomes available per time unit is proportional to the tissue degradation rate (notice that, because the host loses structural volume, $\frac{\mathrm{d}V}{\mathrm{d}t}$ is negative and, consequently, $\mathcal{S}$ is positive). The parameter ω is an efficiency coefficient. The thermodynamic upper limit

$\omega = 1$ means 100% efficiency, which, however, can never be achieved. In the realistic case that $\omega < 1$, part of the degraded structural biomass is actually wasted. Figure V.7 shows the predicted body-weight loss associated with the growth of the tumors depicted in Figure V.5. According to our model, tumor-mediated decrease in body weight involves a depletion in both structure and reserve materials. This is in agreement with the observation that most cancer patients suffer a progressive decrease in both adipose tissue and skeletal muscle.

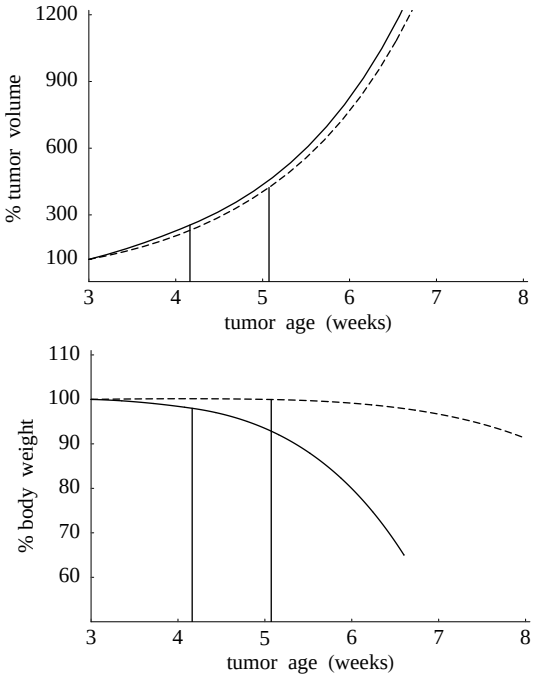

Figure V.7: Tumor growth affects host body weight. The results concern the same computer-simulation study as Figure V.5. Left: Tumor size as a fraction (in %) of its volume 3 days after tumor implantation. Right: Body weight as a fraction (in %) of the host's body weight 3 days after tumor implantation. The vertical lines indicate when tumor-mediated loss of structural biomass starts. The earlier decrease in total body-weight (see right panel) is due to a depletion of reserve materials. Tumor transplantation took place at age $t_i = 15$ weeks (solid lines) and $t_i = 45$ weeks (broken lines) in *ad libitum* fed host.

Cancer patients with the same tumor type can significantly vary in the extent to which they suffer from body-weight loss. Such variations also occur in the context of our model. For instance, Figures V.5 and V.7 show the development of the same tumor in two hosts that differ in age and, consequently, also in size and energetic state. The time at which loss of structural biomass begins, t_s, is indicated with a vertical line. Notice that total body-weight (Figure V.7) begins to decrease before t_s, which is due to an earlier depletion of reserve materials. As can be seen from Figure V.5, in the young host, loss of structural biomass initiates when the tumor reaches a size of 28.7 cm^3. In contrast, in the older host, it starts when the tumor has a size of only 8.4 cm^3. The time delay between tumor implantation and

manifestation of structural-biomass loss also varies with host age. Indeed, in the young it concerns a delay of 4.2 weeks, whereas in the older host it concerns a delay of 5.1 weeks. We conclude that body-weight loss is determined by both host and tumor, rather than by the tumor alone.

Cachexia

The loss of body weight shown in Figure V.7 is due to interactions between the energetics of tumor and host. A tumor may enhance body-weight loss by producing (or inducing the production of) factors that interact with the host. This may lead to the syndrome known as cancer cachexia, which is a common cause of morbidity and mortality in cancer patients. Among the proposed cachectic factors are several cytokines [150], a lipid-mobilizing factor [227], and a proteolysis-inducing factor [228]. The degradation of structural biomass induced by such factors can be incorporated into the generalized κ-rule as follows:

$$\begin{aligned} \textit{energy for tumor growth} &= \kappa_u(\kappa C + \mathcal{S}_c) - \textit{tumor maint. costs} \\ \textit{energy for body growth} &= (1-\kappa_u)(\kappa C + \mathcal{S}_c) - \textit{body maint. costs} - \frac{\mathcal{S}_c}{\omega} \end{aligned} \tag{V.6}$$

where $\mathcal{S}_c$ represents the energy obtained from the cachexia-related degradation of structural biomass. The coefficient ω is again the efficiency of energy regain. In the second equation, the term $\frac{\mathcal{S}_c}{\omega}$ stands for the actual costs of the shrinking process for the host. For simplicity, we assume that the cachectic degradation of host tissues occurs at a rate proportional to tumor size: $\sigma_u V_u$, where σ_u indicates the cachectic potency of a tumor (i.e., unit structure degraded per unit tumor volume per unit time). If $\sigma_u > 0$, the cachexia-mediated degradation of structural biomass results in an energy release rate of $\mathcal{S}_c = \omega[G]\sigma_u V_u$. In contrast, if $\sigma_u = 0$ the tumor lacks any cachectic potency and the expressions above reduce to equations V.3. Owing to the energy demand of the tumor and to the cachexia-mediated degradation of structural biomass, the host's energy balance will soon become negative. The host then has to degrade additional structural biomass to continue satisfying both the tumor's energy demand and its own maintenance requirements.

$$\begin{aligned} \textit{energy for tumor growth} &= \kappa_u(\kappa C + \mathcal{S}_c + \mathcal{S}) - \textit{tumor maint. costs} \\ 0 &= (1-\kappa_u)(\kappa C + \mathcal{S}_c + \mathcal{S}) - \textit{body maint. costs} - \frac{\mathcal{S}_c}{\omega} \end{aligned} \tag{V.7}$$

Figure V.8 shows the implications of cachexia for both host and tumor. The tumor type represented here has higher growth costs than the tumor

type displayed in Figure V.5. This explains the lower initial tumor growth rate in Figure V.8.*i*. Nevertheless, the tumor is eventually more aggressive due to its capacity to cause cachexia. Indeed, the host starts to lose structural biomass 3.2 weeks after tumor transplantation. Moreover, a critical 30% body-weight loss is reached just one week later (see Figure V.8.*ii*). Figure V.8.*ii* also shows that, although we did not incorporate anorexia into the model, we predict a decrease in food consumption related to cachexia. Indeed, food intake diminishes progressively to match the lowered body weight. Figures V.8.*iii* and V.8.*iv* reveal that an increased energy expenditure per structural biomass occurs despite the reduced food consumption. An elevated resting energy expenditure has been frequently observed in relation to cancer cachexia [20, 55, 230].

Above we argued that body-weight loss depends on the host physiological parameters (e.g., Figure V.7). The same dependence holds for tumors with a cachectic potential. The time delay between tumorigenesis and disease onset, for example, may significantly vary among hosts. Consequently, the moment of disease onset nor the extent of the disease can be deduced from tumor size.

V.4 Discussion

The main difference between our approach and previous modeling approaches to tumor growth, is that a tumor is conceived as a body part of the host rather than as an independent entity with an intrinsic maximum size. Our approach has the advantage that it can be used not only to describe tumor growth, but also to explore the relevance of interactions between tumor and host. We exemplified this by studying the influence of several host features on tumor behavior and *vice versa*.

Another difference between our approach and others is that it does not assume *a priori* the existence of an asymptotic maximum tumor size. In contrast, for the widely applied Gompertz model [126, 249], maximum tumor size constitutes a model parameter and the associated S-shaped saturating growth pattern is an intrinsic property of the tumor. But not all tumors show saturating growth. The absence of a plateau in certain tumor growth data has been attributed to the early death of the host [66]. That is, the host dies before tumor growth saturates. We doubt whether this is a solid explanation for any fast growing tumor that does not deviate from an exponential growth pattern. But whether or not our doubt is justified, there is good reason not to assume *a priori* the existence of a maximum tumor size.

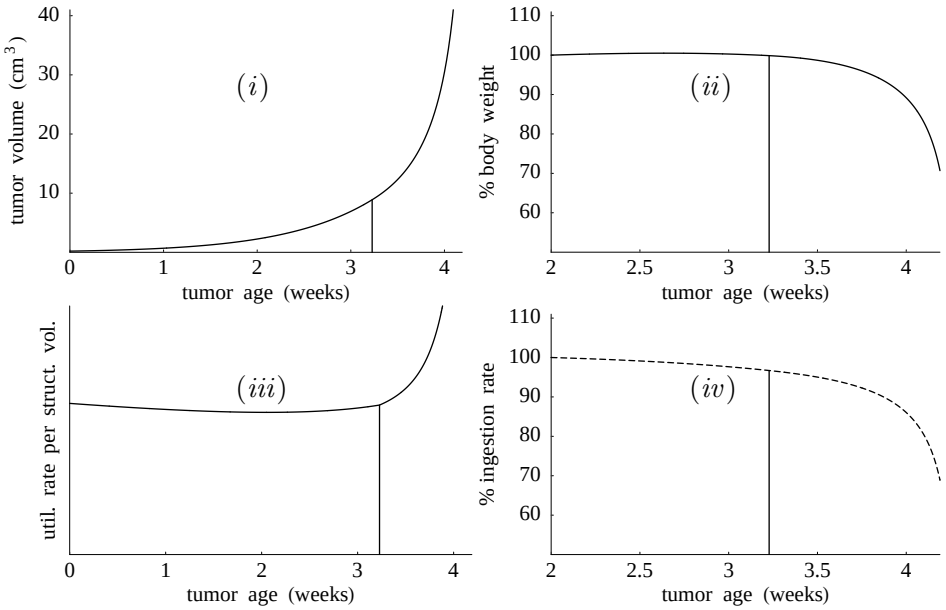

Figure V.8: Implications of cachexia-mediated body-weight loss for tumor and host. (i) Tumor volume as a function of tumor age; (ii) Body weight as a fraction (in %) of body weight 2 days after tumor transplantation; (iii) Predicted energy expenditure per structural biomass; (iv) Food consumption as a fraction (in %) of the ingestion rate 2 days after tumor implantation. The vertical lines indicate the moment at which tumor-mediated loss of structural biomass starts. Tumor transplantation took place at age $t_i = 15$ weeks. Tumor parameters: $[M_u] < [M]$, $[G_u] < [G]$, $\mu_u > 1$ and $\sigma_u > 0$.

Such an assumption hinders the possibility to predict under what physiological conditions a saturating tumor growth can be expected, and how the maximum tumor size depends on host and tumor characteristics.

We analyzed the relation between shape of the tumor growth curve and the parameters of the host. Existence of an asymptotic maximum tumor size is only expected for tumors whose maintenance costs and capacity to extract nutrients from blood satisfy the condition $[M_u] = \mu_u[M]$. As this condition concerns tumor and host parameters, the shape of the tumor growth curve is determined by the energetic characteristics of both tumor and host.

Various factors known to affect tumor growth are not accounted for by our model, for example, diffusion-limited nutrient availability, immune response or the presence of growth inhibitors. The main reason for this is

that when multiple determinants of tumor growth are incorporated at once, it is very difficult to pinpoint the impact of any determinant in particular. Our approach allowed us, for instance, to show that tumor-host interactions in energy dynamics may already cause tumor growth to saturate. This implies that diffusion-limited nutrient availability may be sufficient (e.g., [3]), but not essential to explain an S-shaped growth pattern. If we had included reaction-diffusion of nutrients from the outset, it would have been well-nigh impossible to arrive at this conclusion. To describe describe the growth of particular tumors, however, it may be important to take specific features into account. An advantage of our model is that it can easily be extended to do so. In Appendix C, we exemplify this by showing how our model can be used to describe the growth of solid tumor with a necrotic kernel.

There is general agreement about the main causes of age-dependency of cancer incidence. However, this does not hold for the mechanisms underlying age-dependent tumor progression. Among the mechanisms proposed to explain the latter phenomenon are changes in angiogenic capacity [185], altered apoptotic cell death [100], and immune senescence [192, 233]. As results from various experiments provide evidence for different hypotheses, we preliminarily conclude that several aspects of the natural aging process may affect tumor progression. On the basis of our model predictions we hypothesize that the age-dependent energetic state of the host also plays an important role in determining tumor behavior. Indeed, we argued that age-related differences in tumor growth are due to an age-associated decrease in energy expenditure per structural biomass.

We carried out a theoretical caloric restriction study to investigate the dependence of food consumption on a tumor's growth capacity. Model simulations suggested a strong dependence if tumorigenesis occurs after short-term caloric restriction. In contrast, a weak dependence of tumor growth on caloric intake is expected if tumorigenesis takes place after long-term exposure to caloric restriction. The dependence of tumor growth on food consumption can be understood on the basis of changes in the host energy expenditure.

With regard to the influence of a tumor on host physiology, we focused on tumor-mediated body-weight loss. Computer simulations revealed that body-weight loss can not be unequivocally linked to the increase in tumor size. The main reason is that the severity of body-weight loss is determined by the energetics of both host and tumor, rather than by the tumor alone. Moreover, part of the energy released is actually wasted. These model outcomes may well explain the observation by Plata-Salamán (2000) that

body-weight loss is often more dramatic than one would expect on the basis of the measured tumor growth.

To illustrate the clinical utility of our model, we applied it to understand the energetics behind cancer cachexia. From an energetic point of view, cachexia involves several metabolic alterations, among which are an increase in energy expenditure, a decrease in both structural biomass and reserves, and a reduced food consumption. As a result the host is maintained in a negative energy balance. In the context of our modeling approach, diminished food consumption is a consequence rather than a cause of body-weight loss in cachexia. Yet, in response to the decreased food intake, an acceleration of body-weight loss occurs. From the obtained model predictions, we conclude that the extent of the disease as well as the time delay between tumorigenesis and disease onset strongly depend on the physiological features of the host.

A promising line of research would be to extend the model to include clinical interventions intended to reverse body-weight loss in tumor-bearing patients, such as food intake manipulations and parenteral nutritional support. Food intake manipulations can be incorporated, for instance, as an increase in the assimilation rate. Popp *et al.* (1983) said that "the goal of nutritional therapy in the tumor-bearing host is support of the host carcass in the absence of increased tumor growth." Different food intake manipulations can be analyzed with the aid of our model, to figure out which manipulation may achieve that goal.

Several authors discussed the possible benefits of a low-fat dietary intervention in cancer patients [171, 199]. Because both tumor and host may grow slower or even shrink as a response to the decreased caloric intake, the main issue is whether the tumor or the host suffers more from the effects of caloric restriction. As our model accounts for food consumption, it can be used to examine the implications of such a dietary intervention.

Lazo (1985) argued that "the tumor cell population has to be viewed within the cell community that constitutes the organism." In line with this insight, we formulated our mathematical model within a framework describing the host. We applied the new model to explore several interactions between host and tumor, and were able to capture a number of empirically observed events. Moreover, for some of them we were able to provide an explanation based on energetic features of both tumor and host.

Acknowledgements

The authors thank Bernd Brandt, Paul Hanegraaf, Bob Kooi and two anonymous referees for advice. The work presented in this Chapter is part of the research project DEBtum (VBI-4692), financially supported by STW and DSM.

Appendix

A. Model equations

Tumor-free individual

We assume that the assimilation efficiency is independent of the food ingestion rate (see Appendix, Chapter IV). If an animal receives a fixed fraction ϱ of *ad libitum* food consumption, its assimilation rate is then given by: $A = \varrho A_m$, where A_m denotes the maximum (diet-composition specific) assimilation rate and ϱ is the so-called food-supply coefficient. We define the surface-specific maximum assimilation rate as: $\{A_m\} = A_m V_{1\infty}^{-\frac{2}{3}}$, with $V_{1\infty}$ being the *ad libitum* asymptotic maximum structural volume. The assimilation rate can thus be written as: $A = \varrho\{A_m\}V_{1\infty}^{\frac{2}{3}}$.

According to the DEB-theory, the utilization rate is given by:

$$C = \frac{E}{V}\left(vV^{\frac{2}{3}} - \frac{\mathrm{d}V}{\mathrm{d}t}\right) \tag{V.8}$$

where E denotes the amount of reserves and $v = \frac{\{A_m\}}{[E_m]}$ is the energy conductance, with $[E_m]$ being the maximum reserve density. The change in the amount of reserves is then given by the difference between assimilation and utilization (see Figure V.1), that is: $\frac{\mathrm{d}E}{\mathrm{d}t} = A - C$. Substitution of the expressions for C into this equation leads to:

$$\frac{\mathrm{d}e}{\mathrm{d}t} = \frac{v}{V^{\frac{1}{3}}}\left(\varrho\frac{V_{1\infty}^{\frac{2}{3}}}{V^{\frac{2}{3}}} - e\right) \tag{V.9}$$

with e being the scaled energy density $e = \frac{E}{[E_m]V}$. At the beginning of the study, the host's age is t_0 weeks and its initial reserve density is $e(t_0) = e_0$.

In the context of the DEB-model (Figure V.1), the body has two components. Total body weight is therefore a function of both structure and reserves: $W = d_V(1+\xi e)V$, where d_V is the density of structural biomass and ξ is a dimensionless compound parameter (see Appendix, Chapter IV). As explained in the body of the Chapter, the change in structural volume is given by equation V.2, which can be written as:

$$\frac{\mathrm{d}V}{\mathrm{d}t} = \frac{1}{g[E_m]}C(t) - mV(t) \tag{V.10}$$

where $g = \frac{[G]}{\kappa[E_m]}$ is the energy-investment ratio and $m = \frac{[M]}{[G]}$ the maintenance-rate coefficient. Substitution of the expression for C (equation V.8) gives:

$$\frac{\mathrm{d}V}{\mathrm{d}t} = \frac{veV^{\frac{2}{3}} - gmV}{g+e} \tag{V.11}$$

From equations V.9 and V.11, it can be shown that $V(t)$ tends to an asymptotic maximum value, $V_{\varrho\infty}$, which satisfies $V_{\varrho\infty} = \varrho V_{1\infty} = \varrho(\frac{v}{gm})^3 = \varrho(\frac{\kappa\{A_m\}}{[M]})^3$. Consequently, $A = \varrho^{\frac{1}{3}}\{A_m\}V_{\varrho\infty}^{\frac{2}{3}}$ and the scaled reserve density can be expressed as:

$$\frac{\mathrm{d}e}{\mathrm{d}t} = \frac{v}{V^{\frac{1}{3}}}\left(\varrho^{\frac{1}{3}}\frac{V_{\varrho\infty}^{\frac{2}{3}}}{V^{\frac{2}{3}}} - e\right) \tag{V.12}$$

In sum, the change in size of a tumor-free organism is characterized by equations V.11 and V.12, with initial conditions $V(t_0) = V_0$ and $e(t_0) = e_0$.

Tumor-bearing individual

If tumorigenesis (or tumor implantation) happens at time t_i, let V_{ui} denote the initial tumor size. At t_i the host's structural body-volume is $V_i = V(t_i)$ and its reserve density $e(t_i) = e_i$. As the tumor appropriates reserves originally destined to be spent on physiological processes such as body growth, the host is no longer able to reach its maximum size. To account for this, we generalized the expressions for the scaled reserve density (equation V.12) and the assimilation rate:

$$\frac{\mathrm{d}e}{\mathrm{d}t} = \frac{v}{V(t)^{\frac{1}{3}}}\left(\varrho^{\frac{1}{3}}\frac{\mathcal{V}_{\varrho\infty}(t)^{\frac{2}{3}}}{V(t)^{\frac{2}{3}}} - e(t)\right) \tag{V.13}$$

$$A(t) = \varrho^{\frac{1}{3}}\{A_m\}\mathcal{V}_{\varrho\infty}(t)^{\frac{2}{3}} \tag{V.14}$$

where $\mathcal{V}_{\varrho\infty}(t)$ is defined as the "expected" ultimate structural biomass predicted at time t. We assume that $\mathcal{V}_{\varrho\infty}$ is a function of tumor volume:

$$\mathcal{V}_{\varrho\infty}(t) = \varrho\frac{V(t)}{V_u(t) + V(t)}V_{1\infty}$$

For a tumor-free animal in diet-group ϱ, the function $\mathcal{V}_{\varrho\infty}$ is constant and equal to $V_{\varrho\infty}$.

For both tumor and host, we assume that growth costs are proportional to the increase in structural volume, whereas the maintenance costs are proportional to structural volume. Consequently, the generalized κ-rule (equations V.3) can be written as:

$$\frac{\mathrm{d}V}{\mathrm{d}t} = \frac{1-\kappa_u(t)}{g[E_m]}C(t) - mV(t) \tag{V.15}$$

$$\frac{\mathrm{d}V_u}{\mathrm{d}t} = \frac{\kappa_u(t)}{g_u[E_m]}C(t) - m_uV_u(t) \tag{V.16}$$

where $g_u = \frac{[G_u]}{\kappa[E_m]}$ and $m_u = \frac{[M_u]}{[G_u]}$. The expression for κ_u is given in equation V.4. In the absence of a tumor, equation V.15 reduces to equation V.10. Substitution of the expression for the utilization rate (equation V.8) into the equations above leads to:

$$\frac{\mathrm{d}V}{\mathrm{d}t} = \frac{(1-\kappa_u)veV^{\frac{2}{3}} - gmV}{g + (1-\kappa_u)e} \tag{V.17}$$

$$\frac{\mathrm{d}V_u}{\mathrm{d}t} = \frac{(vV^{\frac{2}{3}} + mV)g\kappa_u e}{gg_u + (1-\kappa_u)g_u e} - m_u V_u \tag{V.18}$$

These equations, together with equation V.13 and the initial conditions $V(t_i) = V_i$, $V_u(t_i) = V_{ui}$, and $e(t_i) = e_i$, specify the change in size of both host and tumor. If the condition $m_u g_u = \mu_u mg$ holds, the tumor grows according to an S-shaped pattern. Moreover, this condition marks the bifurcation between tumors growing ($m_u g_u < \mu_u mg$) or dying off ($m_u g_u > \mu_u mg$).

As explained in the body of the Chapter, equations V.17 and V.18 are reliable thermodynamically as long as $\frac{\mathrm{d}V}{\mathrm{d}t} \geq 0$. Let t_s denote the time (age) at which increase in structure ceases. We define $V_s = V(t_s)$, $V_{us} = V_u(t_s)$ and $e_s = e(t_s)$. For $t \geq t_s$ the following equations, together with equation V.13, describe the loss of structural body mass and the increase in tumor size:

$$\frac{\mathrm{d}V}{\mathrm{d}t} = \frac{(1-\kappa_u)veV^{\frac{2}{3}} - gmV}{(\omega g + e)(1-\kappa_u)} \tag{V.19}$$

$$\frac{\mathrm{d}V_u}{\mathrm{d}t} = \frac{gm\kappa_u V}{g_u(1-\kappa_u)} - m_u V_u \tag{V.20}$$

with initial conditions $V(t_s) = V_s$, $V_u(t_s) = V_{us}$ and $e(t_s) = e_s$. Equations V.19 and V.20 result from the substitution of the expression for C (equation V.8) and $\mathcal{S} = -\omega[G]\frac{\mathrm{d}V}{\mathrm{d}t}$ into equations V.5. Notice that if the condition $m_u g_u = \mu_u mg$ holds, we have $\frac{\mathrm{d}V_u}{\mathrm{d}t} = 0$.

Cachexia equations

Substitution of the expression for C (equation V.8) and $\mathcal{S}_c = \omega[G]\sigma_u V_u$ into equations V.6 gives:

$$\frac{\mathrm{d}V}{\mathrm{d}t} = \frac{(1-\kappa_u)(veV^{\frac{2}{3}} + \sigma_u\omega V_u) - gmV - g\sigma_u V_u}{g + (1-\kappa_u)e} \tag{V.21}$$

$$\frac{\mathrm{d}V_u}{\mathrm{d}t} = \frac{(vV^{\frac{2}{3}} + mV)g\kappa_u e + (\omega g + e)\kappa_u g\sigma_u V_u}{gg_u + (1-\kappa_u)g_u e} - m_u V_u \tag{V.22}$$

These equations, together with equation V.13 and initial conditions $V(t_i) = V_i$, $V_u(t_i) = V_{ui}$, and $e(t_i) = e_i$, specify the change in body size and in tumor volume. If $\sigma_u = 0$, equations V.21 and V.22 reduce to equations V.17 and V.18, respectively.

Let t_s denote the time (age) at which equation V.21 satisfies $\frac{\mathrm{d}V}{\mathrm{d}t}|_{t_s} = 0$. For $t \geq t_s$ the following equations apply:

$$\frac{\mathrm{d}V}{\mathrm{d}t} = \frac{(1-\kappa_u)(veV^{\frac{2}{3}} + \sigma_u\omega V_u) - gmV - g\sigma_u V_u}{(\omega g + e)(1-\kappa_u)} \tag{V.23}$$

$$\frac{\mathrm{d}V_u}{\mathrm{d}t} = \frac{g\kappa_u(mV + \sigma_u V_u)}{g_u(1-\kappa_u)} - m_u V_u \tag{V.24}$$

The initial conditions at t_s are determined by equations V.13, V.21, and V.22. Equations V.23 and V.24 result from the substitution of the expression for C (equation V.8), $\mathcal{S} = -\omega[G]\frac{\mathrm{d}V}{\mathrm{d}t}$ and $\mathcal{S}_c = \omega[G]\sigma_u V_u$ into equations V.7. If $\sigma_u = 0$, equations V.23 and V.24 reduce to equations V.19 and V.20, respectively.

Table V.1: Model variables. Dimensions: − no dimension; e energy; L length; M mass; t time.

Variable	Dimension	
e	-	Host scaled reserve-density
κ_u	-	Tumor reserve-demand function
A	et^{-1}	Assimilation rate
C	et^{-1}	Host utilization-rate
$[C]$	$et^{-1}L^{-3}$	Utilization-rate per structural volume
V	L^3	Host structural-volume
$\mathcal{V}_{\varrho\infty}$	L^3	Expected ultimate structural-volume
V_u	L^3	Volume of tumor's viable cell population
V_T	L^3	Tumor total volume
$V_\dagger$	L^3	Volume of tumor's dead kernel
W	M	Host body-weight
L_T	L	Tumor radius
$\mathcal{S}$	et^{-1}	Energy release-rate
$\mathcal{S}_c$	et^{-1}	Cachectic energy release-rate

B. Parameter values

Hubert *et al.* (2000) consider three different feeding regimes, *ad libitum* ($\varrho = 1$), 25% caloric restriction ($\varrho = 0.75$), and 55% caloric restriction ($\varrho = 0.45$). The animals were 35 days (5 weeks) old at study initiation. As the rats were split into three groups at the beginning of the study, the values of $W_0 = W(t_0)$ and $e_0 = e(t_0)$ can be assumed to be the same for any diet-group. Moreover, because all animals received *ad libitum* feeding until the beginning of the caloric-restriction study, the assumption $e_0 = 1$ holds. In addition we fixed d_V on a value of 1 g/cm^3. During the least-square fitting procedure, we only varied the value of the food-supply

coefficient among the different diet-groups. The estimated parameter values are: $\bar{g} = 7.1$, $\bar{W}_0 = 142.84$ g, $\bar{\xi} = 0.94$, $\bar{V}_{1\infty} = 436.93$ cm^3 and $\bar{v} = 2.22$ cm/week. Consequently: $\bar{m} = \frac{\bar{v}}{\bar{g}}(\bar{V}_{1\infty})^{-1/3} = 0.041$ week^{-1}. The body growth curves corresponding to the estimated parameter values are shown in Figure V.2.

For any displayed tumor: $V_{ui} = 0.2$ cm^3. All computer simulations include a 'switch' of equations at time t_s, with t_s the time (age) at which loss of structural biomass begins, i.e., $\frac{\mathrm{d}V}{\mathrm{d}t}|_{t_s} = 0$.

- *Figure V.4* (shape of the tumor growth curve).
  For any tumor: $\omega = 0.75$ and $\sigma_u = 0$ week^{-1}.
  Solid line: $\mu_u = 4$, $g_u = 3.5$, and $m_u = \mu_u mg/g_u \approx 0.33$ week^{-1}.
  Broken line: $\mu_u = 2$, $g_u = 2.1$, and $m_u = 0.14$ week^{-1}.
  Dotted line: $\mu_u = 1$, $g_u = 2.1$, and $m_u = 0.027$ week^{-1}.

- *Figure V.5* (influence of host age on tumor growth): $\mu_u = 9$, $g_u = 5.1$, $m_u = 10^{-3}$ week^{-1}, $\omega = 0.5$, and $\sigma_u = 0$ week^{-1}.

- *Figure V.6* (effect of caloric restriction on tumor growth): $\mu_u = 3$, $g_u = g$, $m_u = m$, $\omega = 0.75$, and $\sigma_u = 0$ week^{-1}.

- *Figure V.7* (tumor-mediated body-weight loss): $\mu_u = 9$, $g_u = 5.1$, $m_u = 10^{-3}$ week^{-1}, $\omega = 0.5$, and $\sigma_u = 0$ week^{-1}
  (same values as in Figure V.5).

- *Figure V.8* (implications of cachexia-mediated body-weight loss for tumor and host): $\mu_u = 9$, $g_u = 6.1$, $m_u = 0.01$ week^{-1}, $\omega = 0.5$, and $\sigma_u = 1$ week^{-1}.

C. Model extension

An important advantage of our modeling approach is that it can be easily extended to account for specific features of a particular tumor. To exemplify this, we show how it can be used to describe the growth of a tumor with a dead kernel (see Figure II.11). For simplicity, we assume that the the whole tumor is spherical in shape. When the tumor reaches a critical size, defined by a radius δ_m, the tumor starts to develop a dead kernel. In mathematical terms, this implies that an additional cause of tumor-cell death has to be added to our model.

Let us denote as $\frac{\mathrm{d}V_u}{\mathrm{d}t} = \mathcal{X}(V_u)$ our expression for the change in tumor volume (equations V.18, V.20, V.22, or V.24). The growth of the viable cell population in the tumor developing a dead kernel is then:

$$\frac{\mathrm{d}V_u}{\mathrm{d}t} = \mathcal{X}(V_u) - \mathcal{Y}(V_u) \tag{V.25}$$

where $\mathcal{Y}$ represents the death of tumor cells due to insufficient nutrient availability within the tumor. We assume that the volume of cells starved to death gives rise to an equal volume of dead biomass. As the necrotic core can only increase by death

Table V.2: Model parameters. Dimensions: − no dimension; e energy; L length; M mass; t time.

Parameter	Dimension	
d_V	ML^{-3}	Host structure-specific weight
ϱ	-	Host food-supply coefficient
v	Lt^{-1}	Host energy conductance
$[E_m]$	eL^{-3}	Host maximum reserve-density
$V_{\varrho\infty}$	L^3	Host asymptotic maximum structural-volume
V_{ui}	L^3	Tumor initial size
W_0	M	Host initial body-weight
$[M]$	$eL^{-3}t^{-1}$	Host volume-specific maintenance rate
$[M_u]$	$eL^{-3}t^{-1}$	Tumor volume-specific maintenance rate
m	t^{-1}	Host maintenance-rate coefficient
m_u	t^{-1}	Tumor maintenance-rate coefficient
$[G]$	eL^{-3}	Host volume-specific costs for growth
$[G_u]$	eL^{-3}	Tumor's volume-specific costs for growth
g	-	Host energy-investment ratio
g_u	-	Tumor energy-investment ratio
t_i	t	Host age at initiation of tumor growth
ξ	-	Host scaled reserve-specific weight
κ	-	Host reserve-allocation coefficient
ω	-	Efficiency-coefficient of energy regain
σ_u	t^{-1}	Cachectic potency
μ_u	-	Tumor gluttony coefficient
I_m	L^3t^{-1}	Host *ad libitum* food-ingestion rate
A_m	et^{-1}	Host *ad libitum* assimilation rate
δ_m	L	Maximum thickness of the living layer

of cells in the living layer [152], we then have that $\mathcal{Y} = \frac{\mathrm{d}V_\dagger}{\mathrm{d}t}$, with $V_\dagger$ the volume of dead biomass. Substitution of this expression for $\mathcal{Y}$ in equation V.25, leads to:

$$\frac{\mathrm{d}V_u}{\mathrm{d}t} + \frac{\mathrm{d}V_\dagger}{\mathrm{d}t} = \mathcal{X}(V_u)$$

Because the total volume of the tumor satisfies $V_T = V_u + V_\dagger$, the expression above is equivalent to $\frac{\mathrm{d}V_T}{\mathrm{d}t} = \mathcal{X}(V_u)$. As the whole tumor is spherical in shape: $V_T = \frac{4}{3}\pi L_T^3$, with L_T the radius of the tumor. From derivating this expression, we obtain:

$$\frac{\mathrm{d}L_T}{\mathrm{d}t} = \frac{\mathcal{X}(V_u)}{4\pi L_T^2} \tag{V.26}$$

To exhaustively describe the growth of the whole tumor, we now have to fill in the expression for V_u in the equation above. If we assume that the thickness of the

living layer remains constant during tumor growth, the radius of the dead kernel is given by $L_\dagger = L_T - \delta_m$ and:

$$V_u = 4\pi \left(\delta_m L_T^2 - L_T \delta_m^2 + \frac{\delta_m^3}{3} \right) \tag{V.27}$$

because $V_u = V_T - V_\dagger$ and $V_\dagger = \frac{4}{3}\pi L_\dagger^3$. Equation V.27 together with equation V.26 describes the change in the radius of a tumor with a necrotic core. In the particular case that the living biomass grows exponentially (i.e., $\mathcal{X}(V_u) = z_u V_u$), these equations reduce to the tumor growth equation proposed by Mayneord (1932).

Samenvatting

Wiskundige modellen voor de risicobeoordeling van carcinogene stoffen

In het jaar 2000 was kanker de oorzaak van 12% van de 56 miljoen sterfgevallen over de hele wereld. De Wereldgezondheidsorganisatie schat bovendien dat het aantal nieuwe gevallen van kanker in de komende 20 jaar met nog eens 50% zal stijgen. Hiermee is kanker definitief doorgedrongen tot de top-5 van de lijst van belangrijkste doodsoorzaken. Kanker is echter beslist geen nieuwe ziekte. Zo zijn er bijvoorbeeld tumoren ontdekt in Egyptische (1500–500 voor Christus) en Italiaanse (vijftiende eeuw) mummies. Rond het jaar 400 voor Christus vergeleek Hippocrates de aderen die uit sommige borsttumoren groeien met de ledematen van een krab. Vandaar de benamingen *karkinos* ($\kappa\alpha\rho\kappa\iota\nu o\varsigma$) in het Grieks en *cancer* in het Latijn, die oorspronkelijk "krab" betekenden.

Tot de Middeleeuwen werd algemeen gedacht dat tumoren een straf van God waren. Meer recent wordt kanker geassocieerd met veroudering en met blootstelling aan diverse risicofactoren zoals straling, virussen, en natuurlijke en synthetische stoffen. De hypothese dat bepaalde chemicaliën kanker kunnen veroorzaken is minstens zo oud als het epidemiologisch onderzoek van Percival Pott (1775). Deze Engelse arts wees roet aan als schuldige van het hoge aantal scrotumkankergevallen bij schoorsteenvegers. Inmiddels heeft onderzoek uitgewezen dat veel chemicaliën het ontstaan van tumoren kunnen veroorzaken, een proces dat bekend staat als chemische carcinogenese. We noemen zulke kankerverwekende chemicaliën carcinogenen.

Er zijn nu meer dan 100.000 verschillende stoffen op de markt en ieder jaar komen er ongeveer 2.000 nieuwe bij. Uiteraard is het niet wenselijk dat zo'n nieuwe stof risico met zich meebrengt voor de mens. Daarom moet tevoren, in een zogenaamde risicobeoordeling, worden vastgesteld dat de nieuwe stof niet carcinogeen is (of anderszins toxisch). De richtlijnen voor

het uitvoeren van risicobeoordelingen worden bepaald door instellingen zoals de EU, IARC, OECD, en USEPA[1].

Onder risicobeoordeling van (mogelijk) carcinogene stoffen verstaat men het schatten van het kankerrisico voor mensen na blootstelling aan een chemische stof. Meestal wordt deze risicobeoordeling uitgevoerd op basis van dierproeven. De meest gebruikelijke proef is een twee jaar durende test waarbij groepen muizen (of ratten) worden blootgesteld aan verschillende hoeveelheden van de betrokken stof. Er is altijd één groep die een nuldosis krijgt (de controlegroep), om de frequentie te controleren van tumoren die niet door de stof worden veroorzaakt. In standaard carcinogeniciteitsproeven, zoals die van de Amerikaanse NTP, is voor ieder dier de volgende informatie beschikbaar:

Identificatiecode van het individu
Geslacht
Blootstelling (dosis)
Verblijftijd in de proef
Reden van het verlaten van de proef
(b.v. natuurlijke dood, verongelukt, of vermist)
Aanwezigheid van tumoren bij overlijden

Met behulp van deze informatie wordt het kankerrisico van de stof bepaald.

Modellen voor chemische carcinogenese

De resultaten van een carcinogeniciteitsproef kunnen geanalyseerd worden met behulp van wiskundige modellen die de relatie tussen blootstelling aan een stof en het aantal gevallen van kanker beschrijven. Zo kunnen er doses berekend worden die bepaalde verwachte verhogingen van de kans op kanker veroorzaken. Een voorbeeld hiervan is de TD_{50}, de dosis waarvan verwacht wordt dat zij tumoren veroorzaakt in 50% van de dieren die anders (bij een dosis van nul) geen tumoren zouden hebben ontwikkeld. Modellen kunnen ook worden gebruikt om de risico's voor dieren te vertalen naar risico's voor de mens. Een andere toepassing van modellen voor chemische carcinogenese is het voorspellen van tumorfrequenties veroorzaakt door blootstellingen beneden de laagst onderzochte dosis. Dit is belangrijk omdat dierproeven worden uitgevoerd met doses die erg hoog zijn in verhouding tot de niveaus waaraan mensen worden blootgesteld.

[1] Zie lijst met afkortingen op pagina 169

Invloed van voedselopname op groei en veroudering

Zoals in de inleiding gezegd komen tumoren ook voor in de controlegroep. De kans dat een dier een tumor ontwikkelt neemt tijdens de observatieperiode toe. Dit geldt ook voor de mens: hoe ouder, hoe groter de kans op kanker. Ofwel, het ontstaan van tumoren hangt samen met het verouderingsproces. Twee andere aspecten van veroudering spelen ook een belangrijke rol in carcinogeniciteitsproeven. In de eerste plaats: het aantal "normale" sterfgevallen beïnvloedt het aantal dieren in de proef en, daarom, ook het aantal nieuwe kankergevallen. In de tweede plaats: of een dier een tumor heeft kan meestal pas na zijn dood worden vastgesteld. De tijdstippen waarop dieren overlijden bepalen dus de tijdstippen waarop tumoren worden geconstateerd.

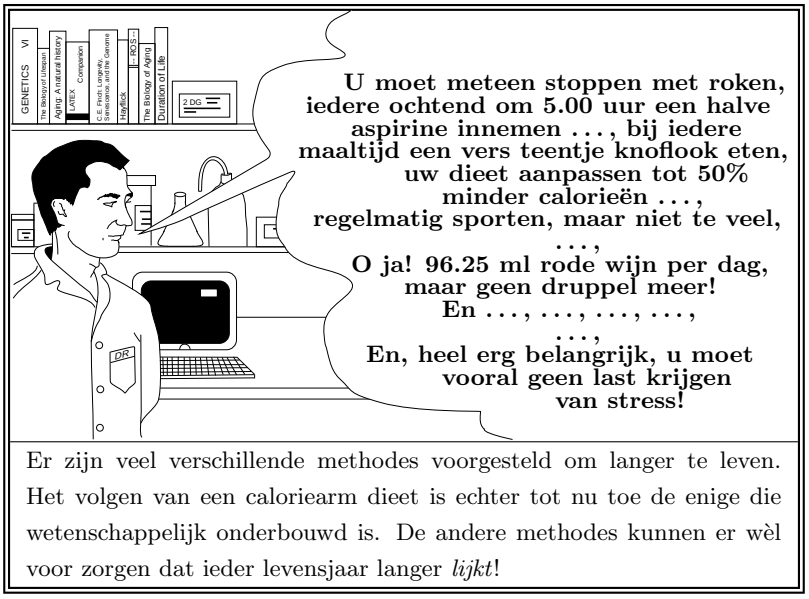

Er zijn veel verschillende methodes voorgesteld om langer te leven. Het volgen van een caloriearm dieet is echter tot nu toe de enige die wetenschappelijk onderbouwd is. De andere methodes kunnen er wèl voor zorgen dat ieder levensjaar langer *lijkt*!

We hebben een model ontwikkeld dat de relatie tussen het verouderingsproces en de procesen van voedselopname en groei vastlegt. Dit model bestaat uit twee modules. De eerste beschrijft de energiedynamica van een organisme, en geeft kwantitatieve formules voor de eetsnelheid, hoeveelheid vet, verandering in lichaamsgrootte en metabole snelheid. Een hoge metabole snelheid is gekoppeld aan een hoge respiratiesnelheid en een hoog hartritme. De tweede module beschrijft het verouderingsproces gebaseerd op de theorie dat veroudering het resultaat is van oxidatieve schade veroorzaakt door vrije

radicalen. Een belangrijk verband tussen beide modules is dat de productiesnelheid van vrije radicalen afhangt van de metabole snelheid. Omdat de metabole snelheid wordt beïnvloed door energie-opname en lichaamsgrootte, kunnen we een formule voor de overlevingskans afleiden die afhangt van voedselniveau en groei.

Een eigenschap van ons model is dat, voor dieren die niet meer groeien, de formule voor de overlevingskans kan worden vereenvoudigd tot de bekende Gompertzformule. Dankzij deze eigenschap zijn we te weten gekomen hoe de parameters van het Gompertzmodel afhangen van metabole snelheid, eetgedrag en lichaamsgrootte. We hebben ons model getoetst aan bestaande gegevens van Weindruch en medewerkers, die groepen muizen met verschillende voedselbeschikbaarheid hebben gevolgd. De dieren die een caloriearm dieet krijgen leven aanmerkelijk langer. Ons model bleek in staat de verschillen in groei en overlevingskans goed te beschrijven.

Interacties tussen tumor en gastheer

Wiskundige modellen die de groei van tumoren beschrijven worden ontwikkeld in verschillende specialisaties binnen het kankeronderzoek, zoals in risicobeoordeling en behandeling. De meeste van deze modellen beschouwen een tumor als een zelfstandige eenheid, los van de "gastheer" waarin de tumor groeit. Deze modellen kunnen dus niets zeggen over de mogelijke interacties tussen tumor en gastheer. Om de relevantie van zulke interacties te bestuderen hebben we een nieuw tumorgroeimodel ontwikkeld, waarin de tumor onderdeel is van het lichaam van de gastheer. In de context van ons model, nemen we aan dat tumoren ontstaan door veranderingen die het energetisch mogelijk maken dat tumorcellen sneller delen dan normale cellen.

Met behulp van computersimulaties hebben we gekeken naar de invloed van de fysiologie van de gastheer op het gedrag van een tumor. Daarbij bleek bijvoorbeeld dat de tumorgroeisnelheid wordt beïnvloed door de leeftijdsafhankelijke metabole snelheid van de gastheer. We voorspellen dat –in het algemeen– tumoren zich sneller zullen ontwikkelen in jonge dan in oude gastheren. Dit is te verklaren door dat de energiebeschikbaarheid per cel afneemt met de leeftijd. Ook voorspellen we hoe tumorgroei beïnvloed kan worden door het "eetgedrag" van de gastheer.

Wat betreft de invloed van de tumor op de gastheer hebben we gekeken naar het gewichtsverlies waaraan veel kankerpatiënten lijden. Als de energetische eisen van de tumor te hoog worden, gaat de gastheer eigen

weefsel afbreken om zijn onderhoudskosten te kunnen betalen. Als gevolg hiervan verliest de gastheer niet alleen vetweefsel maar ook spierweefsel. Een deel van de energie die vrijkomt tijdens dit proces wordt hergebruikt door zowel gastheer als tumor. Omdat de efficiëntie van dit hergebruikproces minder is dan 100%, kan het gewichtsverlies erger zijn dan verwacht op basis van de energetische eisen van de tumor. Daarnaast voorspelt ons model dat de snelheid waarmee het gewicht afneemt beïnvloed wordt door de metabole snelheid van de gastheer. Deze voorspellingen verklaren mogelijk waarom, in de praktijk, geen eenduidige relatie wordt geobserveerd tussen de gewichtsverlies- en tumorgroeisnelheid.

Resumen

Modelos matemáticos para la evaluación de pruebas de carcinogenicidad

En el año 2000 el cáncer fue responsable del 12% de la mortalidad mundial. La Organización Mundial de la Salud (2003) prevé además que el número de nuevos casos crecerá al menos en un 50% en los próximos 20 años. Estas cifras demuestran que el cáncer se ha convertido definitivamente en una de las principales causas de mortalidad. Sin embargo, el cáncer no es, ni mucho menos, una enfermedad nueva. De hecho, se ha constatatdo la presencia de tumores en momias egípcias (1500–500 a.C.) e italianas (siglo XV), y alrededor del año 400 a.C. Hipócrates comparó las venas que irradian de algunos cánceres de mama con las extremidades de un cangrejo, lo cual dió lugar a las denominaciones *karkinos* ($\kappa\alpha\rho\kappa\iota\nu o\varsigma$) en griego y *cancer* en latín.

Hasta bien entrada la Edad Media era creencia generalizada que la aparición de un tumor se debía a la aplicación de algún castigo divino. Posteriormente se ha relacionado el cáncer con el proceso natural de envejecimiento, así como con la acción de diversos factores como radiación, virus, y compuestos naturales y sintéticos. La idea de que ciertos compuestos químicos pueden causar la enfermedad se remonta como mínimo a 1775, año en que Percival Pott (1775) publicó su estudio epidemiológico. En él este médico inglés propuso que el alquitrán presente en el hollín era el agente causante de la elevada incidencia de cáncer de escroto en deshollinadores. Desde entonces se han identificado numerosos compuestos que poseen la capacidad de inducir la formación de tumores mediante un proceso conocido como carcinogénesis química. Estos compuestos reciben el nombre de carcinógenos.

Actualmente hay unos 100.000 compuestos químicos en el mercado, y cada año se añaden alrededor de 2.000 nuevos. Naturalmente, es deseable que la comercialización de estos nuevos compuestos no entrañe un riesgo para el consumidor, por lo que es necesario evaluar la toxicidad y la carcinogenicidad de cada uno de ellos antes de permitir su acceso al mercado.

Las directrices para llevar a cabo estas evaluaciones son establecidas por instituciones como la OCDE[1], la IARC[2], la Unión Europea, y la USEPA[3].

El proceso de evaluación del riesgo carcinógeno se ha definido como un intento científico de identificar y estimar el riesgo de cáncer asociado a la exposición a un compuesto químico. Normalmente esta evaluación es llevada a cabo a partir de los resultados obtenidos mediante experimentos con animales de laboratorio. La prueba de carcinogenicidad más común consiste en un ensayo de dos años de duración en el cual grupos de ratas o ratones son expuestos a diferentes niveles de la sustancia química de interés. Estos experimentos siempre incluyen un grupo al que se le administra una dosis nula, con el fin de controlar la incidencia de tumores no causados por el compuesto químico. Una prueba estándar de carcinogenicidad proporciona la siguiente información sobre cada animal:

Código de identificación individual
Sexo
Dosis
Número de días presente en la prueba
Razón de abandono de la prueba (muerte natural, muerte accidental, desaparición, etc.)
Presencia de tumores

Con esta información se estima el aumento en el riesgo de cáncer debido a un determinado compuesto.

Modelos matématicos de carcinogénesis química

Los resultados de una prueba de carcinogenicidad pueden analizarse mediante modelos matemáticos que describen la relación entre la dosis de un compuesto químico y la incidencia de cáncer. Mediante un modelo de este tipo puede calcularse –por ejemplo– la dosis asociada a un cierto incremento en la incidencia, como la denominada TD_{50}, que es aquella dosis de la que se espera que induzca tumores en la mitad de los individuos que no los habrían desarrollado en ausencia de la sustancia. Los modelos también pueden utilizarse para estimar el riesgo para personas a partir de los resultados obtenidos con animales de laboratorio, o para predecir la incidencia de cáncer por debajo de la dosis más baja empleada. Esta última extrapolación

[1] Organización para la Cooperación y el Desarrollo Económico
[2] Agencia Internacional de Investigación del Cáncer
[3] Agencia de Protección Ambiental de los Estados Unidos

es de gran relevancia, ya que las dosis utilizadas en pruebas de carcinogenicidad son, en general, muy elevadas en comparación con las dosis a las que los seres humanos se ven expuestos.

Un modelo matemático de envejecimiento

Como se ha mencionado en la introducción, normalmente se dan casos de cáncer también en el grupo control. La probabilidad de que un animal desarrolle un tumor aumenta a lo largo de los dos años que dura el ensayo de carcinogenicidad. Un patrón similar de dependencia temporal se ha observado en personas: cuanto más viejo es un ser humano, mayor es la probabilidad de que desarrolle un cáncer. Estas observaciones indican que existe una relación entre la aparición de tumores y el proceso natural de envejecimiento. Al menos otros dos aspectos de este último son de gran importancia para una correcta evaluación de los resultados de una prueba de carcinogenicidad. En primer lugar, el número de muertes por envejecimiento afecta al numero de sujetos presentes en la prueba y, por lo tanto, también al número de nuevos casos de cáncer. En segundo lugar, un tumor no se detecta por lo general hasta que se produce la muerte del animal. Es decir, el instante de la muerte determina el momento en el cual la presencia de un tumor es registrada.

Hemos desarrollado un nuevo modelo matemático que describe la relación entre el proceso de envejecimiento y los procesos de crecimiento e ingestión de alimento. El modelo consta de dos partes; la primera describe la dinámica energética de un organismo y proporciona ecuaciones para características fisiológicas básicas como la variación en la cantidad de grasa corporal, las velocidades de ingestión y crecimiento, y la denominada velocidad metabólica. Una alta velocidad metabólica va asociada a una velocidad de respiración elevada y un ritmo cardiaco rápido.

La segunda parte de nuestro modelo describe el proceso de envejecimiento, y está basada en la teoría de este es consecuencia de la acumulación de daños causados por radicales libres. Un enlace fundamental entre ambas partes del modelo es que la producción de radicales libres depende de la velocidad metabólica; como ésta depende a su vez del consumo calórico y del tamaño del organismo, hemos podido deducir una expresión para la probabilidad de supervivencia –en funcion de la edad– que depende del consumo calórico y del patrón crecimiento.

Una propiedad importante de nuestro modelo es que, para animales que han alcanzado su tamaño final, la expresión para la probabilidad de supervi-

Aunque han sido muchos los métodos propuestos para alargar la vida, sólo el de reducir la ingesta de calorías dispone hasta ahora de testimonios científicos a favor. Los otros métodos, no obstante, posiblemente sí puedan lograr que cada año de vida parezca increíblemente largo.

vencia puede simplificarse hasta la conocida ecuación de Gompertz (1825). Gracias a esta propiedad nos ha sido posible obtener una interpretación en términos fisiológicos de los parámetros de este modelo clásico; en particular, hemos podido averiguar como dependen de la velocidad metabólica, el consumo calórico y el tamaño del organismo. Puesto a prueba con datos de un conocido experimento de Weindruch y col. (1986) en el que varios grupos de ratones fueron mantenidos a diferentes niveles de consumo calórico, nuestro modelo resultó ser capaz de describir las diferencias en crecimiento y supervivencia observadas entre los distintos grupos. Los animales con las dietas más bajas en calorías mostraron poseer la mayor esperanza de vida.

Interacciones entre tumor y organismo hospedador

Modelos matemáticos del crecimiento de tumores han sido desarrollados en diversas subdisciplinas de investigación del cáncer. No obstante, la mayoría de estos modelos consideran al tumor como una entidad independiente y, por lo tanto, no tienen en cuenta posibles interacciones entre el mismo y su organismo hospedador. Para estudiar la relevancia de estas interacciones hemos desarrollado un nuevo modelo matemático partiendo de la premisa de que un tumor es siempre parte de un organismo. En nuestro modelo determinadas mutaciones pueden dar origen al desarrollo de un tumor por

medio de mecanismos que permiten que sea energéticamente factible que las células cancerosas proliferen más rápidamente que las celular normales.

Mediante simulaciones de ordenador hemos investigado la influencia de las características fisiológicas del organismo hospedador sobre el comportamiento de un tumor. Así, hemos descubierto –por ejemplo– que la velocidad de crecimiento del tumor depende de la edad del hospedador o, más concretamente, de su velocidad metabólica, que a su vez varía con la edad. Según las predicciones de nuestro modelo, un mismo tipo de tumor crece por lo general con más rapidez en individuos jóvenes que en individuos maduros, debido a que la energía disponible para cada célula decrece con la edad del organismo. Nuestro modelo también predice que el consumo calórico puede afectar al proceso de crecimiento de un tumor.

Con respecto a la influencia de un tumor sobre su hospedador, nos hemos concentrado en la pérdida de peso que sufren muchos pacientes de cáncer. Según nuestros resultados, cuando las demandas energéticas del tumor alcanzan valores demasiado elevados, el organismo hospedador se ve obligado a degradar tejidos propios con el fin de disponer de la energía suficiente para llevar a cabo sus procesos esenciales de mantenimiento. Como consecuencia el paciente no sólo pierde tejido adiposo, sino también músculo esquelético.

Una parte de la energía liberada durante le proceso de adelgazamiento es aprovechada tanto por el hospedador como por el tumor. Como la eficiencia de esta reutilización no del cien por cien, la pérdida de peso sufrida puede ser mucho más acentuada de lo que cabría esperar a partir de las demandas energéticas del tumor. Además, la magnitud del proceso de adelgazamiento depende tanto de estas últimas como de la velocidad metabólica del hospedador. Posiblemente, estas predicciones de nuestro modelo explican por qué en estudios clínicos no se ha observado una relación unívoca entre la velocidad de crecimiento del tumor y la progresiva pérdida de peso sufrida por el paciente.

References

[1] Abbott WS (1925). A method of computing the effectiveness of an insecticide. *Journal of Economic Entomology* 18:265–267.

[2] Adam JA and Bellomo N (editors) (1997). *A survey of models for tumor-immune system dynamics*. Modeling and simulation in science, engineering and technology. Birkhäuser, Boston.

[3] Afenya EK and Calderón CP (2000). Diverse ideas on the growth kinetics of disseminated cancer cells. *Bulletin of Mathematical Biology* 62(3):527–542.

[4] Ahn H, Kodell RL, and Moon H (2000). Attribution of tumor lethality in the absence of cause-of-death information. *Applied Statistics* 49:157–169.

[5] Allsopp RC, Vaziri H, Patterson C, Golsdtein S, Younglai EV, Futcher AB, Greider CW, and Harley CB (1992). Telomere length predicts replicative capacity of human fibroblasts. *Proceedings of the National Academy of Sciences U.S.A.* 89(21):10114–10118.

[6] Ames BN and Gold LS (1990). Chemical carcinogenesis: Too many rodent carcinogens. *Proceedings of the National Academy of Sciences U.S.A.* 87(19):7772–7776.

[7] Ames BN and Gold LS (1990). Too many rodent carcinogens: Mitogenesis increases mutagenesis. *Science* 249:970–971.

[8] Ames BN and Gold LS (1997). Environmental pollution, pesticides, and the prevention of cancer: Misconceptions. *FASEB Journal* 11:1041–1052.

[9] Andersen ME (1995). Development of physiologically based pharmacokinetic and physiologically based pharmacodynamic models for applications in toxicology and risk assessment. *Toxicology Letters* 79:35–44.

[10] Andersen ME and Krishnan K (1994). Physiologically based pharmacokinetics and cancer risk assessment. *Environmental Health Perspectives* 102:103–108. Suppl. 1.

[11] Armitage P and Doll R (1954). The age distribution of cancer and a multistage theory of carcinogenesis. *British Journal of Cancer* 8(1):1–12.

[12] Armitage P and Doll R (1957). A two-stage theory of carcinogenesis in relation to the age distribution of human cancer. *British Journal of Cancer* 9(2):161–169.

[13] Bailer AJ and Portier CJ (1993). An index of tumorigenic potency. *Biometrics* 49(2):357–365.

[14] ten Berge WF (1999). Kaplan-Meier tumour probability as starting point for dose-response modelling provides accurate life-time risk estimates from rodent carcinogenicity studies. *Annals New York Academy of Sciences* 895:112–124.

[15] von Bertalanffy L (1957). Quantitative laws in metabolism and growth. *Quarterly Review of Biology* 32:217–231.

[16] Bishop JM (1991). Molecular themes in oncogenesis. *Cell* 64:235–248.

[17] Bogen KT (1990). Risk extrapolation for chlorinated methanes as promoters vs initiators of multistage carcinogenesis. *Fundamental & Applied Toxicology* 15:536–557.

[18] Bois FY and Compton-Quintana PJE (1992). Sensitivity analysis of a new model of carcinogenesis. *Journal of Theoretical Biology* 159:361–375.

[19] Borek C and Sachs L (1967). The number of cell generations required to fix the transformed state in X-ray-induced transformation. *Proceedings of the National Academy of Sciences U.S.A.* 59:83–85.

[20] Bosaeus I, Daneryd P, and Lundholm K (2002). Dietary intake, resting energy expenditure, weight loss and survival in cancer patients. *Journal of Nutrition* 132(11):3465–3466. Suppl.

[21] Boucher KM and Yakovlev AY (1997). Estimating the probability of initiated cell death before tumor induction. *Proceedings of the National Academy of Sciences U.S.A.* 94(24):12776–12779.

[22] Brown CC and Chu KC (1989). Additive and multiplicative models and multistage carcinogenesis theory. *Risk Analysis* 9(1):99–105.

[23] Brown D and Rothery P (1993). *Models in biology: Mathematics, statistics and computing*. Wiley and Sons, Chichester.

[24] Burham KP and Anderson DR (1998). *Model selection & inference: A practical information-theoretic approach*. Springer-Verlag, New York.

[25] Butel JS (2000). Viral carcinogenesis: Revelation of molecular mechanisms and etiology of human disease. *Carcinogenesis* 21(3):405–426.

[26] Cameron IL, Pavlat WA, Stevens MD, and Rogers W (1979). Tumor-host responses to various nutritional feeding procedures in rats. *Journal of Nutrition* 109(4):671–684.

[27] Canolty NL and Koong LJ (1976). Utilization of energy for maintenance and for fat and lean gains by mice selected for rapid postweaning growth rate. *Journal of Nutrition* 106:1202–1208.

[28] Casey AE (1934). The experimental alteration of malignancy with an homologous mammalian tumor material. *American Journal of Cancer* 21:760–775.

[29] Charnley G and Wilson JD (1991). Evaluation of the form of the cell growth rate function of the two-stage model for carcinogenesis. In: Butterworth BE, Slaga TJ, Farland W, and McClain M (editors), *Chemically induced cell proliferation: Implications for risk assessment*, pages 291–301. Wiley-Liss, New York.

[30] Chen CW (1993). Armitage-Doll two-stage model: Implications and extension. *Risk Analysis* 13(3):273–279.

[31] Chen JJ, Kodell RL, and Gaylor DW (1988). Using the biological two-stage model to assess risk from short-term exposures. *Risk Analysis* 8(2):223–230.

[32] Choy WN (1993). A review of the dose-response induction of DNA adducts by aflatoxin-B1 and its applications to quantitative cancer-risk assessment. *Mutation Research* 296(3):181 – 198.

[33] Clewell III HJ, Quinn DW, Andersen ME, and Conolly RB (1995). An improved approximation to the exact solution of the two-stage clonal growth model of cancer. *Risk Analysis* 15(4):467–473.

[34] Cohen SM and Ellwein LB (1990). Cell proliferation in carcinogenesis. *Science* 249:1007–1011.

[35] Conolly RB and Andersen ME (1991). Biologically based pharmacodynamic models: Tools for toxicological research and risk assessment. *Annual Reviews of Pharmacology & Toxicology* 31:503–523.

[36] Conolly RB, Reitz RH, Clewell HJ, and Andersen ME (1988). Pharmacokinetics, biochemical mechanism and mutation accumulation: A comprehensive model of chemical carcinogenesis. *Toxicology Letters* 43:189–200.

[37] Cornfield J (1977). Carcinogenic risk assessment. *Science* 198:693–699.

[38] Cox DR and Oakes D (1984). *Analysis of survival data*. Chapman and Hall, London.

[39] Cox LA (1992). Extending the stochastic two-stage model of carcinogenesis to include self-regulation of the non-malignant cell population. *Risk Analysis* 12(1):129–138.

[40] Crouch E and Wilson R (1979). Interspecies comparison of carcinogenic potency. *Journal of Toxicology & Environmental Health* 5:1095–1118.

[41] Crump KS, Hoel DG, Langley CH, and Peto R (1976). Fundamental carcinogenic processes and their implications for low dose risk assessment. *Cancer Research* 36:2973–2979.

[42] Davidson IWF, Parker JC, and Beliles RP (1986). Biological basis of extrapolation across mammalian species. *Regulatory Toxicology & Pharmacology* 6:211–237.

[43] Denes J and Krewski D (1996). An exact representation for the generating function for the Moolgavkar-Venzon-Knudson two-stage model of carcinogenesis with stochastic stem cell growth. *Mathematical Biosciences* 131(2):185–204.

[44] Dewanji A, Goddard MJ, Krewski D, and Moolgavkar SH (1999). Two stage models for carcinogenesis: Number and size distributions of premalignant clones in longitudinal studies. *Mathematical Biosciences* 155(1):1–12.

[45] Dewanji A, Krewski D, and Goddard MJ (1993). A Weibull model for the estimation of tumorigenic potency. *Biometrics* 49(2):367–377.

[46] Dewanji A, Moolgavkar SH, and Luebeck EG (1991). Two-mutation model for carcinogenesis: Joint analysis of premalignant and malignant lesions. *Mathematical Biosciences* 104(1):97–109.

[47] Dewanji A, Venzon DJ, and Moolgavkar SH (1989). A stochastic two-stage model for cancer risk assessment II. The number and size of premalignant clones. *Risk Analysis* 9(2):179–187.

[48] Dinse GE (1991). Constant risk differences in the analysis of animal tumorigenicity data. *Biometrics* 47(2):681–700.

[49] Dodds PS, Rothman DH, and Weitz JS (2001). Re-examination of the "3/4-law"of metabolism. *Journal of Theoretical Biology* 209:9–27.

[50] Donin N, Sinai J, Staroselsky A, Mahlin T, Nordenberg J, and Leibovivi J (1997). Comparison of growth rate of two B16 melanomas differing in metastasic potential in young versus middle-aged mice. *Cancer Investigations* 15(5):416–421.

[51] Duclaux E (1898). *Traité de microbiologie*, chapter Vie aérobie et anaérobie, pages 208–212. Masson and cie, Paris.

[52] Dybing E, Doe J, Groten J, Kleiner J, O'Brien J, Renwick AG, Schlatter J, Steinberg P, Tristscher A, Walker R, and Younes M (2002). Hazard characterisation of chemicals in food and diet: Dose-response, mechanisms and

extrapolation issues. *Food & Chemical Toxicology* 40:237 – 282.

[53] ECETOC (1988). The mutagenicity and carcinogenicity of vinyl chloride: A historical review and assessment. Technical Report 31, European Centre for Ecotoxicology and Toxicology of Chemicals, Brussels.

[54] ECETOC (1996). Risk assessment for carcinogens. Monograph 24, European Centre for Ecotoxicology and Toxicology of Chemicals, Brussels.

[55] Emery PW (1999). Cachexia in experimental models. *Nutrition* 15(7/8):600–603.

[56] Farmer JH, Kodell RL, and Gaylor DW (1982). Estimation and extrapolation of tumor probabilities from a mouse bioassay with survival/sacrifice components. *Risk Analysis* 2(1):27–34.

[57] Fearon ER and Vogelstein B (1990). A genetic model for colorectal tumorigenesis. *Cell* 61:759–767.

[58] Feron VJ, Schwarz M, Hemminki K, and Krewski D (1999). Long- and medium-term carcinogenicity studies in animals and short-term genotoxicity tests. In: Moolgavkar S, Krewski D, Zeise L, Cardis E, and Møller H (editors), *Quantitative Estimation & Prediction of Human Cancer Risks*, chapter 5, pages 103–129. IARC Scientific Publications, Lyon.

[59] Fey SJ and Larsen PM (1988). DNA viruses and human cancer. *Cancer Letters* 41:1 – 19.

[60] Finch CE and Pike MC (1996). Maximum life span predictions from the Gompertz mortality model. *Journal of Gerontology A (Biological Sciences)* 51(3):183–194.

[61] Finkel T and Holbrook NJ (2000). Oxidants, oxidative stress and the biology of aging. *Nature* 408:239–247.

[62] Finkelstein DM (1991). Modeling the effect of dose on the lifetime tumor rate from an animal carcinogenicity experiment. *Biometrics* 47(2):669–680.

[63] Folkman J and Klagsbrun M (1987). Angiogenic factors. *Science* 235:442–447.

[64] Fornaciari G (1999). Renaissance mummies in Italy. *Medicina nei Secoli* 11:85–105.

[65] Freeze RA (2000). *The Environmental Pendulum*. University of California Press, Berkeley.

[66] Friberg S and Mattson S (1997). On the growth rates of human malignant tumors: Implications for medical decision making. *Journal of Surgical Oncology* 65(4):284–297.

[67] Fulgoni VL and Ramirez AG (1998). Cancer: The role of diet, nutrition, and fitness. *Cancer* 83(8):1775–1783.

[68] Gavrilov LA and Gavrilova NS (2001). The reliability theory of aging and longevity. *Journal of Theoretical Biology* 213:527–545.

[69] Gold LS, Slone TH, and Ames BN (1998). What do animal cancer tests tell us about human cancer risk? Overview of analysis of the carcinogenic potency database. *Drug Metabolism Reviews* 30(2):359–404.

[70] Goldin BR (1990). Intestinal microflora: Metabolism of drugs and carcinogens. *Annals of Medicine* 22(2):43–48.

[71] Goldman M (1996). Cancer risk of low-level exposure. *Science* 271:1821–1822.

[72] Gompertz B (1825). On the nature of the function expressive of the law of human mortality, and on a new mode of determining the value of life contingencies. *Philosophical Transactions of the Royal Society London* 115:513–585.

[73] Grasl-Kraupp B, Luebeck EG, Wagner A, Löw-Baselli A, de Gunst M, Waldhör T, Moolgavkar SH, and Schulte-Hermann R (2000). Quantitative analysis of tumor initiation in rat liver: Role of cell replication and cell death (apoptosis). *Carcinogenesis* 21(7):1411–1421.

[74] Greenspan HP (1972). Models for the growth of a solid tumor by diffusion. *Studies in Applied Mathematics* 51:317–340.

[75] Groebe K and Mueller-Klieser W (1991). Distributions of oxygen, nutrient, and metabolic waste concentrations in multicellular spheroids and their dependence on spheroid parameters. *European Biophysics Journal* 19:169–181.

[76] Guengerich FP (2000). Metabolism of chemical carcinogens. *Carcinogenesis* 21(3):345–351.

[77] de Gunst MC and Luebeck EG (1998). A method for parametric estimation of the number and size distribution of cell clusters from observations in a section plane. *Biometrics* 54(1):100–112.

[78] Halliwell B and Gutteridge JMC (1999). *Free radicals in biology & medicine*. Clarendon Press, Oxford, third edition.

[79] Hanahan D and Weinberg RA (2000). The hallmarks of cancer. *Cell* 100:57–70.

[80] Hanes B and Wedel T (1985). A selected review of risk models: One hit, multihit, multistage, probit, Weibull, and pharmacokinetic. *Journal of the American College of Toxicology* 4(4):271–278.

[81] Hanin LG and Yakovlev AY (1996). A nonidentifiability aspect of the two-stage model of carcinogenesis. *Risk Analysis* 16(5):711–715.

[82] Harman D (1956). Aging: A theory based on free radical and radiation chemistry. *Journal of Gerontology* 11:298–300.

[83] Harman D (1981). The aging process. *Proceedings of the National Academy of Sciences U.S.A.* 78(11):7124–7128.

[84] Health Council of the Netherlands (1994). Risk assessment of carcinogenic chemicals in The Netherlands. *Regulatory Toxicology & Pharmacology* 19:14 – 30.

[85] Heidenreich WF (1996). On the parameters of the clonal expansion model. *Radiation Environmental Biophysics* 35:127–129.

[86] Heidenreich WF and Hoogenveen R (2001). Limits of applicability for the deterministic approximation of the two-step clonal expansion model. *Risk Analysis* 21(1):103–105.

[87] Heidenreich WF, Luebeck EG, and Moolgavkar SH (1997). Some properties of the hazard function of the two-mutation clonal expansion model. *Risk Analysis* 17(3):391–399.

[88] Henderson BE, Ross RK, and Pike MC (1991). Toward the primary prevention of cancer. *Science* 254:1131–1138.

[89] Herman JG, Umar A, Polyak K, Graff JR, Ahuja N, Issa JPJ, Markowitz S, Willson JKV, Hamilton SR, Kinzler KW, Kane MF, Kolodner RD, Vogelstein B, Kunkel TA, and Baylin SB (1998). Incidence and functional consequences of *hMLH1* promoter hypermethylation in colorectal carcinoma. *Proceedings of the National Academy of Sciences U.S.A.* 95(12):6870–6875.

[90] Hodgson SV and Maher ER (1999). *A practical guide to human cancer genetics*. Cambridge University Press, Cambridge, second edition.

[91] Hoekstra JA (1991). Estimation of the LD50, a review. *Environmetrics* 2:139–152.

[92] Hoel DG (1980). Incorporation of background in dose-response models. *Federation Proceedings* 39(1):73–75.

[93] Holmes F (1989). Clinical evidence for a change in tumor aggressiveness with age. *Seminars in Oncology* 16:34–40.

[94] Hoogenveen RT, Clewel HJ, Andersen ME, and Slob W (1999). An alternative exact solution of the two-stage clonal growth model of cancer. *Risk Analysis* 19(1):9–14.

[95] Huang HJS, Yee JK, Shew JY, Chen PL, Bookstein R, Friedmann T, and Lee E. Y. H. P. Lee WH (1988). Suppression of the neoplastic phenotype by replacement of the *RB* gene in human cancer cells. *Science* 242:1563–1566.

[96] Hubert MF, Laroque P, Gillet JP, and Keenan KP (2000). The effects of diet, *ad libitum* feeding, and moderate and severe dietary restriction on body weight, survival, clinical pathology parameters, and cause of death in control Sprague-Dawley rats. *Toxicological Science* 58:195–207.

[97] Hunter T (1991). Cooperation between oncogenes. *Cell* 64:249–270.

[98] Huxley JS (1972). *Problems of Relative Growth*. Dover Publications, New York, second edition.

[99] Ingram AJ and Grasso P (1991). Evidence for and possible mechanisms of non-genotoxic carcinogenesis in mouse skin. *Mutation Research* 248(2):333–340. ECETOC Monograph 16.

[100] Itzhaki O, Skutelsky E, Kaptzan T, Siegal A, Michowitz, Sinai J, Huszar M, Nafar S, and Leibovici J (2000). *Biology & pathology of innate immunity mechanisms*, volume 479 of *Advances in Experimental Medicine & Biology*, chapter Macrophage-recognized molecules of apoptotic cells are expressed at higher levels in AKR lymphoma of aged as compared to young mice, pages 251–261. Kluwer Academic Publishers, Dordrecht.

[101] Iversen S and Arley N (1950). On the mechanism of experimental carcinogenesis. *Acta Pathologica & Microbiologica Scandinavica* 27:773–803.

[102] Jen J, Powel S, Papadopoulos N, Smith K, Hamilton S, Vogeltein B, and Kinzler K (1994). Molecular determinants of dysplasia in colorectal lesions. *Cancer Research* 54(21):5523–5526.

[103] Jones PA and Laird PW (1999). Cancer epigenetics comes of age. *Nature Genetics* 21(2):163–167.

[104] Kaplan EL and Meier P (1958). Nonparametric estimation from incomplete observations. *Journal of the American Statistical Association* 53:457–481.

[105] Kendall DG (1960). Birth-and-death processes, and the theory of carcinogenesis. *Biometrika* 47:13–21.

[106] Kerbel RS (2000). Tumor angiogenesis: Past, present and the near future. *Carcinogenesis* 21(3):505–515.

[107] Kimmel M and Flehinger BJ (1991). Nonparametric estimation of the size-metastasis relationship in solid cancers. *Biometrics* 47(3):987–1004.

[108] King RJB (2000). *Cancer Biology*. Pearson Education, Harlow, second edition.

[109] Kirkwood TBL (1977). Evolution of ageing. *Nature* 270:301–304.

[110] Kirkwood TBL, Kapahi P, and Shanley DP (2000). Evolution, stress, and longevity. *Journal of Anatomy* 197:587–590.

[111] Kluyver HN (1961). Food consumption in relation to habitat in breeding chickadees. *Auk* 78:532–550.

[112] Knight EV, Barrett DS, Keenan CM, Kimball JP, Eitzen BH, Bryant S, Smith LN, Szot RJ, and Powers WJ (1998). Influence of origin or controlled feeding on longevity of Sprague-Dawley rats. *International Journal of Toxicology* 17(Suppl. 2):57–78.

[113] Knudson AG (1971). Mutation and cancer: Statistical study of retinoblastoma. *Proceedings of the National Academy of Sciences U.S.A.* 68:820–823.

[114] Kodell RL, Krewski D, and Zielinski JM (1991). Additive and multiplicative relative risk in the two-stage clonal expansion model of carcinogenesis. *Risk Analysis* 11(3):483–490.

[115] Kooijman SALM (1988). The von Bertalanffy growth rate as a function of physiological parameters; a comparative analysis. In: Hallam TG, Gross LJ, and Levin SA (editors), *Mathematical Ecology*, pages 3–45. World Scientific, Singapore.

[116] Kooijman SALM (1993). *Dynamic Energy Budgets in biological systems*. Cambridge University Press, Cambridge.

[117] Kooijman SALM (2000). *Dynamic Energy & Mass Budgets in biological systems. Theory and applications*. Cambridge University Press, Cambridge.

[118] Kooijman SALM (2001). Quantitative aspects of metabolic organization; a discussion of concepts. *Philosophical Transactions of the Royal Society London* 356:331–349.

[119] Kooijman SALM and Bedaux JJM (1996). *The analysis of aquatic toxicity data*. VU University Press, Amsterdam.

[120] Kopp-Schneider A (1997). Carcinogenesis models for risk assessment. *Statistical Methods in Medical Research* 6:317–340.

[121] Kopp-Schneider A and Portier CJ (1989). A note on approximating the cumulative distribution function of the time to tumor onset in multistage models. *Biometrics* 45(4):1259–1263.

[122] Kopp-Schneider A and Portier CJ (1994). A stem cell model for carcinogenesis. *Mathematical Biosciences* 120(2):211–232.

[123] Kopp-Schneider A, Portier CJ, and Sherman CD (1994). The exact formula for the tumor incidence in the two-stage model. *Risk Analysis* 14(6):1079–1080.

[124] Krewski D, Cardis E, Zeise L, and Feron VJ (1999). Empirical approaches to risk estimation and prediction. In: Moolgavkar S, Krewski D, Zeise L, Cardis E, and Møller H (editors), *Quantitative Estimation & Prediction of Human Cancer Risks*, pages 131–178. IARC Scientific Publications.

[125] Kroese ED, Muller JJA, Mohn GR, Dortant PM, and Wester P (2001). Tumorigenic effects in Wistar rats orally administered benzo[*a*]pyrene for two years (gavage studies). Implications for human cancer risks associated with oral exposure to polycyclic hydrocarbons. Technical report, RIVM report nr. 658603 010, Bilthoven.

[126] Laird AK (1964). Dynamics of tumor growth. *British Journal of Cancer* 18:490–502.

[127] Lala PK and Patt HM (1966). Cytokinetic analysis of tumor growth. *Proceedings of the National Academy of Sciences U.S.A.* 56:1735–1742.

[128] Lane N (2002). *Oxygen: The molecule that made the world*. Oxford University Press, Oxford.

[129] Lazo PA (1985). Tumour-host metabolic interaction and cachexia. *FEBS* 187(2):189–192.

[130] Lee HC and Wei YH (2001). Mitochondrial alterations, cellular response to oxidative stress and defective degradation of proteins in aging. *Biogerontology* 2(4):231–244.

[131] van Leeuwen CJ and Hermens JLM (editors) (1995). *Risk Assessment of Chemicals: An Introduction*. Kluwer Academic Publishers, Dordrecht.

[132] van Leeuwen IMM, Kelpin FDL, and Kooijman SALM (2002). A mathematical model that accounts for the effects of caloric restriction on body weight and longevity. *Biogerontology* 3(6):373–381.

[133] van Leeuwen IMM and Zonneveld C (2001). From exposure to effect: A comparison of modeling approaches to chemical carcinogenesis. *Mutation Research* 489(1):17–45.

[134] Lenhard-Rudolph K, Chang S, Lee HW, Blasco M, Gottlieb GJ, Greider C, and DePinho RA (1999). Longevity, stress response, and cancer in aging telomerase-deficient mice. *Cell* 96:701–712.

[135] Levine AJ, Momand J, and Finlay CA (1991). The *p53* tumour suppressor gene. *Nature* 351:453–456.

[136] Lewin B (1991). Oncogenic conversion by regulatory changes in transcription factors. *Cell* 64:303–312.

[137] Liotta LA, Steeg PS, and Stetler Stevenson WG (1991). Cancer metastasis and angiogenesis: An imbalance of positive and negative regulation. *Cell* 64:327–336.

[138] Little MP (1995). Are two mutations sufficient to cause cancer? Some generalizations of the two-mutation model of carcinogenesis of Moolgavkar, Venzon, and Knudson, and of the multistage model of Armitage and Doll. *Biometrics* 51(4):1278–1291.

[139] Little MP, Muirhead CR, and Charles MW (1999). Describing time and age variations in the risk of radiation-induced solid tumor incidence in the japanese atomic bomb survivors using generalized relative and absolute risk models. *Statistics in Medicine* 18:17–33.

[140] Littlefield NA, Farmer JH, Taylor PW, and Sheldon WE (1979). Effects of dose and time in a long-term, low-dose carcinogenesis study. *Journal of Environmental Pathology & Toxicology* 3:17–34.

[141] Lovell DP and Thomas G (1996). Quantitative risk assessment and the limitations of the linearized multistage model. *Human & Experimental Toxicology* 15:87–104.

[142] Lowe SW and Lin AW (2000). Apoptosis in cancer. *Carcinogenesis* 21(3):485–495.

[143] Lubin JH, Blot WJ, Berrino F, Flamant R, Cillis CR, Kunze M, Schmahl D, and Visco G (1984). Modifying risk of developing cancer by changing habits in cigarette smoking. *British Medical Journal* 288:1953–1956.

[144] Luebeck EG and Moolgavkar SH (1991). Stochastic analysis of intermediate lesions in carcinogenesis experiments. *Risk Analysis* 11(1):149–157.

[145] Luebeck EG and Moolgavkar SH (1994). Simulating the process of malignant transformation. *Mathematical Biosciences* 123(2):127–146.

[146] Luebeck EG, Moolgavkar SH, Buchmann A, and Schwarz M (1995). Growth kinetics of enzyme-altered liver foci in rats treated with phenobarbital or α-hexachlorocyclohexane. *Toxicology & Applied Pharmacology* 130:304–315.

[147] Lutz WK (1998). Dose-response relationships in chemical carcinogenesis: superposition of differential mechanisms of action, resulting in linear-

nonlinear curves, practical thresholds, J-shapes. *Mutation Research* 405(2):117–124.

[148] MacPhee DG (1998). Epigenetics and epimutagens: Some new perspectives on cancer, germ line effects and endocrine disrupters. *Mutation Research* 400(1-2):369–379.

[149] Marnett LJ (2000). Oxyradicals and DNA damage. *Carcinogenesis* 21(3):361–370.

[150] Matthys P and Billiau A (1997). Cytokines and cachexia. *Nutrition* 13(9):763–770.

[151] Maugh TH (1978). Chemical carcinogenesis: How dangerous are low doses? *Science* 202:37–41.

[152] Mayneord WV (1932). On a law of growth of Jensen's rat sarcoma. *American Journal of Cancer* 16:841–846.

[153] McElwain DLS and Ponzo PJ (1977). A model for the growth of a solid tumor with non-uniform oxygen consumption. *Mathematical Biosciences* 35:267–279.

[154] Medinsky MA (1995). The application of physiologically based pharmacokinetic/pharmacodynamic (PBPK/PD) modeling to understanding the mechanism of action of hazardous substances. *Toxicology Letters* 79:185–191.

[155] Meier KL, Bailer AJ, and Portier CJ (1993). A measure of the tumorigenic potency incorporating dose-response shape. *Biometrics* 49(3):917–926.

[156] Mendelsohn ML (1960). The growth fraction: A new concept applied to tumors. *Science* 123:1496.

[157] Miller EC and Miller JA (1981). Searches for ultime chemical carcinogens and their reactions with cellular macromolecules. *Cancer* 47:2327–2345.

[158] Mills JJ and Andersen ME (1993). Dioxin hepatic carcinogenesis: Biologically motivated modeling and risk assessment. *Toxicology Letters* 68:177–189.

[159] Miquel J, Economos AC, Fleming J, and Johnson JEJ (1980). Mitochondrial role in aging. *Experimental Gerontology* 15:579–591.

[160] van der Molen GW (1996). A generic toxicokinetic model for persistent lipophilic compounds in humans: An application to TCDD. *Fundamental & Applied Toxicology* 31:83–94.

[161] Moolgavkar SH (1986). Hormones and multistage carcinogenesis. *Cancer Surveys* 5(3):635–648.

[162] Moolgavkar SH (1988). Biologically motivated two-stage model for cancer risk assessment. *Toxicology Letters* 43:139–150.

[163] Moolgavkar SH (1992). A population perspective on multistage carcinogenesis. In: Harris CC, Hirohashi S, and Ito N (editors), *Proceedings of the 22nd International Symposium of the Princess Takamatsu Cancer Research Foundation*, pages 381–391. Japan Scientific Societies Press, Tokyo.

[164] Moolgavkar SH (1993). Cell proliferation an carcinogenesis models: General principles with illustrations from the rodent liver system. *Environmental Health Perspectives* 101:91–94.

[165] Moolgavkar SH and Dewanji A (1988). Biologically based models for cancer risk assessment: A cautionary note. *Risk Analysis* 8(1):5–6.

[166] Moolgavkar SH, Dewanji A, and Venzon DJ (1988). A stochastic two-stage models for cancer risk assessment I. The hazard function and the probability of tumor. *Risk Analysis* 8(3):383–392.

[167] Moolgavkar SH, Krewski D, and Schwarz M (1999). Mechanisms of carcinogenesis and biologically based models. In: Moolgavkar SH, Krewski D, Zeise L, Cardis E, and Møller H (editors), *Quantitative Estimation & Prediction of Human Cancer Risks*, chapter 7, pages 179–237. IARC Scientific Publications, Lyon.

[168] Moolgavkar SH, Krewski D, Zeise L, Cardis E, and Møller H (editors) (1999). *Quantitative Estimation & Prediction of Human Cancer Risks*. IARC Scientific Publications, Lyon.

[169] Moolgavkar SH and Luebeck EG (1990). Two-event model for carcinogenesis: Biological, mathematical and statistical considerations. *Risk Analysis* 10:323–341.

[170] Moolgavkar SH and Venzon DJ (1979). Two-event models for carcinogenesis: Incidence curves for childhood and adult tumors. *Mathematical Biosciences* 47:55–77.

[171] Mukherjee P, El-Abbadi MM, Kasperzyk JL, Ranes MK, and Seyfriend TN (2002). Dietary restriction reduces angiogenesis and growth in an orthotopic mouse brain tumour model. *British Journal of Cancer* 86(10):1615–1621.

[172] Nordling CO (1953). A new theory on the cancer-inducing mechanism. *British Journal of Cancer* 7:68–72.

[173] Nowel PC (1976). The clonal evolution of tumor cell populations. *Science* 194:23–28.

[174] NTP (1993). Toxicology and carcinogenesis studies of 1,3-butadiene in $B6C3F_1$ mice. National Toxicology Program 93-3165, U.S. Department of Health and Human Services, Research Triangle Park, North Carolina.

[175] NTP (2002). Tenth annual report on carcinogens. National toxicology program, U.S. Department of Health and Human Services, Research Triangle Park, North Carolina.

[176] Ochsenbein AF, Klenerman P, Karrer U, Ludewig B, Pericin M, Hengartner H, and Zinkernagel RM (1999). Immune surveillance against a solid tumor fails because of immunological ignorance. *Proceedings of the National Academy of Sciences U.S.A.* 96(5):2233–2238.

[177] O'Flaherty EJ (1989). Interspecies conversion of kinetically equivalent doses. *Risk Analysis* 9(4):587–598.

[178] Olovnikov AM (1973). A theory of marginotomy. *Journal of Theoretical Biology* 41:181–190.

[179] Papa S and Skulachev VP (1997). Reactive oxygen species, mitochondria, apoptosis and aging. *Molecular & Cellular Biochemistry* 174:305–319.

[180] Payne PR and Waterlow JC (1971). Relative energy requirements for maintenance, growth, and physical activity. *Lancet* 2:210–211.

[181] Pearl R (1928). *The rate of living*. Knopf, New York and London.

[182] Peer PG, Dijck JA, Hendriks JH, and Verbeek AL (1993). Age-dependent growth rate of primary breast cancer. *Cancer* 71(11):3547–3551.

[183] Pendergrass WR, Lane MA, Bodkin NL, Hansen BC, Ingram DK, Roth GS, Yi L, Bin H, and wolf NS (1999). Cellular proliferation potential during aging and caloric restriction in rhesus monkeys (*Macaca mulatta*). *Journal of Cellular Physiology* 180:123–130.

[184] Peto R, Lopez AD, Boreham J, Thun M, Health CJ, and Doll R (1996). Mortality from smoking worldwide. *British Medicine Bulletin* 52(1):12–21.

[185] Pili R, Guo Y, Chang J, Nakanishi H, Martin GR, and Passaniti A (1994). Altered angiogenesis underlying age-dependent changes in tumor growth.

Journal of the National Cancer Institute 86(17):1303–13014.

[186] Pirt SJ (1965). The maintenance energy of bacteria in growing cultures. *Proceedings of the Royal Society of London B (Biological Sciences)* 163:224–231.

[187] Plata-Salamán CR (2000). Central nervous system mechanisms contributing to the cachexia-anorexia syndrome. *Nutrition* 16(10):1009–1012.

[188] Popp MB, Wagner SC, and Brito OJ (1983). Host and tumor responses to increasing levels of intravenous nutritional support. *Surgery* 94(2):301–308.

[189] Portier C and El Masri H (1997). Statistical research needs in mechanistic modelling for carcinogenic risk assessment. *Statistical Methods in Medical Research* 6:305–315.

[190] Portier CJ and Kopp-Schneider A (1991). A multistage model of carcinogenesis incorporating DNA damage and repair. *Risk Analysis* 11(3):535–543.

[191] Pott P (1775). *Chirurgical Observations Relative to the Cataracts, the Polypus of the Nose, the Cancer of the Scrotum, the Different Kinds of Ruptures & the Mortifications of the Toes and Feet*. Hawes, Clarke and Collins, London.

[192] Prehn RT (1972). The immune reaction as a stimulator of tumor growth. *Science* 176:170–171.

[193] Ramsey JJ, Harper ME, and Weindruch R (2000). Restriction of energy intake, energy expenditure and aging. *Free Radical Biology & Medicine* 29(10):946–968.

[194] Rand GM (editor) (1995). *Fundamentals of Aquatic Toxicology*. Taylor and Francis, Washington, second edition.

[195] Reitz RH, Gargas ML, Andersen ME, Provan WM, and Green TL (1996). Predicting cancer risk from vinyl chloride exposure with a physiologically based pharmacokinetic model. *Toxicology & Applied Pharmacology* 137:253–267.

[196] Remedi MM, Hliba E, Demarchi M, and Depiante-Depaoli M (1998). Relationship between immune state and tumor growth rate in rats bearing progressive and non-progressive mammary tumors. *Cancer Immunology, Immunotherapy* 46(6):350–354.

[197] Ries LAG, Kosery CL, Hankey BF, Miller BA, Clegg L, and Edwards BK (2000). *SEER Cancer Statistics Review, 1973-1996*. National Cancer Institute, Bethesda.

[198] Robertson JR and Salt GW (1981). Responses in growth, mortality, and reproduction to variable food levels by the rotifer *Asplanchia girodi*. *Ecology* 62(2):1585–1596.

[199] Rose DP, Connolly JM, and Meschter CL (1991). Effect of dietary fat on human breast cancer growth and lung metastasis in nude mice. *Journal of the National Cancer Institute* 83(20):1491–1495.

[200] Rosenkranz HS, Pollack N, and Cunningham AR (2000). Exploring the relationship between the inhibition of gap junctional intercellular communication and other biological phenomena. *Carcinogenesis* 21(5):1007–1011.

[201] Rubin H, Chow M, and Yao A (1996). Cellular aging, destabilization and cancer. *Proceedings of the National Academy of Sciences U.S.A.* 93(5):1825–1830.

[202] van Ryzin J (1980). Quantitative risk assessment. *Journal of Occupational Medicine* 22(5):321–326.

[203] van Ryzin J and Rai K (1987). A dose-response model incorporat-

ing nonlinear kinetics. *Biometrics* 43(1):95–105.

[204] Sawyer C, Peto R, Bernstein L, and Pike MC (1984). Calculation of carcinogenic potency from long-term animal carcinogenesis experiments. *Biometrics* 40(1):27–40.

[205] Schulte-Hermann R, Bursch W, Marian B, and Grasl-Kraupp B (1999). Active cell death (apoptosis) and cellular proliferation as indicators of exposure to carcinogens. In: McGregor DB, Rice JM, and Venitt S (editors), *The use of short- & medium-term tests for carcinogens & data on genetic effects in carcinogenic hazard evaluation*, pages 273–285. IARC Scientific Publications, Lyon.

[206] Sherman CD and Portier CJ (1997). The two-stage model of carcinogenesis: Overcoming the nonidentifiability dilemma. *Risk Analysis* 17(3):367–374.

[207] Sherman CD and Portier CJ (2000). Calculation of the cumulative distribution function of the time to a small observable tumor. *Bulletin of Mathematical Biology* 62:229–240.

[208] Sherman CD, Portier CJ, and Kopp-Schneider A (1994). Multistage models of carcinogenesis: An approximation for the size and number distribution of late-stage clones. *Risk Analysis* 14(6):1039–1048.

[209] Shigenaga MK, Hagen TM, and Ames BN (1994). Oxidative damage and mitochondrial decay in aging. *Proceedings of the National Academy of Sciences U.S.A.* 91(23):10771–10778.

[210] Slob W (1999). Thresholds in toxicology and risk assessment. *International Journal of Toxicology* 18:259–268.

[211] Sohal RS and Weindruch R (1996). Oxidative stress, caloric restriction, and aging. *Science* 273:59–63.

[212] Steel GG (1977). *Growth kinetics of tumors*. Clarendon Press, Oxford.

[213] Steel GG and Lamerton LF (1966). The growth rate of human tumours. *British Journal of Cancer* 20:74–86.

[214] Steward BW and Kleihues P (editors) (2003). *World Cancer Report*. IARC Press, Lyon.

[215] Sutherland RM (1988). Cell and environment interactions in tumor microregions: The multicell spheroid model. *Science* 240:177–182.

[216] Tan WY (1991). *Stochastic models of carcinogenesis*. Marcel Dekker, New York.

[217] Tan WY and Chen CW (1990). Multiple-pathway model of carcinogenesis involving one- and two-stage models. In: Arino O, Axelrod D, and Kimmel M (editors), *Mathematical population dynamics*, chapter 31, pages 469–482. Marcel Dekker, New York.

[218] Tan WY and Chen CW (1998). Stochastic modeling of carcinogenesis: Some new insights. *Mathematical & Computer Modelling* 28(11):49–71.

[219] Tan WY and Singh KP (1987). Assessing the effects of metabolism of environmental agents on cancer tumor development by a two-stage model of carcinogenesis. *Environmental Health Perspectives* 74:203–210.

[220] Tannock IF (1983). Biology of tumor growth. *Hospital Practice* 18:81–93.

[221] Tannock IF and Hill RP (editors) (1998). *The basic science of oncology*. McGraw-Hill, New York, third edition.

[222] Thomas CE and Kalyanaraman B (editors) (1997). *Oxygen radicals and the disease process*. Harwood Academic Publishers, Amsterdam.

[223] Thomlison RH and Gray LH (1955). The histological structure of some hu-

man lung cancers and the possible implications for radiotherapy. *British Journal of Cancer* 9:539–549.

[224] Thompson D (1961). *On growth and form*. Cambridge University Press, Cambridge.

[225] Thorslund TW, Brown CC, and Charnley G (1987). Biologically motivated cancer risk models. *Risk Analysis* 7(1):109–119.

[226] Timbrell J (2000). *Principles of Biochemical Toxicology*. Taylor and Francis, London, third edition.

[227] Tisdale MJ (2000). Metabolic abnormalities in cachexia and anorexia. *Nutrition* 16(10):1013–1014.

[228] Tisdale MJ (2001). Cancer anorexia and cachexia. *Nutrition* 17(5):438–442.

[229] Tomatis L, Huff J, Hertz-Picciotto I, Sander DP, Bucher J, Boffeta P, Axelson O, Blair A, Taylor J, Stayner L, and Barret JC (1997). Avoided and avoidable risks of cancer. *Carcinogenesis* 18(1):97–105.

[230] Toomey D, Redmond HP, and Bouchierhayes D (1995). Mechanisms mediating cancer cachexia. *Cancer* 76(12):2418–2426.

[231] Travis CC (1988). Interspecific scaling of toxicity data. *Risk Analysis* 8(1):119–125.

[232] Tsao JL, Yatabe Y, Salovaara R, Järvinen HJ, Mecklin JP, Aaltonen LA, Tavarè S, and Shibata D (2000). Genetic reconstruction of individual colorectal tumor histories. *Proceedings of the National Academy of Sciences U.S.A.* 97(3):1236–1241.

[233] Tsuda T, Kim YT, and Siskind GW (1987). Role of the thymus and T cells in slow growth of B16 melanoma in old mice. *Cancer Research* 47:3097–3102.

[234] USEPA (1996). Proposed guidelines for carcinogen risk assessment. Technical Report EPA/600/P-92/003C, Office of Research and Development U.S. Environmental Protection Agency, Washington.

[235] van der Vaart AW (1998). *Asymptotic Statistics*. Cambridge Series in Statistical and Probabilistic Mathematics. Cambridge University Press, Cambridge.

[236] Vaidya VG and Alexandro FJ (1982). Evaluation of some mathematical models for tumor growth. *International Journal of Bio-Medical Computing* 13:19–35.

[237] Varmus H and Weinberg RA (1993). *Genes & the Biology of Cancer*. Scientific American Library, New York.

[238] Velazquez SF, Schoeny R, Rice GE, and Cogliano VJ (1996). Cancer risk assessment: Historical perspectives, current issues, and future directions. *Drug & Chemical Toxicology* 19:161–185.

[239] Verhulst PF (1838). Notice sur la loi que la population suit dans son accroissement. *Correspondence Mathématique & Physique* 10:113–121.

[240] Vestal RE (1997). Aging and pharmacology. *Cancer* 80(7):1302–1310.

[241] Ward JP and King JR (1997). Mathematical modelling of avascular-tumour growth. *IMA Journal of Mathematics Applied in Medicine & Biology* 14:39–69.

[242] Ward JP and King JR (1999). Mathematical modelling of the effects of mitotic inhibitors on avascular tumour growth. *Journal of Theoretical Medicine* 1(4):287–311.

[243] Waters MD, Stack HF, and Jackson MA (1999). Genetic toxicology data in the evaluation of potential human environmental carcinogens. *Mutation Research* 437(1):21–49.

[244] Wei Q, Matanoski GM, Farmer ER, Hedayati MA, and Grossman L (1993). DNA repair and aging in basal cell carcinoma: A molecular epidemiology study. *Proceedings of the National Academy of Sciences U.S.A.* 90:1614–1618.

[245] Weibull W (1951). A statistical distribution of wide applicability. *Journal of Applied Mechanics* 18:293–297.

[246] Weindruch R, Walford RL, Fligiel S, and Guthrie D (1986). The retardation of aging in mice by dietary restriction: Longevity, cancer, immunity and lifetime energy intake. *Journal of Nutrition* 116:641–654.

[247] Weismann A (1889). The duration of life. In: Poulton B, Schonland S, and Shipley AE (editors), *Assays upon Heredity & Kindred Biological Problems*. Clarendon Press, Oxford.

[248] Whang YE, Wu X, Suzuki H, Reiter RE, Tran C, Vessela RL, Said JW, Isaacs WB, and Sawyers CL (1998). Inactivation of the tumor suppressor *PTEN/MMAC1* in advanced human prostate cancer through loss of expression. *Proceedings of the National Academy of Sciences U.S.A.* 95:5246–5250.

[249] Winsor CP (1932). The Gompertz curve as a growth curve. *Proceedings of the National Academy of Sciences U.S.A.* 18:1–8.

[250] Winter JE (1973). The filtration rate of *Mytilus edulis* and its dependence on algal concentrations, measured by a continuous automatic recording apparatus. *Marine Biology* 22:317–328.

[251] Wiseman H and Halliwell B (1996). Damage to DNA by reactive oxygen and nitrogen species: Role in inflammatory disease and progression to cancer. *Biochemical Journal* 313:17–29.

[252] Wolfram S (1996). *The Mathematica Book*. Cambridge University Press, Cambridge.

[253] Yakovlev AY and Tsodikov AD (1996). *Stochastic models of tumor latency & their biostatistical applications*, volume 1 of *Mathematical Biology & Medicine*. World Scientific, Singapore.

[254] Yamasaki H (1996). Role of disrupted gap junctional intercellular communication in detection and characterization of carcinogens. *Mutation Research* 365(1-3):91–105.

[255] Yang GL and Chen CW (1991). A stochastic two-stage carcinogenesis model. A new approach to computing the probability of observing tumor in animal bioassays. *Mathematical Biosciences* 104(2):247–258.

[256] Yokota J (2000). Tumor progression and metastasis. *Carcinogenesis* 21(3):497–503.

[257] Yoshida K, Inoue T, Nojima K, Hirabayashi Y, and Sado T (1997). Calorie restriction reduces the incidence of myeloid leukemia induced by a single whole-body radiation in C3H/He mice. *Proceedings of the National Academy of Sciences U.S.A.* 94(6):2615–2619.

[258] Youngman LD, Park JYK, and Ames BN (1992). Protein oxidation associated with aging is reduced by dietary restriction of protein or calories. *Proceedings of the National Academy of Sciences U.S.A.* 89(19):9112–9116.

[259] Yu BP (1996). Aging and oxidative stress: Modulation by dietary restriction. *Free Radical Biology & Medicine* 21(5):651–668.

[260] Zainal TA, Oberley TD, Allison DB, Szweda LI, and Weindruch R (2000). Caloric restriction of rhesus monkeys lowers oxidative damage in skeletal muscle. *FASEB Journal* 14(12):1825–1836.

[261] Zhao CQ, Young MR, Diwan BA, Coogan TP, and Waalkes MP (1997). Association of arsenic-induced malignant transformation with DNA hypomethylation and aberrant gene expression. *Proceedings of the National Academy of Sciences U.S.A.* 94(20):10907–10912.

[262] Zheng Q (1994). On the exact hazard and survival functions of the MVK stochastic carcinogenesis model. *Risk Analysis* 14(6):1081–1084.

[263] Zheng Q (1995). On the MVK stochastic carcinogenesis model with Erlang distributed cell life lengths. *Risk Analysis* 15(4):495–502.

[264] von Ziglinicki T, Pilger R, and Sitte N (2000). Accumulation of single-strand breaks is the major cause of telomere shortening in human fibroblasts. *Free Radical Biology & Medicine* 28(1):64–74.

[265] Zingg JM and Jones PA (1997). Genetic and epigenetic aspects of DNA methylation on genome expression, evolution, mutation and carcinogenesis. *Carcinogenesis* 18(5):869–882.

[266] Zink A, Rohrbach H, Szeimies U, Hagedorn HG, Haas CJ, Weyss C, Bachmeier B, and Nerlich AG (1999). Malignant tumors in ancient Egyptian population. *Anticancer Research* 19(5B):4273–4277.

Abbreviations

	Name or Description
ACI	Adjusted Cumulative Incidence
AD	Armitage-Doll model
ADI	Acceptable Daily Intake
AIR	Acceptable Increase in Risk
B[*a*]P	Benzo[a]Pyrene
B[*a*]P-RIVM	B[a]P carcinogenicity test
BUT-NTP	1,3-butadiene NTP carcinogenicity test
CA	Chromosomal Aberrations
CAS	Chemical Abstracts Service
CDF	Cumulative Distribution Function
CPDB	Carcinogenic Potency Database
CR	Caloric Restriction
DCC	Deleted in Colorectal Carcinoma gene
DEB	Dynamic Energy Budget theory
DNA	DeoxyriboNucleic Acid
ECETOC	European Centre for Ecotoxicology and Toxicology of Chemicals
EHS	Engleberth-Holm-Swarm carcinoma
ERR	Excess Risk Rate
FCTI	Final Cumulative Tumor Incidence
FT	Failure Time
EU	European Union
IARC	International Agency for Research on Cancer
IPCS	International Programme on Chemical Safety
KM	Kaplan-Meier
kpa	Kilogram per year
LD_{50}	50% Lethal Dose
LMS	Linearized Multi-Stage dose-response model
LOAEL	Lowest Observed Adverse Effect Level
MeCCNU	1-(2-Chloroethyl)-3-(4-MethylCyclohexyl)-1-NitrosoUrea
MHFT	Multi-Hit Failure-Time model

continued on next page

continued from previous page

	Name or Description
ML	Maximum Likelihood
MTD	Maximum Tolerated Dose
MVK	Moolgavkar-Venzon-Knudson model
NCI	National Cancer Institute (USA)
NIH	National Institutes of Health (USA)
NKI	Nederlands Kanker Instituut
NOAEL	No Observed Adverse Effect Level
NOEL	No Observed Effect Level
NTP	National Toxicology Program (USA)
OECD	Organization for Economic Cooperation and Development
OHFT	One-Hit Failure-Time model
PBPK	Physiologically-Based Pharmaco-Kinetics
PDF	Probability Density Function
QRA	Quantitative Risk Assessment
RB	RetinoBlastoma
RIVM	Rijksinstituut voor Volksgezondheid en Milieu
RNS	Reactive Nitrogen Species
ROS	Reactive Oxygen Species
RS	Reactive Species
SAR	Structure-Activity Relationships
STW	Netherlands Technology Foundation
TCDD	2,3,7,8-Tetrachlorodibenzo-*p*-dioxin
TD_{50}	Tumorigenic 50% Dose
T_2	Tumor doubling time
tpa	Ton per year
UCL	Upper Confidence Limit
USEPA	Environmental Protection Agency (USA)
UV	UltraViolet
VSD	Virtually Safe Dose
WHO	World Health Organization